Polycytotoxic CD8+ T cells with restricted TCR repertoires typify T lymphocytes in Toxic Epidermal Necrolysis patients

Single Sentence Summary

This study highlights the key role of polycytotoxic CD8+ T cells in the severity of toxic epidermal necrolysis, opening major opportunities to improve diagnostic approaches.

Axel Patrice VILLANI[1-2]*, Aurore ROZIERES[1]*, Benoît BENSAID[2], Klara ERIKSSON[3], Amandine MOSNIER[1], Floriane ALBERT[1], Virginie MUTEZ[1], Océane BRASSARD[1], Tugba BAYSAL[1], Mathilde TARDIEU[1], Omran ALLATIF[1], Floriane FUSIL[1], Thibault ANDRIEU[1-5], Denis JULLIEN[1-2], Valérie DUBOIS[6], Catherine GIANNOLI[6], Henri GRUFFAT[1], Marc PALLARDY[7], François-Loïc COSSET[1], Audrey NOSBAUM[1-4], Osami KANAGAWA[1], Janet L. MARYANSKI[8], Daniel YERLY[3], Jean-François NICOLAS[1-4], Marc VOCANSON[1]

*Equal contributors

Affiliations:

[1] CIRI-Centre International de Recherche en Infectiologie; INSERM, U1111; Univ Lyon; Université de Lyon 1; Ecole Normale Supérieure de Lyon; CNRS, UMR 5308, Lyon, France

[2] Drug allergy reference center, Hospices Civils de Lyon, Hôpital Edouard Herriot, Service de Dermatologie, Lyon, France

[3] Drug allergy research laboratory, Bern University, Switzerland

[4] Département d'Allergologie et d'immunologie Clinique, Höpital Lyon-Sud, Pierre-Bénite, France

[5] SFR Biosciences Gerland, US8, UMS3444, Lyon, France

[6] EFS, Etablissement Français du Sang, Décines, France

[7] INSERM, UMR 996, Châtenay-Mallabry, France

[8] Unité de Thérapie Cellulaire et Génique (UTCG), Centre Hospitalier Universitaire de Nice, 06101 Nice, France

Corresponding author

Email : marc.vocanson@inserm.fr

Abstract

Toxic epidermal necrolysis (TEN) is a life-threatening cutaneous adverse drug reaction (cADR), characterized by massive epidermal necrosis. Diverse studies have reported that TEN onset correlates with a robust skin infiltration by cytotoxic lymphocytes (T, NK cells) and inflammatory monocytes. To better understand why skin symptoms are so severe in TEN disease versus other benign cARDs such as maculopapular exanthema (MPE), we conducted a prospective immunophenotyping study on skin samples and blood from 18 TEN and 14 MPE patients, using mass cytometry and next generation TCR sequencing. Our results confirmed that cytotoxic CD8+ T cells (CTLs) are the main leucocyte subsets found in TEN blisters, at the acute phase, while we failed to repeatedly detect unconventional lymphocytes such as NKT, MAIT, NK or gamma-delta T cells. Strikingly, deep sequencing of the T cell receptor CDR3 repertoire revealed massive expansion of unique CDR3 clonotypes in blister cells. Over-represented clonotypes were mainly effector memory CD8+CD45RA-CCR7- T cells, and expressed high levels of cytotoxic (Granulysin or Granzymes A & B) and activation (CD38) markers. By comparison, TCR repertoire bias and polycytotoxic phenotype were far less marked in MPE patients. By transfecting α and β chains of the expanded clonotypes into immortalized T cells, we confirmed in some patients that those cells were drug-specific. Collectively, our results suggest that the quantity (clonal expansions) and quality (cytotoxic phenotype) of skin-recruited CTLs condition the clinical presentation of cADRs. Importantly, they open major opportunities for the development of new prognostic avenues in TEN.

Introduction

Toxic epidermal necrolysis (TEN) is characterized as a rapidly progressing blistering eruption accompanied by an important mucosal involvement and skin detachment. Hence, TEN is associated with an important mortality rate of approximately 25-40%, and nearly constant and invalidating sequelae (blindness, respiratory disturbance…), which are responsible for profound loss of quality of life in surviving patients (*1*) (*2*) (*3*).

The etiopathogenesis of TEN, like other cutaneous adverse drug reactions (cADRs), involves the activation of drug-specific T cells, which have been isolated and cloned from the blood and the skin lesions of TEN patients (*4-6*) (*7*). Similarly to chemical allergens, the majorities of the drugs responsible for TEN are protein-reactive, and generate new drug-peptide epitopes which trigger an hypersensitivity/allergic reaction (*8*) (*9*) (*10*). Of note, recent works suggest that T cell stimulation could also be consecutive to a direct and non-covalent interaction of the drug with the T Cell Receptor (TCR), or the major histocompatibility complex (MHC)-binding groove (a process referred to as "p-i concept") (*11*), as well as *via* the presentation of an altered repertoire of self-peptides (*12*) (*13*).

Although it remains only partially understood, the most probabilistic scenario for TEN onset postulates that, once they have been primed in lymphoid organs, drug-specific cytotoxic CD8+ T cells are recruited at the dermo-epidermal junction, where they kill keratinocytes presenting drug epitopes at their cell surface, through mechanisms involving Perforin/Granzyme B and MHC class I-restricted pathways (*6*) (*10*). To explain extensive blister formation and subsequent skin detachment, several investigators have reported that specific T cells produce massive amounts of soluble mediators like Granulysin (*14*), interferon-gamma (IFN-γ) or tumor necrosis factor-alpha (TNF-α), that further amplify and extend keratinocyte cell death. IFN-γ and TNF-α promote Fas-L expression on keratinocytes, and subsequent cell-cell suicide (*via* Fas-FasL presentation) to explain the disseminated epidermal apoptosis in some patients (*15*). Alternatively, other works have suggested that natural killer (NK) cells and inflammatory monocytes exert additional contribution to epidermal necrolysis, notably via Granulysin-, TWEAK (CD255)-, TRAIL (CD253)- or Annexin A1-dependent mechanisms (*16*) (*17*) (*18*).

If these immunological features are now well established, including the skin infiltration by CTLs (*19*), most of them were also detected in patients suffering from less severe cADRs, such as maculopapular exanthema (MPE) (*20*) (*21*). MPE patients harbor limited spots of epidermal apoptosis/necrolysis (*22*) (*23*), but no blisters, and fast healing upon drug discontinuation. Hence, to date, it is still largely unknown why some patients, who sometimes take the same drugs (*24, 25*), develop a severe and life-threatening disease (TEN) or mild reaction (MPE). The fact that drug-specific CTLs were shown to be involved in diverse types of cADRs questions whether their number,

89 their functions or their activation parameters (epitope number and persistence, regulatory
90 mechanisms…) are peculiar/specific to TEN disease. Moreover, the differential recruitment of
91 unconventional cytotoxic leucocytes could also precipitate the severity of this disease.
92 To gain further insight on TEN pathogenesis we conducted, here, a comprehensive
93 immunophenotyping study to characterize the immune cells infiltrating the skin or circulating in the
94 blood of patients suffering from TEN or MPE, at time of disease onset. Our main results revealed that
95 there is a dramatic expansion of polycytotoxic CD8+ T cell clones in the blood and the skin of TEN
96 patients, which largely outnumbers the frequency of cells expanding in less severe MPE patients.

RESULTS

Skin and blood samples were collected from 18 TEN patients during the course of their intensive care, and from 14 hospitalized MPE controls. Demographic data are shown in **Table 1**. Samples were recovered within a minimal delay of 0-2 days after patient's arrival at clinic. Hence, majority of samples were collected before the peak of the disease, characterized for TEN patients by the percentage of maximal skin detachment (**Table 1 & Table S1**). Noteworthy, the majority of patients displayed very diverse HLA genotypes, with A*02 and B*44 as the most represented loci. For this group of patients, a careful investigation of causative drug(s) associated to skin symptoms revealed a large variability in terms of drug nature or mode of action. The same molecule was reported as culprit drug only for pairs of TEN patients (Allopurinol for patients TEN-1 & -3; Sulfamethozaxole/Trimethoprim for TEN-2 & -5; and Ceftriaxone for TEN-10 & -11, (**Table 1**)).

Immunophenotype of leukocytes infiltrating the skin of TEN patients

We first examined the immunophenotype of cells infiltrating the skin of TEN patients by mass cytometry and subsequent computational data analysis. Blister cell samples obtained from 7 TEN patients were analyzed by CyTOF using a panel of 29 antibodies (**Table S2**), enabling mapping of all major peripheral blood mononuclear cell subsets (lineage gating strategy is represented in **Figure S1**). We detected a large predominance of conventional T lymphocytes (TCR$\alpha\beta$+; 71.3±18.8%) among hematopoietic CD45+ cells, along with a minor infiltration of monocytes (CD14+ subset, 13.47±8.6%), NK (TCR$\alpha\beta$-CD56+, 5.8±7.2%) cells, and very few gamma delta T (TCR$\gamma\delta$+, 1.9±2.8%), B (CD19+, 0.6±0.6%) or dendritic cells (CD11c+, 3.4±5.9%) (**Figure 1, A1**). Conventional T lymphocytes were CD8+ (56.64±21.6%), CD4+ (29.24±20.4%) and double-negative (DN) (9.6±4.4%) T cells (**Figure 1, A2**). Very few or no double positive (DP, 2.0±3.4%), MAIT (CD4-CD8β-TCRVα7.2+, 0.2±0.1%) or invariant NKT (iNKT; TCR$\alpha\beta^{int}$TCRVα24+, 1.0±1.5%) cells were recorded for all the patients (**Figure 1, A2**). Interestingly, when skin TEN biopsies were collected, instead of blister fluids, we detected similar results, except for an increased representation of CD4+ versus CD8+ fraction cells (**Figure S2**).

Similarly to TEN, the inflamed skin of MPE patients was infiltrated by conventional T lymphocytes (63.8±19.5% of hematopoietic CD45+ cells), and to a lesser extent, by CD14+ monocytes (12.3±8.1%) and NK cells (4.8±5.8%) (**Figure 1, B1**). In contrast to TEN, the CD4+ fraction (51.58±13.2%) dominated over its CD8+ counterpart (17.6%±13.4) (**Figure 1, B2**). Interestingly, such frequencies were comparable to those found in the skin of healthy donors (**Figure 1, C**).

Finally, we detected no major difference in the immunophenotype of cells circulating in the blood of TEN, MPE patients and healthy volunteers, with CD8+ T cells representing approximately 1/4 of total TCR$\alpha\beta$+ cells in all the tested samples (**Figure S3**).

Collectively, our results thus confirm that the blistering and inflamed skin of TEN patients is extensively infiltrated by CD8+ T cells (*20*) (*26*) (*14*). By contrast, no major skewing was recorded for unconventional lymphocytes, NK cells or monocytes, when compared to MPE or healthy individuals.

FlowSOM clusterization of skin CD8+ T cells into 7 phenotypic subsets

As CD8+T cell-mediated cytotoxicity is key in the initiation and formation of drug-induced lesions, we investigated in detail the molecular cytotoxic expression patterns of CD8+ T cells in TEN blisters versus MPE skin. We performed high dimensional profiling and scrutinized the (co-)expression of several cell death-associated molecules (Granulysin, Granzyme B, Granzyme A, Perforin, but also TRAIL (CD253), TWEAK (CD255), Annexin A1, CD107a), as well as different activation markers (CD27, CD38, CD56, CD57, CD137, CD226). Using concatenated CyTOF data from different samples (skin and PBMCs from TEN, MPE but also healthy individuals), we ran FlowSOM, a self-organizing map (SOM) clustering algorithm, to assess the heterogeneity of CD8+ T cell population present in the different patients. FlowSOM first stratified CD8+ T population in 100 nodes. Projected as minimal spanning tree in **Figure 2A & Figure S4**, each SOM node groups cells with similar phenotypes, with the node size representing the number of cells within that node (illustrations of minimal spanning tree obtained for each tissue sample are also shown in **Figures S5-S11**). SOM nodes were next gathered in 4 main clusters, as automatically calculated using K-finder Tree-level approach algorithm. Because K-finder approach did not capture the full diversity of the concatenated population (**data not shown**), we decided to increase the FlowSOM clusterization to 7 distinct clusters. To define the phenotype identity of each cluster, we generated a heatmap showing the integrated median fluorescence intensity (iMFI) values of each marker in each FlowSOM cluster (**Figure 2B**).

Cluster A displayed a phenotypic identity coincident with naïve T cells (characterized by high levels of CD45RA, CCR7 or CD27, and by the lack of classical cytotoxic markers such as Granulysin, Granzyme B, Granzyme A or Perforin), while cluster E, F and G recapitulated T_{EMRA} features (high levels of CD45RA, CD57 and low levels of CCR7), with Granzyme A, Granzyme B, Perforin and Granulysin as main variables between clusters (moderate and high cytotoxicity, respectively for clusters E, F and G, but with no Granulysin expression in cluster F) (**Figure 2B & Figure S12**). Alternatively, clusters B and C both displayed a phenotype of effector memory lymphocytes (T_{EM}; CCR7-, CD45RA-), but conversely to the former, cluster C denoted activated cytotoxic cells, as illustrated by their high level of CD38, Granzyme B and Granulysin expression. Finally, we identified a

last subpopulation (cluster D), which bore some of the hallmarks of central memory T cells (T_{CM}; $CCR7^+$, $CD45RA^-$), and also a substantial expression of CD38, Annexin A1 or CD253 markers (**Figure 2B & Figure S12**).

A polycytotoxic signature typifies lesional CD8+ TEN T cells

In-depth analysis of the frequency of the 7 CD8+ T cell clusters in skin and blood of TEN versus MPE patients and healthy individuals revealed clear phenotypic differences between individuals and samples (**Figure 2C**). Most of the clusters were present in all patient samples, except for clusters D and F found only in a few. A degree of inter-individual variation was found for most clusters. Notably, the activated effector memory subset (cluster C) was consistently elevated in TEN (mean: 55% of infiltrating CD8+ T cells) and to a lesser extent in MPE (mean: 30%) skin samples, relative to healthy (mean: 1%) samples (**Figure 2C**). Unlike the other clusters, cluster C expresses high levels of the cell surface activation marker CD38.

These results thus establish that the major subset of CD8+ T cells infiltrating the skin of TEN patients displays a hallmark CD38+ polycytotoxic effector memory cell phenotype (cluster C).

Restricted TCR Vβ repertoire among TEN CD8+ T cells

Parallel to these studies, we also addressed TCR usage of T cells present in TEN blisters. FACS analysis conducted on 24 of the most common Vbeta (Vβ) chains demonstrated a highly restricted TCRVβ repertoire usage in 12 out of 13 TEN patients tested, with single Vβ expansions ranging from up to 20% to 80% of total TCR-Vβ chains expression (only patient TEN-5 showed no expansion), when compared to healthy donors) (**Figure 3 & Figure S13**). This preferential usage concerned almost exclusively CD8+ (**Figure 3A**) and poorly CD4+ T cells (**Figure 3C**). It concerned quasi all the 24 Vβ chains (with the exception of Vβ5, Vβ5.2, Vβ13.6 (using antibody Vβ nomenclature)), and Vβ3, Vβ7.2, Vβ13.2 and Vβ14 were the most overrepresented Vβ chains, each found in 3-5/13 of TEN patients. TEN-1, TEN-2, TEN-4 and TEN-6 patients showed overexpression of at least 3 TCR-Vβ chains (**Figure 3A**).

In contrast to TEN skin, TCR Vβ expansion were less marked but still significant in CD8+ T cells (but not CD4+ T cells) from TEN PBMCs, with notable biases in TEN-3, -4, -6, -10, -11, -13 and -15 patients (**Figure S14**), while a very limited number of TCR Vβ expansion was detected in cells (CD8+, CD4+ or CD3+) isolated from MPE skin and PBMC samples (**Figures 3B & 3D** and **Figures S15 & S16)**, when compared to healthy individuals (**Figure S13**).

Massive oligoclonal expansion of distinct CDR3 clones in the skin and blood of TEN patients

As FACS cannot catch the full spectrum of the TCR repertoire, we next took advantage of high-throughput sequencing (HTS) of the TCR CDR3 regions (the antigen recognition domains) to evaluate sample clonality. Investigations of TCRBV repertoire first confirmed the preferential usage of the same Vβ chains in TEN blister cells as those observed by FACS (**Tables S3 to S7**). More importantly, the TCR biases in TEN were the result of very limited numbers of CDR3 clonotype expansions, which ranged from >10% to 90% of total TCR sequences for combined top 5 clones (except TEN-2, -8 and -14) (**Figure 4, Tables S4**). Of note, clone-tracking analyses revealed no sharing of identical TCR CDR3 nucleotide (**Figure S17**) or amino acid (**Figure S18**) sequences among the 15 TEN patients, suggesting a lack of public TCR repertoire usage in cells infiltrating TEN induced by different drugs. An interesting exception was noted for one clone from patients TEN-6 and TEN-10, which shared amino acid but not nucleotide sequence (**Figures S17 & S18**). As these patients were exposed respectively to Norfloxacin and Ciprofloxacin quinolones) (**Table 1**), potential epitope cross-reactivity could have lead to the expansion of the same clone.

Importantly, similar TCRBV repertoire analysis (**Figure 4 & Table S6**), and subsequent clonality index measures (which serves to quantify TCR repertoire diversity; **Figure 5**), revealed that in contrast to TEN patients, clonal expansions were rare for MPE patients, and were usually lower than 5%, with the exception of patient MPE-6 with a combined top 5 clone expansion corresponding to approximately 20% of TCR sequences.

Clonotypes that were massively expanded in the TEN skin were also found elevated in the blood of respective patients, at least for the top 5 clones (**Figures S19 & S20, Tables S5 & S7**). This result then indicates that the massive infiltration of unique clonotypes in TEN blisters was likely consecutive to a previous clonal expansion in the lymphoid organs. Only for patient TEN-15, and to a lesser extent for patients TEN-6 and TEN-11, were some of the highly expanded skin clones not represented in the blood (**Figure S18**).

T cell repertoire diversity and clonal expansion of skin clones circulating in blood correlates with TEN severity

TEN severity, assessed here as percent of final skin detachment, varied significantly after patient's arrival to the clinic (**Figure 6A**), and was maximal between 1 to 7 days (mean ±SD = 3.2 ±1.6 days) depending on patients (**Table 1**). We then searched to determine whether correlations existed between clonal expansions in the skin or the blood of TEN patients (measured at days 0-2 after patient's arrival to the clinic) and final skin detachment. While no association was detected with skin clonality indices (R=0.00003, p=NS; **Figure 6B**), by contrast, we observed that patients with the highest PBMC clonality indices presented the highest percentages of final skin detachment (R=0.4, p=0.01; **Figure 6C**). Besides, substantial correlations were also noted with the percentage of top skin

clones circulating in blood, as shown for top 1 (R=0.29, p=0.04; **Figure 6D**) and for the highly expanded clones (i.e. clones represented at a frequency > 0.05% of TCRBV repertoire in each patient; R=0.36, p=0.02; **Table S3 & Figure 6E**).

Combined with the lack of major TCR CDR3 biases recorded in MPE samples (skin or blood) (**Figure 4**), our results thus demonstrate that the massive expansion of unique clonotypes is a major feature of TEN pathology and that the level of expansion of those unique clonotypes among PBMCs is directly related to clinical severity.

Expanded clones match with the polycytotoxic clones over-represented in TEN samples

Thereafter, by taking advantage of mass cytometry, we were able to track back highly expanded clones in the skin and blood of TEN patients to analyze their phenotype. We first demonstrated that CD8+ T cells expressing dominant Vβ chains (FACS analysis) displayed very high levels of Granulysin and CD38 markers, when compared to their non-dominant CD8+Vβ+ T cell counterparts (**Figure 7A**). By superimposing dominant and non-dominant TCRVβ+ markers on our concatenated CD8+ T cell clusters, we next demonstrated that skin dominant TCRVβ+ cells mainly expressed the cytotoxic cluster C phenotype (**Figure 7B**). Conversely, the non-dominant TCRVβ+ cells were detected in all the different clusters.

These data then confirmed that the expanded clones correspond to the polycytotoxic CD8+ T cells that are over-represented in TEN samples.

Expanded clones in both skin and blood are drug-specific

Ultimately, we sought to determine whether highly expanded and activated clones were drug specific. To this end, we FACS sorted dominant CD8+TCRVβ+ T cells present in the blister fluids or the blood of 5 TEN patients (TEN-3,-7,-9,-10,-15), and sequenced their TCRAV repertoire. Results demonstrated that dominant specimens used a principal TCR-Vα+ chain (**Table S8**), despite parallel expression of a defective TCRVA segment (data not shown). Intriguingly, CD8+TCRVβ13.2+ and CD8+TCRVβ22+ cells isolated from patient TEN-9 (and expressed at similar percentages (**Figure 3**)) showed the expression of the same pair of overexpressed Vα chains (TCRVA19-01*01) but with distinct TCRAJ segments (respectively TCVA30-01*01 and TCVA29-01*01). We then subsequently transfected the rearranged V(D)J regions of respective TCRα and TCRβ chains into CD8+ Skw3 cell lines, to force the expression of a unique TCR bearing the cognate α and β chains (**Table S9**). After verification of sustained and stable TCR expression (data not shown), transfectants were restimulated with autologous EBV-transformed B cells pulsed with the culprit drug for 24h. The following day, we measured CD69 expression at the surface of Skw3 cells. Results showed a positive

dose response for TEN-3 with oxypurinol (the metabolite of allopurinol, the culprit drug for TEN-3), but not with the parent drug or an irrelevant drug (sulfamethoxazole) (**Table 2**). A positive response was also recorded for TEN-7 with the culprit pantoprazole, as well as for patient TEN-9 with Rifampicin (but not with all the other drugs taken by this patient) (**Table 2**). Interestingly, Rifampicin was positive for the 4 transfectants generated for TEN-9. Indeed, we generated two transfectants for the respective CD8+TCRVβ13.2+ and CD8+TCRVβ22+ cells, each expressing one of the two different TCRVα chains detected (**Table 2 & Table S9**; transfectants expressing all 4 TCR Vβ and Vα sequences were not tested here). Of note, Ibuprofen induced a false positive response, as it also provided positive reactions with control Skw3 transfectants (**Table 2**). By contrast, we failed to detect CD69+ expression in transfectants generated from patients TEN-10 and TEN-15, and stimulated respectively with Ceftriaxone and Ciprofloxacin or Levofloxacin and Metronidazole (**Table 2**).

DISCUSSION

The main objective of our study was to gain further insight on TEN pathophysiology by tracking immune cells that are present in the skin and the blood of patients at disease onset. Our results confirm that CTLs are the main leucocyte subset found in TEN blisters, followed by a minor infiltration of CD14+ monocytes and NK cells; but we failed to repeatedly detect unconventional cytotoxic lymphocytes such as NKT, MAIT or gamma-delta T cells. Strikingly, deep sequencing of the T cell receptor CDR3 repertoire revealed that there is a massive expansion of unique CD8+ T cell clones in TEN patients (both in skin and blood), which expressed an effector memory phenotype and an elevated level of cytotoxic or inflammatory / activation markers such as Granulysin, Granzymes A & B or CD38. By comparison, TCR repertoire bias and polycytotoxic phenotype were far less marked in MPE patients revealing clear phenotypic differences between the two diseases. By transfecting α and β chains of the expanded clones into immortalized T cells, we succeeded to demonstrate that some of these clones were drug-specific. Importantly, T cell repertoire diversity analysis revealed that clonal expansion of skin clones circulating in the blood of TEN patients correlates with the final clinical severity (as defined by the maximal percentage of skin detachment).

Massive expansion of unique TCR clonotypes in TEN patients

The most striking observation of our study is certainly the demonstration that there is a dramatic expansion of unique polycytotoxic CD8+ T cell clones in TEN patients, which largely outnumbers the frequency of clonotypes expanding in less severe MPE patients. Few studies have already described oligoclonal expansion in TEN (or in the less severe Stevens-Johnson syndrome (SJS)), but such studies mainly focused on *in vitro* T cell (re)activation experiments, or used samples which were isolated from individuals with restricted HLA genotype (for instance HLA-B*15.02 (*4*) (*28*)) and reactive to a limited number of compounds (mainly allopurinol and carbamazepine) (*4, 29*) (*30*) (*28*). All of these studies showed preferential usage of TCRBV subtypes, clonal expansion of specific CDR3 and less TCR diversity, but observations were compared to data obtained from healthy or drug-tolerant donors only. Hence, results were not surprising in as much as antigen-specific T cell expansion obviously deforms TCR repertoires, when compared to homeostasis (*31*). The infiltration of predominant T cell clones has already been reported in many benign inflammatory skin diseases such as psoriasis, atopic dermatitis and contact dermatitis (*32*) (*33*) (and in MPE, as shown in our study (**Figure 5**)). Here, novelty then resides in the demonstration that the strength of clonal expansions reached levels (both in skin and blood) that were only described in skin neoplasic disorders, such as cutaneous T cell lymphomas (CTCLs) (*33*). Additionally, the fact that our results can be generalized to patients expressing highly diverse HLA genotypes and reactive to very different drugs (**Table 1**), thus reinforces the idea that a massive clonal bias is a major immunological hallmark

of TEN disease. Of note, compared to a recent study from Pan et al. (*28*), which showed an expansion of public TCRβ clonotypes in carbamazepine allergic SJS/TEN patients, we failed to detect any public pattern in our cohort.

It will then be crucial to determine in the future the reasons for such clonal expansion in TEN disease compared to less severe MPE. (i) The massive production of inflammatory mediators noticed in the sera and the blister fluid of TEN patients (*14*) (*34*), or the reported defective Treg functions (*35*), certainly participates to enlarge the proliferation of drug-specific cells, but whether it is a consequence, a cause or both remains to clarify. (ii) Alternatively, it could be hypothesized that TEN patients own a drug-specific preimmune repertoire that is prone to considerable enlargement compared to MPE patients. Several preclinical studies have shown that the breadth of immune response strongly depends on the number of specific T cell precursors (*36*). (iii) Another assumption addresses heterologous immunity, and a possible accumulation of pathogenic clones due to cross-reactivity with a reservoir of virus-specific memory T cells (*37*). (iv) Finally, it is still completely unknown whether drug accumulation (due to defective drug detoxification mechanisms (*38*)) predominates within TEN versus MPE skin, fostering continuous T cell stimulation.

Immunophenotype of TCR clonotypes in TEN patients

Another novelty brought by our study is the extended characterization of the expanded clonotypes, which mostly comprises CD8+ T cells endowed with a polycytotoxic phenotype. We observed that the dominant skin TCRVβ+ CTLs mainly expressed the cluster C phenotype, which was assigned to effector memory T cells. As expected (*26*) (*14*), this subset expressed high levels of Granzyme A, Granzyme B and especially Granulysin markers, and it was the sole subset (with cluster D, poorly represented in skin samples) to express the CD38 protein, which is classically associated with T cell activation and/or diapedesis (*39*). By contrast, it lacked the expression of the senescence marker CD57 (classically assigned to T_{EMRA} subsets), indicating that the expanded CTL clones correspond to recently activated T cells.

By comparison, CD8+ T cells infiltrating the skin of MPE or healthy donors displayed a distinct functional phenotype, as shown both at the global population level (**data not shown**) and after multidimensional analysis (**Figure 2**). We notably detected less (MPE) or no (healthy donors) cluster C subset, but more non activated effector memory T cells (cluster B), and a T_{EMRA} subset (cluster E) endowed with moderate expression of cytotoxic markers (when compared to other T_{EMRA} subsets). It is probable than the main differences recorded between TEN and MPE are due to the strong clonotype expansions. It will be interesting to determine in future works whether drug-specific skin MPE T cells are also found in cluster C, as for TEN (*20*) (*26*). Besides, it will be important to uncover whether drug-specific T cells from TEN patients possess unique ability to expand and/or to

differentiate into potent killer cells, when compared to MPE T cells. This difficult task might become feasible with T cell clones generated *in vitro* from precursors collected in TEN and MPE patients allergic to the same molecules.

Drug specificity

A major finding of our study is the antigenic specificity of the highly expanded clones found in TEN patients. Indeed, we were able to demonstrate that several of our engineered transfectants (produced from TEN-3, -7 and -9) responded to their putative culprit drugs *in vitro.* Interestingly, although no clear culprit drug was identified for TEN-9, one of the many putative offending molecules, Rifampicin, responded to the 4 different TCRα/β transfectants we engineered for this patient. However, transfectants generated from sequences identified in patients TEN-10 and TEN-15 failed to respond to the tested drugs (Ceftriaxone, Ciprofloxacin, Levofloxacin, Metronidazole; **Table 2**). Various reasons might explain these TEN-10 and TEN-15 results. The simplest hypothesis is that we did not transfect the appropriate pathogenic TCR sequences. Besides, conversely to the results obtained with TEN-3 transfectants, which confirmed that T cells from allopurinol allergic patients are reactive to its metabolite (oxypurinol), but not to the parent molecule (Chung et al., 2015), it is possible that our *in vitro* drug exposure conditions (during Skw3 / EBV-transformed B cell cultures) did not generate enough metabolites or drug-induced epitopes necessary to activate all transfectants (notably for Ciprofloxaxin, Levofloxacin or Metronidazole). Similarly, we cannot exclude that a specific mode of drug-epitope presentation (using peculiar non-conventional HLA-presentation (*40*)) or the involvement of an altered peptide repertoire (*12*) (*13*), govern T cell expansion from patients TEN-10 or -15. A final hypothesis addresses the immunomodulatory properties of Ceftriaxone, Levofloxacin or Metronidazole (*41*) (*42*) (*43*), which could have inhibited the stimulatory properties of EBV-transformed B cells and hindered the activation of respective transfectants.

Correlation with disease severity

The identification of early biomarkers, which predict final severity, is a highly desirable goal to improve clinical management of TEN patients. Recent work from Xiong et al. suggests that TCR repertoire diversity in patients suffering from SJS or TEN (only 4 TEN patients were included in the study (*29*)) correlates to disease severity. So far, it is still debated whether SJS is an early stage of TEN (SJS is a bullous cADRs characterized by <10% of skin detachment) or a different pathology (both at the etiological and mechanistic levels). Here, we enrolled patients with progressing but established TEN phenotype (with 40-100% of skin detachment at the peak of disease; except for patient TEN-2 who displayed an SJS/TEN intermediate phenotype with 20% of skin detachment). Despite extensive clonal expansion in TEN skin at disease onset, we failed to detect any correlation between skin TCR

repertoire diversity (or the percentage of top skin clones, **data not shown**) and final skin severity (**Figure 6**). However, we observed substantial correlations with the same metrics (TCR repertoire diversity, percentage of highly expanded skin clones) when assessed in PBMCs at disease onset (**Figure 6**), thus expanding findings reported by Xiong et al. (*29*). Hence, to track clonal expansion (or TCR repertoire diversity) could prove of paramount value for clinicians who want to anticipate the evolution of this life-threatening disease, and develop adequate care measures. However, due to the low number of patients (n=15) tested in our TCR repertoire study, it will be crucial to validate these important results with an extended cohort. Besides, it will be important to determine why we failed to detect any correlation with TCR repertoire metrics in the skin. Because of the high diversity of culprit drug and/or drug regimen (**Table 1**), it was impossible to estimate how fast molecules were metabolized/eliminated from patient's skin upon drug discontinuation (after patient's arrival to the clinic). Hence, differences in drug metabolization may have prolonged the number of skin recruited clones, as well as their time of stimulation by keratinocytes or skin dendritic cells, leading to extended/maximal skin damages for certain patients. Alternatively, it is also important to emphasize that TCR repertoire diversity among PBMCs from TEN patients proved not different from that of MPE (**Figure 5**) but also healthy subjects ((**data not shown;** for healthy donor comparison, data were retrieved from Adaptive Biotechnologies project on normal human PBMCs at https://www.adaptivebiotech.com/products-services/immunoseq/immunoseq-analyzer, and from (27)). This indicates that PBMC TCR diversity analysis in itself is not sufficient to discriminate severe from benign diseases and homeostatic condition, and that it must be associated to a comprehensive clinico and immunophenotyping analysis. To monitor the rise and the possible persistence of the pathogenic CTL clones throughout of the progression and the resolution of the disease should brought major improvement to diagnose and treat this life-threatening disease.

In conclusion, our results demonstrate that the quantity and quality of skin-recruited CTLs conditions the clinical presentation of cADRs. Importantly, they open major opportunities for the development of new prognostic markers in TEN.

MATERIALS & METHODS

Study design

Patients were prospectively recruited by the drug allergy reference center at the *Hospices Civils de Lyon* (France) between 2014 and 2018. TEN or MPE diagnoses were based on the definition by the RegiSCAR study group (*44, 45*). Only patients with a probable or a definite diagnosis of TEN or MPE were enrolled in this study. Culprit drugs in TEN patients were determined according to the Algorithm for Drug Causality for Epidermal Necrolysis (ALDEN) (*46*). For MPE patients, the main putative drug was also determined. We collected demographic and clinical information, including sex and age, as well as underlying diseases (*i.e.* the disease the culprit drug was prescribed for), comorbidities, duration of drug exposure before TEN/MPE onset and HLA-A/B genotyping results. HLA-A/B genotypes were determined by reverse PCR-sequence-specific oligonucleotide hybridization (LABType® SSO, One Lambda). Complementary information were also collected for TEN patients: SCORTEN score at diagnosis (*47*) and percentage of skin detachment assessed by *E-Burn®* smartphone application (Android Play store®). The latter was determined when the patient was first diagnosed with TEN ('initial'), and when maximum involvement was observed ('final'). We enrolled 20 healthy subjects as controls.

The study was approved by local ethical committee and written informed consent was obtained from each participant. Given the observational nature of the translational study, there was no randomization or formal blinding process for the investigators.

Sample collection and processing

Skin samples

Skin samples for TEN mainly consisted of blister fluids (all the patients). Supernatant was collected and cells were repeatedly washed in complete RPMI before subsequent processing. In case of MPE and patients TEN-15, -17 and -18, 6-mm^2 biopsies were performed directly into lesional erythematous skin. Abdominal skin leftovers, from healthy subjects undergoing elective plastic surgery, were used as control biopsies. Skin cells were extracted by mechanical dissociation and enzymatic digestion (2 hours at 37°C in RPMI supplemented with collagenase type 1 (1.25 U/mL, Sigma-Aldrich, Saint Quentin Fallavier, France), DNAse (4KU/mL, Sigma-Aldrich) and HEPES buffer (5%)), before to be passed though a 100μm cell strainer (ThermoFischer Scientific, Dardilly, France) to obtain single cell suspensions. Cell viability was determined by trypan blue exclusion.

Blood samples

PBMCs from healthy donors and patients were isolated from whole blood samples (in Lithium-Heparin coated tubes) using Ficoll-histopaque (Ficoll-Paque PLUS®, GE Healthcare Life Sciences®) density gradient centrifugation, and cell viability was assessed as described above.

Details about sampling days for each patient and corresponding investigations are listed in **Table S1**. Depending on experiments, samples were either frozen in liquid nitrogen according to standard procedures, or immediately stained for immunophenotyping analysis.

Flow cytometry analysis

Flow cytometry was carried out using fluorescently labeled mAbs, recognizing human CD3 (7D6; Thermo Fisher Scientific, Les Ulis, France), CD4 (VIT4; Miltenyi biotech, Bergish Glabach, Germany) and CD8 (SK1; Biolegend, San Diego, California, USA) proteins. V-beta (Vβ) chain repertoire expression was assessed using a kit of 24 TCR-Vβ mAbs (IOTest® BetaMark, Beckman Coulter, Roissy, France; which includes approx. 70% of the expressed human TCR Vβ domains: TCR Vβ 1, 2, 3, 4, 5.1, 5.2, 5.3, 7.1, 7.2, 8, 9, 11, 12, 13.1, 13.2, 13.6, 14, 16, 17, 18, 20, 21.3, 22, 23) and viability discrimination was performed by incubating cells with Live/dead eFluor-506 (eBioscience, San Diego, California, USA).

Cells were analyzed on a LSR FORTESSA flow cytometer (BD Biosciences, Franklin Lakes, New Jersey, USA) and data were analyzed using FlowJo software (v10®, Ashland, Oregon, USA).

For TCR sequencing experiments, some dominant CD8+ TCR Vβ+ cells were sorted on a FACSARIA IIu device (BD Biosciences).

Mass cytometry analysis

Mass cytometry antibodies were obtained as pre-conjugated metal-tagged antibodies from Fluidigm (South San Francisco, California, USA) or generated in-house by conjugating unlabeled purified antibodies (from Myltenyi or Beckman Coulter) to isotope-loaded polymers using Maxpar X8 Multi-Metal Labeling Kit (Fluidigm). After titration on Nanodrop ND 1000 (ThermoFischer) antibodies were diluted in antibody stabilization buffer (Candor-Biosciences, Wangen im Allgäu, Germany) with 0.5% sodium azide (Sigma). A detailed list of the antibodies used in this study is provided in supplementary materials (**Table S2**). Cell identification was performed using Irridium-Intercalator (Fluidigm) and viability discrimination was assessed by staining cells with Cisplatin (194Pt, Fluidigm). In some experiments, cells were fixed and permeabilized using Cytofix/Cytoperm solution (Cytofix/Cytoperm™, BD Biosciences, Le Pont de Claix, France) and next intra-cellularly stained with human anti-Granulysin, anti-Granzyme A, anti-Granzyme B, and anti-Perforin mAbs.

Before acquisition on HELIOS mass cytometer (Fluidigm) cells were resuspended in half-diluted Four Element Calibration Beads (Fluidigm), and data set were normalized with Cytof software using Finck

algorithm (*48*). Flow Cytometry Standard (FCS) 3.0 files were imported into FlowJo software v10®, and analyses included standard gating to remove beads, aggregates or dead cells, and further identify main leucocyte subsets (**Figure S1**).

High-dimensional mass cytometry data analysis

An inverse hyperbolic sine transformation was applied to analyze data from rare populations of TCR$\alpha\beta$+ CD8+ T cells per sample (n=300; all CyTOF samples were used (**Table S1**), except skin samples from MPE-9 and -12, which were excluded from the analysis due to very low CD8+ T cell number, and TEN-18 samples due to technical problem). Data were next clustered using FlowSOM algorithm (*49*) (with FlowSOM R pluging downloaded in FlowJo v10). A self-organizing map (SOM) was first trained to gather all cells into 100 distinct nodes based on their similarities in high dimensional space (i.e considering the relative MFI of 16 markers simultaneously: CCR7, CD45RA, CD27, CD38, CD56, CD57, CD107a, CD137, CD226, CD253, CD255, Granzyme A, Granzyme B, Granulysin, Perforin, Annexin A1, and excluding cell-lineage: CD45, CD14, CD19, TCR$\alpha\beta$, TCR$\gamma\delta$, CD8α, CD8β, CD4, CD38, CD56, NKP46, CD11b, CD11c, TCRVα14-Jα18, TCRVα7.2. SOM nodes were subsequently grouped in different clusters (each representing different CD8+T cell subsets) using K-parameter and/or K-Finder R package (*https://arxiv.org/pdf/1811.07356.pdf*) (based on Tracy Widom algorithm to approximate 'K' in sparse data matrices, 'K' being the number of relevant clusters in a population). FlowSOM clusters were visualized as integrated (i.e. including all samples) or disease phenotype minimal spanning trees, and heatmaps showing the integrated or individual MFI of each marker per cluster were generated with FlowJo or Excel. Additional hierarchical metaclusterings were performed, using the gplots R package based on the Euclidean distance and Ward-linkage (*50*), to determine the immunophenotype or the frequency of each cluster per samples.

DNA isolation and high-throughput sequencing of TCRα/β CD3R regions

DNA was isolated from frozen skin and PBMC samples using QIAamp DNA Micro Kit (Qiagen, Courtaboeuf, France), according to manufacturer's instructions. Then, TCRβ and TCRα CDR3 regions were amplified and sequenced using ImmunoSEQ assay (Adaptive Biotechnologies). In brief, bias-controlled V and J gene primers were used to amplify rearranged V(D)J segments spanning each unique CDR3β/α, and amplicons were next sequenced (at approx. 20x coverage) using the Illumina HiSeq platform. The assay was performed at survey level (detection sensitivity: 1 cell in 40,000). After correcting sequencing errors via a clustering algorithm, TCRβ/α V, D and J genes were annotated according to the IMGT database (http://www.imgt.org).

Sequencing data were analyzed according to the ImmunoSEQ Analyzer V.3.0 (*http://www.immunoseq.com*). Diverse TCR repertoire metrics were explored: frequency and overlap of highly expanded clones, respective nucleotide or amino acid CDR3 sequences, usage and pairing of TCRB/AV, TCRBD and TCRB/AJ families or diversity of the TCR repertoire (clonality index based on Shannon's entropy).

Transfection of the Vα- and Vβ-Chains of the TCR into Skw3-CD8 cell lines

Skw3-CD8 cell lines were transfected as described previously (*51*) according to the method of Vollmer et al. (*52*). In brief, rearranged human variable TCR α- and β genes identified by TCR sequencing were amplified by polymerase chain reaction and cloned into expression vectors containing human constant and regulatory TCR sequences. The resulting vectors were cotransfected by electroporation into the TCR-negative Skw3 cell line, which also expresses the human CD8 coreceptor. The TCR-transfected cells outgrowing in selective medium were picked, and the expression of the correct TCR α and β was further assessed by flow cytometry, using a FACS-Canto-I device (BD-Biosciences, San Jose, CA, USA). The transfected cells with stable TCR expression were selected for assessment of reactivity and specificity, which was measured by TCR-induced CD69 expression.

TCR-Transfectant Stimulation Assay

Skw3-CD8 cell lines transfected expressing the correct TCR α and β were cocultured with autologous EBV-transformed B-lymphoblastoid cell lines (*53*) at 1:2 ratio at 37 °C. Tested drugs were added to the cocultures with the indicated concentrations. After 24h, cells were stained with anti-human CD3 (Biolegend, San Diego, CA, USA) and anti-human CD69 (Biolegend) and analyzed by flow cytometry. Increase of CD69 expression was monitored in 10,000 $CD3^+$ events. Experiments were repeated at least 2 times.

Statistical analysis

In all figures, data are presented as mean ± SD. P-values were calculated with two-tailed independent Student's t tests or one-way analysis of variance (ANOVA) using GraphPad Prism software (v8®, San Diego, Californie, USA). P-values < 0.05 were considered significant.

SUPPLEMENTARY MATERIALS

Table S1. Sampling days and subsequent biological analysis.

Table S2. Antibodies and panel information.

Table S3: Raw parameters of TCRBV repertoire analysis.

Table S4: Comparison of the productive frequency of the 5 most common TCR-β clonotypes found in skin TEN samples, and the frequency of respective TCR Vβ chains detected by FACS.

Table S5: Comparison of the productive frequency of the 5 most common TCR-β clonotypes found in BMC TEN samples, and the frequency of respective TCR-Vβ chains detected by FACS.

Table S6: Comparison of the productive frequency of the 5 most common TCR-β clonotypes found in skin MPE samples, and the frequency of respective TCR-Vβ chains detected by FACS.

Table S7: Comparison of the productive frequency of the 5 most common TCR-β clonotypes found in PBMC MPE samples, and the frequency of respective TCR-Vβ chains detected by FACS.

Table S8: Identification of the main TCR-α chains expressed by dominant TCR-Vβ+ cells.

Table S9. Paired TCRα and TCRβ sequences used to generate Skw3 transfectants.

Figure S1. Lineage gating strategy used for supervised analysis of mass cytometry data.

Figure S2. Comparison of the immunophenotypes present in blister or adjacent skin samples.

Figure S3: Immunophenotypes of the leucocytes present in PBMC samples from TEN, MPE or healthy subjects.

Figure S4: Minimal spanning tree magnification. All samples – TEN, MEP, healthy subjects.

Figure S5: Illustrations of minimal spanning trees obtained after FlowSOM analysis of concatenated CD8+ T cell data from TEN, MPE or healthy samples.

Figure S6: Minimal spanning tree magnification. Skin samples – TEN patients.

Figure S7: Minimal spanning tree magnification. PBMC samples – TEN patients.

Figure S8: Minimal spanning tree magnification. Skin samples – MPE patients.

Figure S9: Minimal spanning tree magnification. PBMC samples – MPE patients.

Figure S10: Minimal spanning tree magnification. Skin samples - healthy donors.

Figure S11: Minimal spanning tree magnification. PBMC samples - healthy donors.

Figure S12. FACS illustrations of the concatenated CD8+ T cell immunophenotypes.

Figure S13: TCR Vβ repertoire usage in T cell subsets isolated from the skin and PBMCs of healthy donors.

Figure S14: TCR Vβ repertoire usage in T cell subsets isolated from PBMCs of TEN and MPE patients.

Figure S15: TCR Vβ repertoire usage in T cell subsets isolated from the skin of TEN, MPE or healthy individuals.

Figure S16: TCR Vβ repertoire usage in T cell subsets isolated from the blood of TEN, MPE or healthy individuals.

Figure S17: Clonotype nucleotide sequence overlap between skin and PBMC samples from TEN and MPE patients.

Figure S18: Clonotype amino acid overlap between skin and PBMC samples from TEN and MPE patients.

Figure S19. Frequency and TCRBV usage of the highly expanded TCRβ clonotypes in PBMC samples.

Figure S20: Frequency of the most expanded TCRβ clonotypes in the blood and the skin of TEN and MPE patients.

REFERENCES AND NOTES

1. A. P. Villani *et al.*, Nécrolyse épidermique toxique : physiopathologie et avancées thérapeutiques *Rev Fr Allergol* **57**, 418-425 (2017).
2. T. A. Duong, L. Valeyrie-Allanore, P. Wolkenstein, O. Chosidow, Severe cutaneous adverse reactions to drugs. *Lancet* **390**, 1996-2011 (2017).
3. C. B. Chen *et al.*, An Updated Review of the Molecular Mechanisms in Drug Hypersensitivity. *J Immunol Res* **2018**, 6431694 (2018).
4. W. H. Chung *et al.*, Oxypurinol-Specific T Cells Possess Preferential TCR Clonotypes and Express Granulysin in Allopurinol-Induced Severe Cutaneous Adverse Reactions. *J Invest Dermatol* **135**, 2237-2248 (2015).
5. A. Nassif *et al.*, Toxic epidermal necrolysis: effector cells are drug-specific cytotoxic T cells. *J Allergy Clin Immunol* **114**, 1209-1215 (2004).
6. A. Nassif *et al.*, Drug specific cytotoxic T-cells in the skin lesions of a patient with toxic epidermal necrolysis. *J Invest Dermatol* **118**, 728-733 (2002).
7. J. Adam *et al.*, Abacavir induced T cell reactivity from drug naive individuals shares features of allo-immune responses. *PloS one* **9**, e95339 (2014).
8. W. Hoetzenecker *et al.*, Toxic epidermal necrolysis. *F1000Res* **5**, (2016).
9. W. J. Pichler, D. J. Naisbitt, B. K. Park, Immune pathomechanism of drug hypersensitivity reactions. *The Journal of allergy and clinical immunology* **127**, S74-81 (2011).
10. M. Vocanson, D. J. Naisbitt, J. F. Nicolas, Current perspective of the etiopathogenesis of delayed-type, and T-cell-mediated drug-related skin diseases. *The Journal of allergy and clinical immunology*, (2020).
11. W. J. Pichler, O. Hausmann, Classification of Drug Hypersensitivity into Allergic, p-i, and Pseudo-Allergic Forms. *International archives of allergy and immunology* **171**, 166-179 (2016).
12. P. T. Illing *et al.*, Immune self-reactivity triggered by drug-modified HLA-peptide repertoire. *Nature* **486**, 554-558 (2012).
13. D. A. Ostrov *et al.*, Drug hypersensitivity caused by alteration of the MHC-presented self-peptide repertoire. *Proceedings of the National Academy of Sciences of the United States of America* **109**, 9959-9964 (2012).
14. W. H. Chung *et al.*, Granulysin is a key mediator for disseminated keratinocyte death in Stevens-Johnson syndrome and toxic epidermal necrolysis. *Nature medicine* **14**, 1343-1350 (2008).
15. I. Viard-Leveugle *et al.*, TNF-alpha and IFN-gamma are potential inducers of Fas-mediated keratinocyte apoptosis through activation of inducible nitric oxide synthase in toxic epidermal necrolysis. *J Invest Dermatol* **133**, 489-498 (2013).
16. C. Schlapbach *et al.*, NKp46+ cells express granulysin in multiple cutaneous adverse drug reactions. *Allergy* **66**, 1469-1476 (2011).
17. E. de Araujo *et al.*, Death ligand TRAIL, secreted by CD1a+ and CD14+ cells in blister fluids, is involved in killing keratinocytes in toxic epidermal necrolysis. *Experimental dermatology* **20**, 107-112 (2011).
18. N. Saito *et al.*, An annexin A1-FPR1 interaction contributes to necroptosis of keratinocytes in severe cutaneous adverse drug reactions. *Science translational medicine* **6**, 245ra295 (2014).
19. M. Hertl *et al.*, Predominance of epidermal CD8+ T lymphocytes in bullous cutaneous reactions caused by beta-lactam antibiotics. *J Invest Dermatol* **101**, 794-799 (1993).

20. Y. Hari *et al.*, T cell involvement in cutaneous drug eruptions. *Clinical and experimental allergy : journal of the British Society for Allergy and Clinical Immunology* **31**, 1398-1408 (2001).
21. N. Yawalkar, W. J. Pichler, Pathogenesis of drug-induced exanthema. *International archives of allergy and immunology* **124**, 336-338 (2001).
22. F. Skowron *et al.*, Comparative histological analysis of drug-induced maculopapular exanthema and DRESS. *Journal of the European Academy of Dermatology and Venereology : JEADV* **30**, 2085-2090 (2016).
23. S. Singh *et al.*, Assessment of histopathological features of maculopapular viral exanthem and drug-induced exanthem. *J Cutan Pathol* **44**, 1038-1048 (2017).
24. M. Mockenhaupt, Epidemiology of cutaneous adverse drug reactions. *Allergol Select* **1**, 96-108 (2017).
25. Y. K. Jee, S. Kim, J. M. Lee, H. S. Park, S. H. Kim, CD8(+) T-cell activation by methazolamide causes methazolamide-induced Stevens-Johnson syndrome and toxic epidermal necrolysis. *Clinical and experimental allergy : journal of the British Society for Allergy and Clinical Immunology* **47**, 972-974 (2017).
26. P. C. Kuechler *et al.*, Cytotoxic mechanisms in different forms of T-cell-mediated drug allergies. *Allergy* **59**, 613-622 (2004).
27. J. Dean *et al.*, Annotation of pseudogenic gene segments by massively parallel sequencing of rearranged lymphocyte receptor loci. *Genome Med* **7**, 123 (2015).
28. R. Y. Pan *et al.*, Identification of drug-specific public TCR driving severe cutaneous adverse reactions. *Nat Commun* **10**, 3569 (2019).
29. H. Xiong *et al.*, Comprehensive assessment of T cell receptor beta repertoire in Stevens-Johnson syndrome/toxic epidermal necrolysis patients using high-throughput sequencing. *Mol Immunol* **106**, 170-177 (2019).
30. T. M. Ko *et al.*, Shared and restricted T-cell receptor use is crucial for carbamazepine-induced Stevens-Johnson syndrome. *The Journal of allergy and clinical immunology* **128**, 1266-1276 e1211 (2011).
31. T. Oakes *et al.*, The T Cell Response to the Contact Sensitizer Paraphenylenediamine Is Characterized by a Polyclonal Diverse Repertoire of Antigen-Specific Receptors. *Front Immunol* **8**, 162 (2017).
32. J. L. Harden, D. Hamm, N. Gulati, M. A. Lowes, J. G. Krueger, Deep Sequencing of the T-cell Receptor Repertoire Demonstrates Polyclonal T-cell Infiltrates in Psoriasis. *F1000Res* **4**, 460 (2015).
33. I. R. Kirsch *et al.*, TCR sequencing facilitates diagnosis and identifies mature T cells as the cell of origin in CTCL. *Science translational medicine* **7**, 308ra158 (2015).
34. S. C. Su *et al.*, Interleukin-15 Is Associated with Severity and Mortality in Stevens-Johnson Syndrome/Toxic Epidermal Necrolysis. *J Invest Dermatol* **137**, 1065-1073 (2017).
35. N. Yoshioka *et al.*, Disturbed balance in three subpopulations of CD4(+)Foxp3(+) regulatory T cells in Stevens-Johnson syndrome and toxic epidermal necrolysis patients. *Clinical immunology* **148**, 89-91 (2013).
36. M. K. Jenkins, H. H. Chu, J. B. McLachlan, J. J. Moon, On the composition of the preimmune repertoire of T cells specific for Peptide-major histocompatibility complex ligands. *Annual review of immunology* **28**, 275-294 (2010).
37. C. A. Almeida *et al.*, Virus-specific T-cell clonotypes might contribute to drug hypersensitivity reactions through heterologous immunity. *The Journal of allergy and clinical immunology*, (2019).

38. S. C. Su *et al.*, HLA Alleles and CYP2C9*3 as Predictors of Phenytoin Hypersensitivity in East Asians. *Clin Pharmacol Ther* **105**, 476-485 (2019).
39. S. Deaglio *et al.*, Human CD38 (ADP-ribosyl cyclase) is a counter-receptor of CD31, an Ig superfamily member. *Journal of immunology* **160**, 395-402 (1998).
40. R. J. Betts *et al.*, Contact sensitizers trigger human CD1-autoreactive T-cell responses. *Eur J Immunol* **47**, 1171-1180 (2017).
41. R. Koziel *et al.*, Ciprofloxacin inhibits proliferation and promotes generation of aneuploidy in Jurkat cells. *J Physiol Pharmacol* **61**, 233-239 (2010).
42. E. Becker *et al.*, Doxycycline, metronidazole and isotretinoin: Do they modify microRNA/mRNA expression profiles and function in murine T-cells? *Sci Rep* **6**, 37082 (2016).
43. A. Forsgren, The immunosuppressive effect of cephalosporins and cephalosporin-gentamicin combinations. *The Journal of antimicrobial chemotherapy* **8 Suppl B**, 183-186 (1981).
44. A. Auquier-Dunant *et al.*, Correlations between clinical patterns and causes of erythema multiforme majus, Stevens-Johnson syndrome, and toxic epidermal necrolysis: results of an international prospective study. *Arch Dermatol* **138**, 1019-1024 (2002).
45. S. H. Kardaun *et al.*, Variability in the clinical pattern of cutaneous side-effects of drugs with systemic symptoms: does a DRESS syndrome really exist? *Br J Dermatol* **156**, 609-611 (2007).
46. B. Sassolas *et al.*, ALDEN, an algorithm for assessment of drug causality in Stevens-Johnson Syndrome and toxic epidermal necrolysis: comparison with case-control analysis. *Clin Pharmacol Ther* **88**, 60-68 (2010).
47. S. Bastuji-Garin *et al.*, SCORTEN: a severity-of-illness score for toxic epidermal necrolysis. *J Invest Dermatol* **115**, 149-153 (2000).
48. R. Finck *et al.*, Normalization of mass cytometry data with bead standards. *Cytometry A* **83**, 483-494 (2013).
49. S. Van Gassen *et al.*, FlowSOM: Using self-organizing maps for visualization and interpretation of cytometry data. *Cytometry A* **87**, 636-645 (2015).
50. R. V. Bruggner, B. Bodenmiller, D. L. Dill, R. J. Tibshirani, G. P. Nolan, Automated identification of stratifying signatures in cellular subpopulations. *Proceedings of the National Academy of Sciences of the United States of America* **111**, E2770-2777 (2014).
51. D. A. Schmid, J. P. Depta, M. Luthi, W. J. Pichler, Transfection of drug-specific T-cell receptors into hybridoma cells: tools to monitor drug interaction with T-cell receptors and evaluate cross-reactivity to related compounds. *Mol Pharmacol* **70**, 356-365 (2006).
52. J. Vollmer, H. U. Weltzien, A. Dormoy, F. Pistoor, C. Moulon, Functional expression and analysis of a human HLA-DQ restricted, nickel-reactive T cell receptor in mouse hybridoma cells. *J Invest Dermatol* **113**, 175-181 (1999).
53. C. Segouffin-Cariou, G. Farjot, A. Sergeant, H. Gruffat, Characterization of the epstein-barr virus BRRF1 gene, located between early genes BZLF1 and BRLF1. *J Gen Virol* **81**, 1791-1799 (2000).
54. D. Mauri-Hellweg *et al.*, Activation of drug-specific CD4+ and CD8+ T cells in individuals allergic to sulfonamides, phenytoin, and carbamazepine. *Journal of immunology* **155**, 462-472 (1995).

729 55. D. J. Smith *et al.*, Genetic engineering of hematopoietic stem cells to generate
730 invariant natural killer T cells. *Proceedings of the National Academy of Sciences of*
731 *the United States of America* **112**, 1523-1528 (2015).
732 56. V. Voillet *et al.*, Human MAIT cells exit peripheral tissues and recirculate via
733 lymph in steady state conditions. *JCI insight* **3**, (2018).
734

735

736 **Acknowledgements:** We thank Sébastien Dessurgey and Joris Gutrin (Plateau technique de
737 cytométrie en flux, US8 / UMS3444 SFR BioSciences Gerland - Lyon) for assistance with flow and
738 mass cytometry. We thank Miltenyi biotech France for providing majority of mAbs used in this study.
739

740 **Funding:** This study was supported by French National Research Agency (ANR; SCARS), French
741 Society of Dermatology and French Society of Allergology.
742

743 **Author contributions:** APV, AR, KE, AM, FA, VM, OB, TB, MT, FF, TA, CG, VD and HG carried out
744 cytometry, HLA typing or transfectants experiments and analysis. BB managed the clinical study,
745 performed sample collections and obtained consent. OA and JLM analyzed TCR sequencing data. All
746 authors, and more specifically JLM and OK, participated in the interpretation of the data. DY, JFN, MV
747 designed the experiments and supervised this study. APV, JFN and MV wrote the manuscript. All
748 authors had final approval of the submitted and published version.
749

750 **Conflict of Interest**: The authors declare no competing financial interests. APV, AR, BB, AM, FF, FA,
751 VM, OB, TB, MT, OA, FF, TA, DJ, CG, VD, CG, HG, MP, FLC, AN, OK, JFN and MV are public employees
752 from INSERM or CNRS or Université de Lyon 1 or Hospices Civils de Lyon (France). JLM is a retired
753 former employee of INSERM."KE and DY are public employees of Bern University (Switzerland).
754

755 **Data and materials availability**: All data associated with this study are available in the main text or
756 the supplementary materials. All data and materials used in the analysis will be made available to any
757 reasonable research demands, for purposes of reproducing or extending the analysis.
758

Table legends.

Table 1: Patients demographics, clinical features and HLA genotype.

Alden's algorithm was used to determine culprit drugs for TEN patients. For MPE patients, the main putative drugs are also indicated.

SCORTEN was evaluated at day 0 (arrival at clinic). Disease severity was also appreciated by calculating percentages of skin detachment (using *E-Burn®* application). The peak of disease was appreciated as the date at which TEN patients displayed maximal percentage of skin detachment.

M=Male. F=Female. ENT= Ear Nose Throat. SLE=Systemic lupus erythematosus. HIV+= Human Immunodeficiency virus positive. HCV+= Hepatitis C virus positive, na=not applicable.

* no culprit drug was identified for patient TEN-9, using ALDEN algorithm. The patient received Ibuprofen, Doxycyclin, Sulfamethoxazole-Trimethoprime, Tetracyclin, Isoniazid, Rifampicin in the days before TEN onset.

Table 2. Drug-induced activation of different transfectants. Skw3 cell lines engineered for the expression of TCRs bearing Vα and Vβ chains from some of the top clones found in patients TEN-3,-7,-9,-10 and -15 were stimulated *in vitro* with EBV-transformed B cells in presence of graded doses of different drugs, or left unpulsed. Table 2 depicts the percentage of CD69 expression in CD3+ transfectants measured by FACS after 24h stimulation. Results from control transfectants generated from Abacavir- (17D), Allopurinol- (AnWeA1) or Sulfamethoxazole- (UNO H13) allergic donors (*54*) (*7*) (*51*) are also shown. Red and blue figures indicate >2 or >1.5 CD69 expression fold increase versus unpulsed cultures.

Transfectant ID are from Table S8.

Autologous EBV-transformed B cells were used for all the patients, except for patient TEN-7 who died in between, and for whom we did not have any autologous PBMCs left; hence we performed the same analysis with heterologous PBMCs from 3 different healthy donors. Heterologous EBV-transformed B cells were also used to stimulate control transfectants.

Culprit drugs defined by ALDEN algorithm are the followings: TEN-3=Allopurinol; TEN-7=Pantoprazole; TEN-10= Ceftriaxone or Ciprofloxacin; TEN-15= Levofloxacin or Metronidazole. For patient TEN-9, no culprit drug was defined due to multiple exposures. Oxypurinol is a metabolite of Allopurinol.

Figure legends

Figure 1. Immunophenotypes of the leucocytes present in skin samples from TEN, MPE or healthy subjects. The leucocytes isolated from the skin of 7 subjects with TEN (**A**), 6 subjects with MPE (**B**) and 4 healthy donors (**C**) were analyzed by mass cytometry. Scatter plots depict percentages of conventional TCRαβ+ lymphocytes, gamma delta T cells, B lymphocytes, NK cells, monocytes or conventional dendritic cells in CD45+ hematopoietic cells (**A1-C1**), and percentages of CD8+, CD4+, double negative and double positive T cell subsets, as well as iNKT and MAIT cells in gated TCRαβ+ population (**A2-C2**). Mean frequencies +/- SD are also shown.

Figure 2. High-dimensional cell analysis of CD8+ T cells identifies TEN-enriched immunophenotypes. FlowSOM analysis with automatic consensus clustering was performed on concatenated CD8+ T cell data (300 cells/sample) from both skin and PBMC samples from TEN and MPE patients and healthy donors. (**A**) Results were presented as minimal spanning tree (MST) of 100 nodes gathered in 7 background colored clusters (A, B, C, D, E, F, G). Each node includes phenotypically similar cells and the size of the node indicates the number of cell events. See MST magnification in **Figure S4** to appreciate marker expression in respective SOM nodes. (**B**) Heat map of the integrated MFI of 16 markers across the 7 FlowSOM clusters identified in A. The colour in the heatmap represents the median of the arcsinh for each cluster (centroid) with 0-1 transformed marker expression. Clusters (columns) and markers (rows) were hierarchically metaclustered using Ward's method to group subpopulations with similar phenotype. (**C**) Cluster frequencies were determined for each sample from each subject, to appreciate tissue abundance. Statistics compared frequencies of each cluster in PBMC or skin samples versus the frequency of the respective cluster in healthy donor samples. ns= not significant, *P<0.05, ***P<0.01, Mann-Whitney test (two-tailed).

Figure 3. TCR Vβ repertoire usage in T cell subsets isolated from the lesional skin of TEN and MPE patients. The leucocytes isolated from the lesional skin of 13 subjects with TEN (**A & C**) and 5 subjects with MPE (**B & D**) were analysed by flow cytometry. Histograms depict percentages of 24 TCR Vβ chains in gated CD8+ (**A & B**) and CD4+ (**C & D**) T cell subsets, using the IOTest® Beta Mark TCR Vb Repertoire Kit (TCR-Vβ 1, 2, 3, 4, 5.1, 5.2, 5.3, 7.1, 7.2, 8, 9, 11, 12, 13.1, 13.2, 13.6, 14, 16, 17, 18, 20, 21.3, 22, 23). Each symbol (triangles for TEN, square for MPE) represents a TCR Vβ chain. Highly expanded Vβ subfamilies in respective CD8+ or CD4+ T cell subsets versus healthy individuals are indicated. The red bar represents 3x the mean of respective Vβ chain in healthy individuals (**Figure S13**).

Figure 4. Frequency and TCRBV usage of the highly expanded TCRβ clonotypes. The leucocytes isolated from the lesional skin of 15 subjects with TEN and 7 subjects with MPE were evaluated using HTS of the TCR. Pie charts illustrate frequencies of the 5 most expanded TCRβ clonotypes (measured as % of unique CDR3 sequence among all productive rearrangements within a sample). Colors indicate the respective TCRBV usage of each TCRβ clonotypes. Gray indicates the remaining clonotypes found in the same sample. TCRβ chain amino acid sequences are also provided.

Figure 5. Increased clonality indices in TEN skin but not PBMC samples. The Shannon entropy-based clonality index for total TCR rearrangements was compared in skin (**A**) and PBMC (**B**) samples from 15 patients with TEN and 7 patients with MPE. Exact dates of sample collection are reported in Table S1. Values approaching 1 indicate a highly clonal repertoire in which a small number of rearrangements comprise a large portion of all immune cells. Conversely values approaching 0 indicate a repertoire where every rearrangement was present at an identical frequency. **P<0.01. Student t test (two-tailed).

Figure 6. The percentage of maximal skin detachment in TEN patients correlates with clonality indices and clonal expansion of skin clones in PBMCs. Quantification of skin detachment (expressed as percentage of total body area) in 15 TEN patients was appreciated at their arrival to the clinic (initial) and at the peak of the skin reaction (maximal) (**A**). The latter was compared with the Shannon entropy-based clonality indices determined in skin (**B**) or PBMCs (**C**). Comparisons with the percentages of the top clone (**C**) and the cumulative percentages of the highly expanded clones (HEC) are also provided (**D**). Respective correlation factors were calculated using Pearson correlation method. The coefficient of determination, R^2, and statistical significance are indicated for each correlation. *P<0.05. Student t test (two-tailed).

Figure 7. Immunophenotype of dominant TCRVβ+ cells. The dominant CD8+TCRVβ+ cell subset isolated from the blister fluids of 4 subjects with TEN (TEN-3, 7, -9 and -10) was analyzed for the expression of CD38 and Granulysin, markers by mass cytometry (**A**). Pictures depict representative gating strategy to select the dominant CD8+TCRVβ+ cell subset (**A1**) and histogram overlays of CD38 and Granulysin expression, when compared with non-dominant CD8+TCRVβ (others) or CD4+ T cell counterparts (**A2**). To characterize the phenotypic identity of respective subsets, Cytof data were superimposed on concatenated CD8+ T cell clusters identified in Figure 2. Donut representations depict the frequency of each cluster in dominant and non-dominant CD8+TCRVβ+ cell subsets (**B**).

Of note, as no anti-Vβ3 mAb exists for Cytof, dominant TCRVβ3+ cells in patient TEN-10 (which represent 90% of total CD8+ T cells in skin) were gated by negative selection. We gated cells negative for TCR-Vβ21.3+, -Vβ13.2+ and -Vβ7.2+ expression.

SUPPLEMENTARY MATERIALS

Supplementary table legends

Table S1. Sampling days and subsequent biological analysis. Table describes the days at which samples were collected after patient's arrival to the clinic (all from day 0 to day 2), as well as the corresponding biological investigations performed on these samples.

*Skin and PBMC samples for TCR sequencing were collected as indicated in the table, except for TEN-2 and TEN-14, for which PBMC samples were performed at 1 day of interval.

Table S2. Antibodies and panel information.

Table S3: Raw parameters of TCRBV repertoire analysis.

Genomic DNA extracted from skin (**A**) and PBMC (**B**) samples from 15 TEN and 7 MPE patients were used for survey level deep sequencing of the TCRβ–chain, using ImmunoSEQ™ platform. Data were analyzed using ImmunoSEQ™ analyser toolset. Table describes raw parameters of TCR repertoire analysis.

Total template: the sum of templates for all rearrangements in the sample. Productive templates: the sum of templates for all productive rearrangements in the sample. Fraction productive: the fraction of productive templates among all templates. Productive rearrangement: the count of unique rearrangements in the sample that are in-frame and do not contain a stop codon. Productive rearrangements can produce a functional protein receptor. Number and cumulative percentage of TCRB sequences, representing > 0.5% of total TCRB repertoire.

Table S4: Comparison of the productive frequency of the 5 most common TCR-β clonotypes found in skin TEN samples, and the frequency of respective TCR Vβ chains detected by FACS. Genomic DNA extracted from skin TEN samples were used for survey level deep sequencing of the TCRβ chain, using ImmunoSEQ™ platform. TCRBV repertoire data were compared to the frequency of respective TCR Vβ+ cells detected among CD3+CD8+ T cells by FACS. Of note, the anti-Vβ mAb nomenclature is distinct from the corresponding TCRBV nomenclature. Information for Vβ family, TCRBV, TCRBD, TCRBJ, template number, amino acid and CDR3 rearrangement are also provided.

Vb familly: the identified V Gene Family that contributed to a specific rearrangement. *TCRBV:* a concise string identifying the most specific V Gene family, gene or allele identified during annotation. *TCRBD:* a concise string identifying the most specific D Gene family, gene or allele identified during annotation. *TCRBJ:* a concise string identifying the most specific J Gene family, gene or allele identified during annotation. *Templates:* the total number of templates for a specific rearrangement in the sample. *CDR3 rearrangement:* a particular nucleotide sequence generated through V(D)J recombination. Only productive rearrangements are shown. Productive rearrangements are in-frame, do not contain a stop

codon and can produce a functional protein receptor. *Productive frequency:* the frequency of a specific « productive rearrangement » among all productive rearrangements within a sample, calculated as the templates for a specific rearragement divided by the sum of productive templates for a sample.

Table S5: Comparison of the productive frequency of the 5 most common TCR-β clonotypes found in PBMC TEN samples, and the frequency of respective TCR-Vβ chains detected by FACS. Genomic DNA extracted from PBMC TEN samples were used for survey level deep sequencing of the TCRβ–chain, using ImmunoSEQ™ platform. The TCRBV repertoire and TCR-Vβ FACS analysis is described in the legend of Table S4.

Table S6: Comparison of the productive frequency of the 5 most common TCR-β clonotypes found in skin MPE samples, and the frequency of respective TCR-Vβ chains detected by FACS. Genomic DNA extracted from skin MPE samples were used for survey level deep sequencing of the TCRβ–chain, using ImmunoSEQ™ platform. The TCRBV repertoire and TCR-Vβ FACS analysis is described in the legend of Table S4.

Table S7: Comparison of the productive frequency of the 5 most common TCR-β clonotypes found in PBMC MPE samples, and the frequency of respective TCR-Vβ chains detected by FACS. Genomic DNA extracted from PBMC skin samples were used for survey level deep sequencing of the TCRβ–chain, using ImmunoSEQ™ platform. The TCRBV repertoire and TCR-Vβ FACS analysis is described in the legend of Table S4.

Table S8: Identification of the main TCR-α chains expressed by dominant TCR-Vβ+ cells. Dominant CD8+TCR-Vβ+ cells were FACS sorted from the skin or PBMC samples of patients TEN-3, -7, -9, -10 and -15. Genomic DNA was extracted and used for survey level deep sequencing of the TCRα–chain, using ImmunoSEQ™ platform. Information for Vα family, TCRAV, TCRAJ, template number, amino acid and CDR3 rearrangement and productive frequency are provided, as described in Table S4.

Table S9. Paired TCRα and TCRβ sequences used to generate Skw3 transfectants. Table shows minimal information (Vβ/Vα family, TCRB/AV, TCRB/AD, TCRB/AJ, CDR3 rearrangement) for the TCRα and TCRβ chain rearrangement CDR3 sequences that were transfected in Skw3 cell lines to test drug-specificity of dominant TCR clonotypes from patients TEN-3,-7,-9,-10 and -15. The targeted top clone in paired skin/PBMC heat map scatters is shown, as well as respective transfectant ID.

Supplementary figure legends

Figure S1. Lineage gating strategy used for supervised analysis of mass cytometry data. Representative example of the gating strategy used to identify leucocyte lineages and T cell subpopulations in the skin and PBMC samples from TEN, MPE or healthy subjects. Cells were detected using irridium staining, and doublets and beads were excluded. Live (cisplatin negative (194 Pt)) CD45+ hematopoietic cells were then progressively subcategorized into different subpopulations: monocytes (CD14+), B cells (CD19+), conventional T cells (TCRαβ+), gamma delta T cells (TCRγδ+), NK cells (TCRαβ-TCRγδ-CD56+), conventional dendritic cells (cDC, CD11c+TCRαβ-TCRγδ-CD56-), invariant natural killer cells (iNKT, TCRαβ^{int} TCRVα24+) (*55*), CD4+ T cells (TCRαβ+CD4+), CD8+ T cells (TCRαβ+CD8β+), double positives (DP, TCRαβ+CD4+CD8β+), double negatives (DN, TCRαβ+CD4-CD8β-TCRVα7.2-) and MAIT cells (TCRαβ+CD4-CD8β-CD8α±TCRVα7.2+) (*56*).

Figure S2. Comparison of the immunophenotypes present in blister or adjacent skin samples. The leucocytes isolated from different bullae or adjacent non-bullous inflammatory skin from 3 subjects with TEN (black, red or blue symbols) were analyzed by mass cytometry. Scatter plots depict percentages of conventional TCRαβ+ lymphocytes, gamma delta T cells, B lymphocytes, NK cells, monocytes or conventional dendritic cells in hematopoietic CD45+ cells (**A**) and percentages of CD8+, CD4+, double negative and double positive T cell subsets, as well as iNKT and MAIT cells in gated TCRαβ+ population. Mean frequencies +/- SD are also indicated.

Figure S3: Immunophenotypes of the leucocytes present in PBMC samples from TEN, MPE or healthy subjects. The PBMCs from 7 subjects with TEN (**A**), 6 subjects with MPE (**B**) and 6 healthy donors (**C**) were analyzed by mass cytometry. Scatter plots depict percentages of conventional TCRαβ+ lymphocytes, gamma delta T cells, B lymphocytes, NK cells, monocytes or conventional dendritic cells in hematopoietic CD45+ cells (**A1-C1**), and percentages of CD8+, CD4+, double negative and double positive T cell subsets, as well as iNKT and MAIT cells in gated TCRαβ+ population (**A2-C2**). Mean frequencies +/- SD are also shown.

Figure S4: Minimal spanning tree magnification. All samples – TEN, MEP, healthy subjects. High-dimensional cell analysis using FlowSOM was conducted, as in Figure 2, on concatenated CD8+ T cell data (300 cells/sample) obtained from both skin and PBMC samples from TEN and MPE patients and healthy donors (as reported in **Table S1)**. Minimal spanning tree (with 100 nodes) and automatically subcategorized clusters (clusters A, B, C, D, E, F, G) are depicted. Each node includes phenotypically

similar cells and the size of the node indicates the number of cell events. At the center of each node is represented a star chart. Each colored star branch corresponds to the specific markers (CD45RA, CCR7, Granzyme B (GzB), Granzyme A (GzA), Granulysin (GNLY), Perforin, CD27, CD38, CD56, CD57, CD107a, CD137, CD226, CD253, CD255, Annexin A1) used for phenotypic comparison. The height of each star branch indicates the mean intensity: if the part reaches the border of the circle, the cells have a high expression for the marker.

Figure S5: Illustrations of minimal spanning trees obtained after FlowSOM analysis of concatenated CD8+ T cell data from TEN, MPE or healthy samples. High-dimensional cell analysis using FlowSOM was conducted on concatenated CD8+ T cell data (300 cells/sample) from either skin or PBMC samples from subjects with TEN (**A**), with MPE (**B**) and from healthy donors (**C**), as reported in **Table S1**.

Figure S6: Minimal spanning tree magnification. Skin samples – TEN patients. High-dimensional cell analysis using FlowSOM was conducted, as in Figure S4, on concatenated CD8+ T cell data (300 cells/sample) obtained from TEN skin samples, as reported in **Table S1**.

Figure S7: Minimal spanning tree magnification. PBMC samples – TEN patients. High-dimensional cell analysis using FlowSOM was conducted, as in Figure S4, on concatenated CD8+ T cell data (300 cells/sample) obtained from TEN PBMC samples, as reported in **Table S1**.

Figure S8: Minimal spanning tree magnification. Skin samples – MPE patients. High-dimensional cell analysis using FlowSOM was conducted, as in Figure S4, on concatenated CD8+ T cell data (300 cells/sample) obtained from MPE skin samples, as reported in **Table S1**.

Figure S9: Minimal spanning tree magnification. PBMC samples – MPE patients. High-dimensional cell analysis using FlowSOM was conducted, as in Figure S4, on concatenated CD8+ T cell data (300 cells/sample) obtained from MPE PBMC samples, as reported in **Table S1**.

Figure S10: Minimal spanning tree magnification. Skin samples - healthy donors. High-dimensional cell analysis using FlowSOM was conducted, as in Figure S4, on concatenated CD8+ T cell data (300 cells/sample) obtained from skin samples of healthy donors, as reported in **Table S1**.

Figure S11: Minimal spanning tree magnification. PBMC samples - healthy donors. High-dimensional cell analysis using FlowSOM was conducted, as in Figure S4, on concatenated CD8+ T cell data (300 cells/sample) obtained from skin samples of healthy donors, as reported in **Table S1**.

Figure S12. FACS illustrations of the concatenated CD8+ T cell immunophenotypes. The 7 FlowSOM clusters (A-G) identified by high-dimensional analysis in Figure 2 were displayed for standard FACS plots visualization, using CCR7, CD45RA, Granulysin (GNLY), CD38, CD57, Granzyme A (GzA), CD27 and Granzyme B (GzB) markers.

Figure S13: TCR Vβ repertoire usage in T cell subsets isolated from the skin and PBMCs of healthy donors. The leucocytes isolated from the skin and PBMCs of 12 (HD-9 to HD-20) healthy donors were analysed by flow cytometry. Histograms depict percentages of 24 TCR Vβ chains in gated CD8+ (**A & C**) and CD4+ (**B & D**) T cell subsets, using the IOTest® Beta Mark TCR Vb Repertoire Kit. Each round symbol represents a TCR Vβ chain. The black bar depicts the mean of respective Vβ chain in CD8+ T cells. The red bar illustrates the threshold value (3x the mean of respective Vβ chain) from which TCR Vβ chain from TEN or MPE patients were considered as highly expanded.

Figure S14: TCR Vβ repertoire usage in T cell subsets isolated from PBMCs of TEN and MPE patients. PBMCs from 13 subjects with TEN (**A & C**) and 5 subjects with MPE **(B & D)** were analysed by flow cytometry. Histograms depict percentages of 24 TCR Vβ chains in gated CD8+ (**A & B**) and CD4+ (**C & D**) T cell subsets, using the IOTest® Beta Mark TCR Vb Repertoire Kit. Each symbol (triangles for TEN, square for MPE) represents a TCR Vβ chain. Highly expanded Vβ subfamilies in respective CD8+ or CD4+ T cell subsets versus healthy individuals are indicated. The red bar represents 3x the mean of respective Vβ chain in healthy individuals (**Figure S13**).
TEN-2 (both CD8 and CD4+ T cells; not done) and TEN-15 (CD4+ T cells; technical issue) data are not depicted in the scatter plots.

Figure S15: TCR Vβ repertoire usage in T cell subsets isolated from the skin of TEN, MPE or healthy individuals. The leucocytes isolated from the lesional skin of 13 subjects with TEN (**A**), 5 subjects with MPE (**B**) and 6 healthy indivuals **(C)** were analysed by flow cytometry, as in **Figure 3**. Each symbol (triangles for TEN, square for MPE, rounds for healthy donors) represents a TCR Vβ chain. Highly expanded Vβ subfamilies in respective CD8+ or CD4+ T cell subsets versus healthy individuals are indicated. The red bar represents 3x the mean of respective Vβ chain in healthy individuals (**Figure S13**).

Figure S16: TCR Vβ repertoire usage in T cell subsets isolated from the blood of TEN, MPE or healthy individuals. PBMCs isolated from the blood of 13 subjects with TEN (**A**), 5 subjects with MPE (**B**) and 6 healthy indivuals **(C)** were analysed by flow cytometry, as in **Figure 3**.

Each symbol (triangles for TEN, square for MPE, rounds for healthy donors) represents a TCR Vβ chain. Highly expanded Vβ subfamilies in respective CD8+ or CD4+ T cell subsets versus healthy individuals are indicated. The red bar represents 3x the mean of respective Vβ chain in healthy individuals (**Figure S13**).

TEN-2 (not done) data are not depicted in the scatter plots.

Figure S17: Clonotype nucleotide sequence overlap between skin and PBMC samples from TEN and MPE patients. Morisita-Horn similarity index heatmap depicts overlap metrics (provided by ImmunoSEQ Analyzer V.3.0) for each possible pair-wise percent sharing between all pairs of TEN and MPE samples. This was computed by averaging across the two ratios of shared sequencing reads for each sample. Blue squares illustrate low (<1%) or no reads sharing between samples, white being intermediate and red being the highest level of sharing. Figures at the center of each square indicate percent sharing.

Figure S18: Clonotype amino acid overlap between skin and PBMC samples from TEN and MPE patients. Morisita-Horn similarity index heatmap depicts overlap metrics (provided by ImmunoSEQ Analyzer V.3.0) for each possible pair-wise percent sharing between all pairs of TEN and MPE samples. This was computed by averaging across the two ratios of shared sequencing reads for each sample. Blue squares illustrate low (<1%) or no reads sharing between samples, white being intermediate and red being the highest level of sharing. Figures at the center of each square indicate percent sharing.

Figure S19. Frequency and TCRBV usage of the highly expanded TCRβ clonotypes in PBMC samples. The leucocytes isolated from the PBMCs of 15 subjects with TEN and 5 subjects with MPE were evaluated using HTS of the TCR. Pie charts illustrate frequencies of the 5 most expanded TCRβ clonotypes (measured as % of unique CDR3 sequence among all productive rearrangements within a sample). Colors indicate the respective TCRBV usage of each TCRβ clonotypes. Gray indicates the remaining clonotypes found in the same sample. TCRβ chain amino acid sequences are also provided.

Figure S20: Frequency of the most expanded TCRβ clonotypes in the blood and the skin of TEN and MPE patients. Comparison of TCRβ-chain CDR3 sequences in paired skin and PBMC samples. Each

dot of the heat map scatters represent one clone and the percentage of total reads of this given clone in skin and PBMC samples of TEN or MPE patients. Clones uniquely found in skin samples are located on the x-axis in red, clones uniquely present in PBMCs are located on the y-axis in blue; and clones found in both samples are in violet. Most expanded clones in the blood are shown with an arrow (such clones were used for correlation calculations in Figure 6).

Demographics		Clinical characteristics						HLA genotype	
Patient ID	Sex/Age	Underlying diseases	Comorbidities	Culprit drug	Drug exposure before onset (days)	SCORTEN	% of skin detachment (initial/final)	Locus A	Locus B
TEN-1	M/48	Hyperuricemia	None	Allopurinol	8	3	2/100	A*02 ; A*33	B*38 ; B*58
TEN-2	M/39	Urine tract infection	None	Sulfamethoxazole/Trimethoprim	7	1	6/20	A*30 ; A*30	B*13 ; B*18
TEN-3	F/40	Hyperuricemia	None	Allopurinol	15	2	20/80	A*02 ; A*03	B*27 ; B*58
TEN-4	M/74	Melanoma	Melanoma	Vemurafenib	22	5	30/100	A*03 ; A*23	B*44 ; B*51
TEN-5	M/32	Pneumocystis prophylaxis	HIV+	Sulfamethoxazole/Trimethoprim	15	3	10/80	A*02 ; A*24	B*44 ; B*45
TEN-6	F/83	Urine tract infection	Cardiac insufficiency	Norfloxacin	8	3	20/50	A*03 ; A*-	B*18 ; B*73:01
TEN-7	M/50	Gastritis	Cirrhosis	Pantoprazole	10	3	20/100	A*02 ; A*11	B*15 ; B*44
TEN-8	F/33	Bipolar disease	None	Lamotrigine	12	2	10/40	A*02 ; A*30	B*08 ; B*44
TEN-9	F/34	Chronic pain	None	*	2	3	10/50	A*02 ; A*02	B*15 ; B*53
TEN-10	F/63	Severe angina	None	Ceftriaxione, Ciprofloxacin	8	2	15/30	A*01:03 ; A*68	B*08 ; B*73:01
TEN-11	M/58	Infectious osteoarthritis	Diabetes, renal insufficiency	Ceftriaxone	15	4	10/60	A*02 ; A*29	B*44 ; B*45
TEN-12	F/27	Cirrhosis	Autoimmune hepatitis	Furosemide	21	3	40/40	A*01 ; A*-	B*08 ; B*51
TEN-13	F/75	Post-surgery infection	Bladder adenocarcinoma	Cefixime	4	4	30/30	A*02 ; A*-	B*44 ; B*57
TEN-14	M/41	Myeloma	Myeloma	Revlimid	15	2	5/25	A*02 ; A*02	B*15 ; B*27
TEN-15	F/69	Lung infection	Ischemic stroke, SLE	Levofloxacin, Metronidazole	5	3	10/50	A*03 ; A*30	B*18 ; B*40
TEN-16	F/69	Lung Infection	Lung infection	Pristinamycin	1	2	10/38	A*02 ; A*03	B*35 ; B*51
TEN-17	H/50	Infection	None	Azithromycin, paracetamol	5	4	20/80	A*02 ; A*03	B*07 ; B*51
TEN-18	H/58	Liver cancer	HCV+	Sorafenib	10	5	5/48	A*03 ; A*11	B*35 ; B*40
MPE-1	M/18	ENT infection	None	Amoxicillin	2	na	na	A*01 ; A*02	B*40 ; B*51
MPE-2	M/61	ENT infection	None	Amoxicillin	3	na	na	A*02 ; A*-	B*08 ; B*40
MPE-3	F/68	breast infection	Breast cancer	Vancomycin	28	na	na	A*24 ; A*25	B*15 ; B*18
MPE-4	F/78	Myeloma	Myeloma	Bortezomid	5	na	na	A*29 ; A*31	B*35 ; B*44
MPE-5	F/71	Cardiac insufficiency	Cardiac insufficiency	Diltiazem	15	na	na	A*02 ; A*-	B*51 ; B*-
MPE-6	F/62	Infectious osteoarthritis	None	Vancomycin	2	na	na	A*01 ; A*02	B*40 ; B*57
MPE-7	M/61	Pulmonary infection	None	Vancomycin	42	na	na	A*02 ; A*32	B*49 ; B*51
MPE-8	F/24	Chronic pain	None	Ibuprofen	9	na	na	A*24 ; A*-	B*15 ; B*38
MPE-9	F/94	Urine tract infection	None	Clindamycin	3	na	na	A*23 ; A*31	B*39 ; B49
MPE-10	F/62	Graft versus Host Disease	Bone marrow transplant	Tazocillin, contrast material	1-2	na	na	A*02 ; A*03	B*15:16 ; B*39
MPE-11	F/39	Hypertension	SLE	Macrogol, Urapidil, Amlodipine	14	na	na	A*32 ; A*34	B*39 ; B*44
MPE-12	F/62	Hypertension, Gout	Hypertension, Gout	Allopurinol, Fibrate	28	na	na	A*23 ; A*68	B*44 ; B53
MPE-13	H/52	Myeloma	Myeloma	Revlimid, Bortezomid	15	na	na	A*01 ; A*02	B*07 ; B*51
MPE-14	F/67	Dermatomyositis	Dermatomyositis	Hydroxychloroquine	15	na	na	A*01 ; A*29	B*08 ; B*44

Table 1

Patient ID	SKW3 transfectant ID	Drug concentrations (µg/ml))	% of CD69 expression		
			No drug	Concentration 1	Concentration 2
TEN-3	C1	Allopurinol (62.5 / 250)	2.34		2.24
		Oxypurinol (62.5 / 250)	2.34		**22.91**
		Sulfamethoxazole (100 / 200)	2.34		1.29
TEN-7	C2	Pantoprazole (50)	31.4		
		Pantoprazole (5 / 20 / 50)			
	C3	Ibuprofen (20 / 100 / 200)	8.5	7.4	8.3
		Sulfamethoxazole (100 / 200)	8.77		7.82
		Rifampicin (50 / 100)	8.77		5.98
		Isoniazid (10 / 50)	8.7		9.11
		Doxycyclin (5 / 10 / 20)	8.5	10.1	9.5
		Tetracyclin (10 / 50 / 100)	8.5	7.4	7.1
	C4	Sulfamethoxazole (100 / 200)	1.02		1
		Rifampicin (50 / 100)	1.02		0.54
		Isoniazid (10 / 50)	1.02		0.7
TEN-9	C5	Ibuprofen (20 / 100 / 200)	13.88	12.9	13.2
		Ibuprofen (50 / 100)	3.5		**4.45**
		Sulfamethoxazole (50 / 100)	3.5		2.46
		Trimethoprim (10 / 50)	3.5		1.75
		Rifampicin (10 / 50)	2.78		3.39
		Doxycyclin (5 / 10 / 20)	13.88	15.8	15.6
		Tetracyclin (10 / 50 / 100)	13.88	15.5	**21.2**
		Tetracyclin (10 / 50)	2.78		3.17
	C6	Ibuprofen (50 / 100)	3.74		5.92
		Sulfamethoxazole (50 / 100)	3.74		3.62
		Rifampicin (10 / 50)	3.74		4.83
		Trimethoprim (10 / 50)	3.74		2.88
		Tetracyclin (10 / 50)	3.74		2.88
TEN-10	C7	Ceftriaxone (25 / 50 / 100)	2.34	3.43	**3.94**
	C8	Ceftriaxone (50 / 100 / 200)	12.22	11.87	11,99
		Ciprofloxacin (12.5 / 25 / 50)	10.92	10.06	11,76
TEN-15	C9	Levofloxacin (25 / 50 / 100)	5,99	5.63	5,42
		Metronidazole (25 / 50 / 100)	6.26	5.66	5,42
Control-1	17D	Abacavir (1 / 10 / 20)	1.43	**93.2**	**88.9**
		Pantoprazole (12.5 / 25 / 50)	1.43	1.81	1.77
Control-2	AnWe A1	Allopurinol (62.5 / 250)	4.31		**17.07**
		Oxypurinol (62.5 / 250)	4.31		5.03
Control-3	UNO H13	Ibuprofen (20 / 100 / 200)	5.2	4.6	**10.5**

Table 2

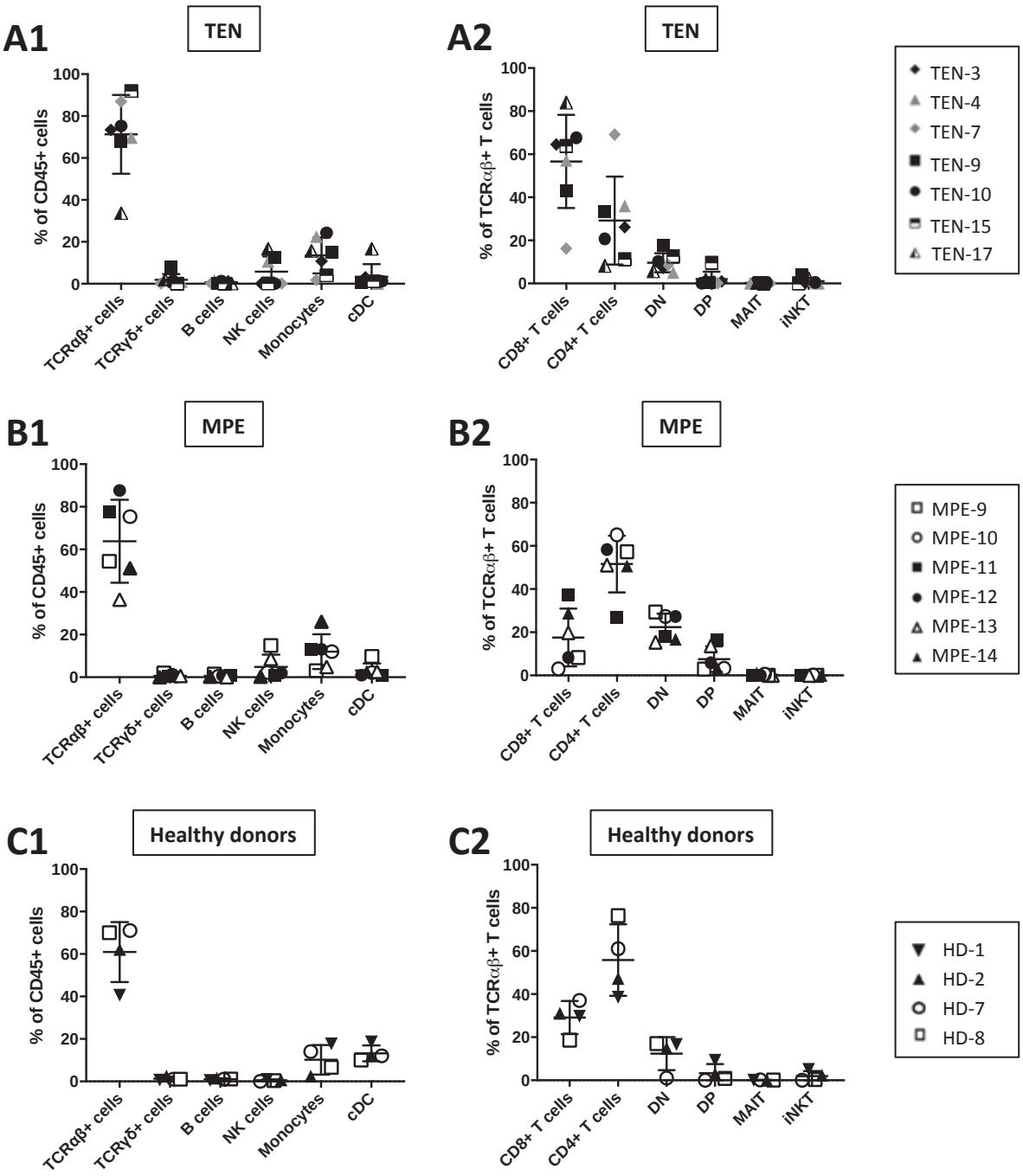
A1
TEN
% of CD45+ cells
TCRαβ+ cells
TCRγδ+ cells
B cells
NK cells
Monocytes
cDC
A2
TEN
% of TCRαβ+ T cells
CD8+ T cells
CD4+ T cells
DN
DP
MAIT
iNKT
TEN-3
TEN-4
TEN-7
TEN-9
TEN-10
TEN-15
TEN-17
B1
MPE
B2
MPE
MPE-9
MPE-10
MPE-11
MPE-12
MPE-13
MPE-14
C1
Healthy donors
C2
Healthy donors
HD-1
HD-2
HD-7
HD-8

Figure 1

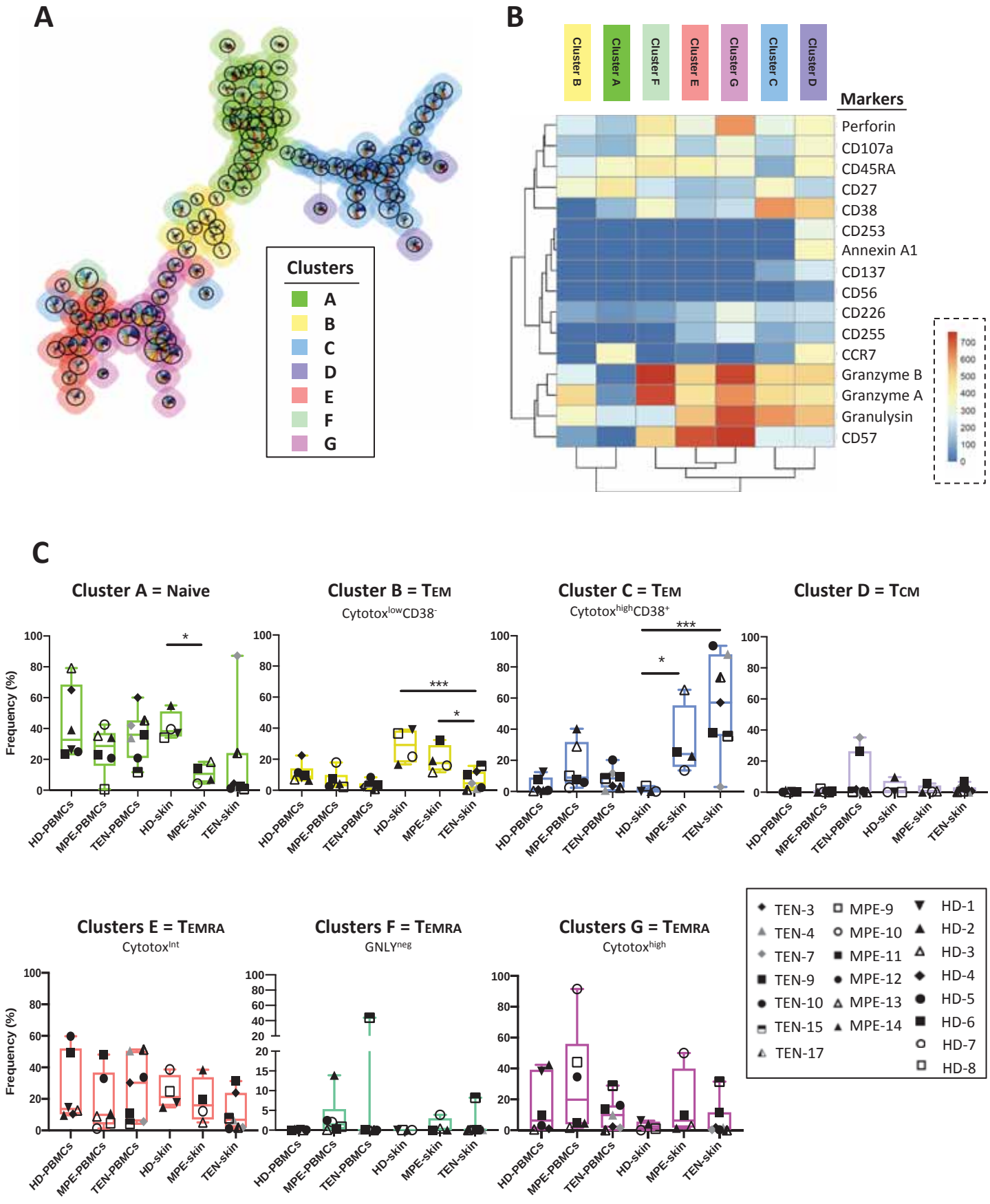
A
Clusters
A
B
C
D
E
F
G
B
Cluster B
Cluster A
Cluster F
Cluster E
Cluster G
Cluster C
Cluster D
Markers
Perforin
CD107a
CD45RA
CD27
CD38
CD253
Annexin A1
CD137
CD56
CD226
CD255
CCR7
Granzyme B
Granzyme A
Granulysin
CD57
700
600
500
400
300
200
100
0
C
Cluster A = Naive
Cluster B = TEM
Cytotox^low CD38^-
Cluster C = TEM
Cytotox^high CD38^+
Cluster D = TCM
Frequency (%)
HD-PBMCs
MPE-PBMCs
TEN-PBMCs
HD-skin
MPE-skin
TEN-skin
Clusters E = TEMRA
Cytotox^Int
Clusters F = TEMRA
GNLY^neg
Clusters G = TEMRA
Cytotox^high
TEN-3
TEN-4
TEN-7
TEN-9
TEN-10
TEN-15
TEN-17
MPE-9
MPE-10
MPE-11
MPE-12
MPE-13
MPE-14
HD-1
HD-2
HD-3
HD-4
HD-5
HD-6
HD-7
HD-8

Figure 2

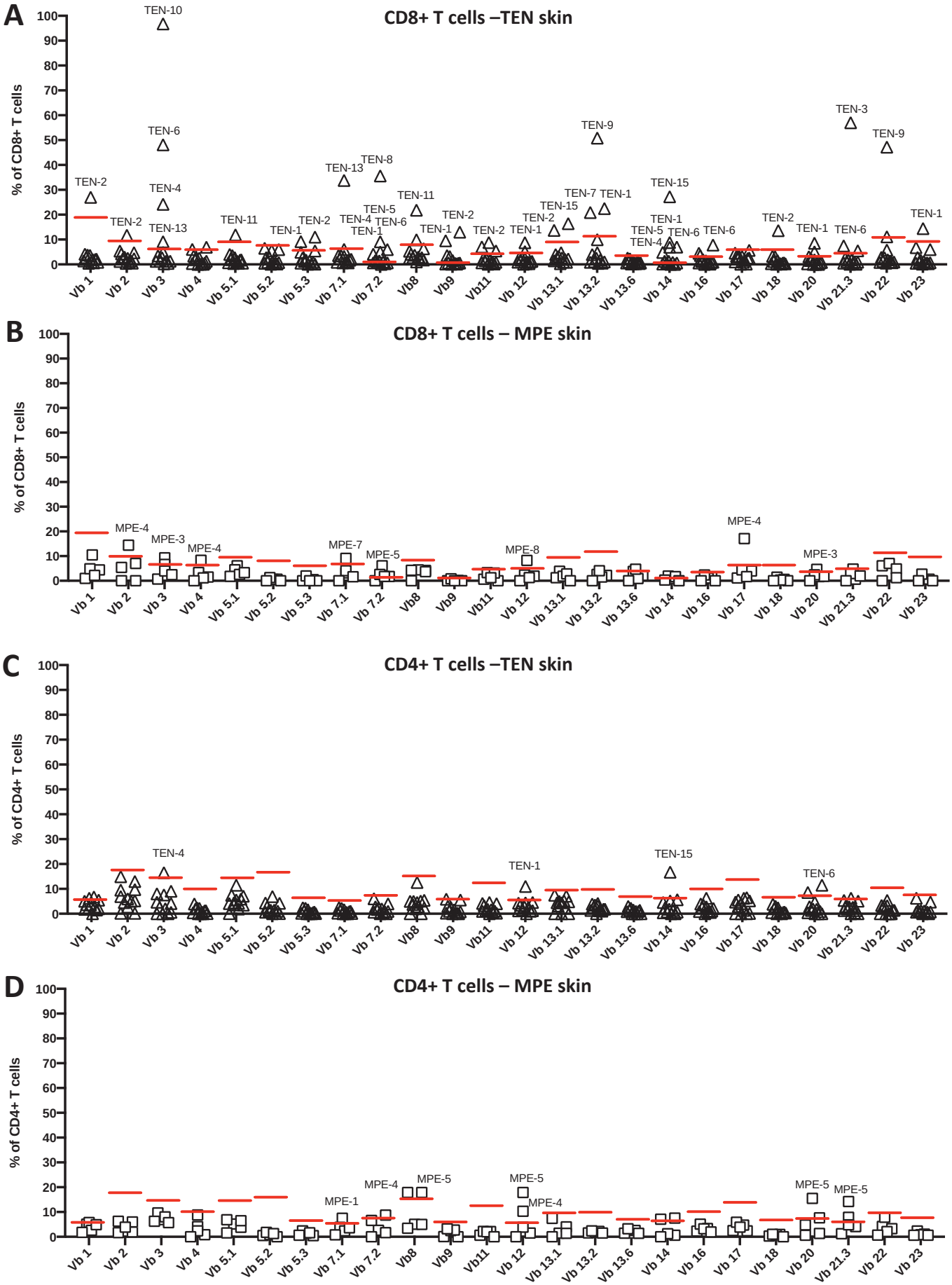
A
CD8+ T cells –TEN skin
% of CD8+ T cells
B
CD8+ T cells – MPE skin
% of CD8+ T cells
C
CD4+ T cells –TEN skin
% of CD4+ T cells
D
CD4+ T cells – MPE skin
% of CD4+ T cells
Vb 1
Vb 2
Vb 3
Vb 4
Vb 5.1
Vb 5.2
Vb 5.3
Vb 7.1
Vb 7.2
Vb8
Vb9
Vb11
Vb 12
Vb 13.1
Vb 13.2
Vb 13.6
Vb 14
Vb 16
Vb 17
Vb 18
Vb 20
Vb 21.3
Vb 22
Vb 23

Figure 3

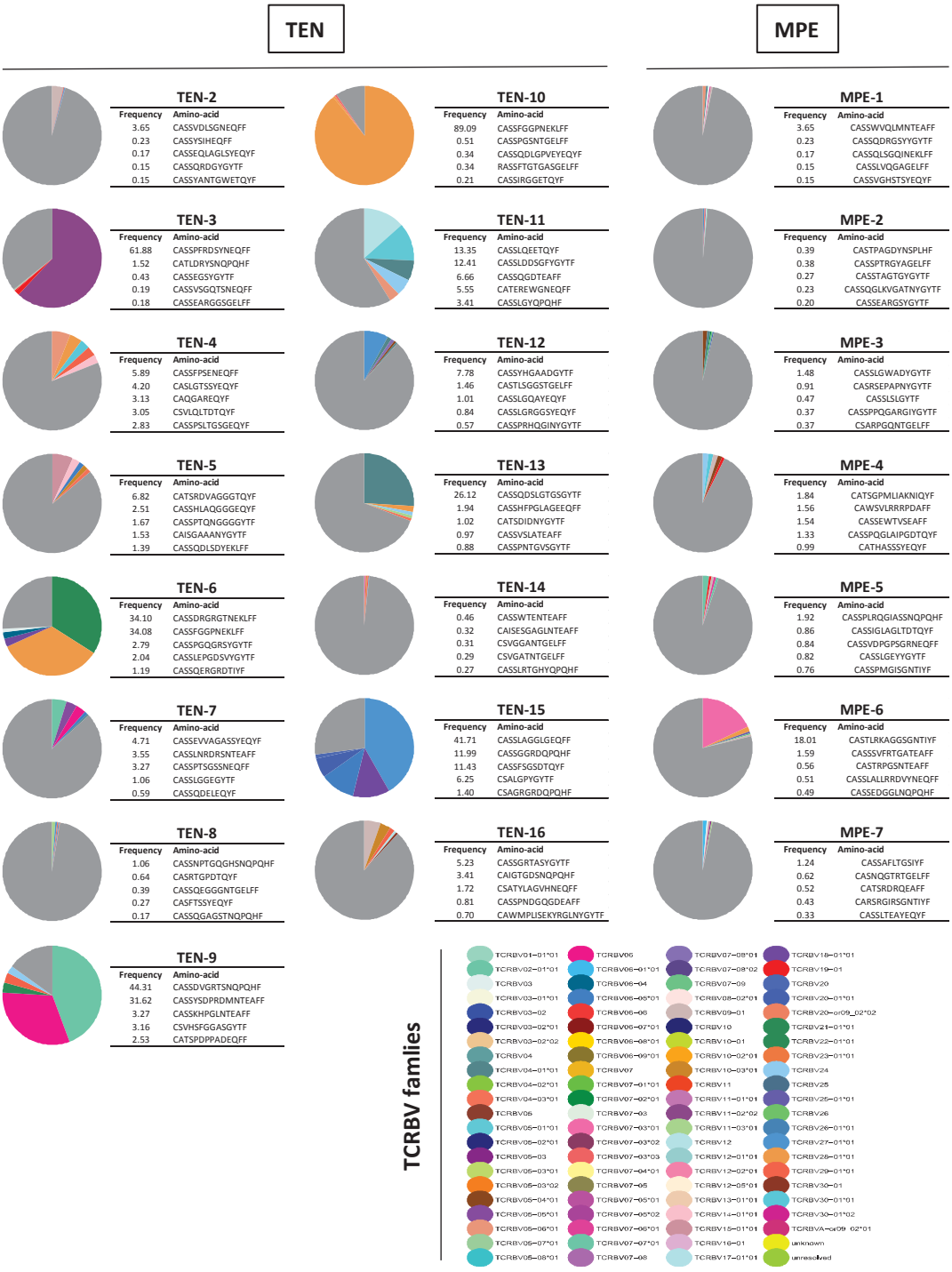
TEN
MPE
TEN-2
Frequency Amino-acid
3.65 CASSVDLSGNEQFF
0.23 CASSYSIHEQFF
0.17 CASSEQLAGLSYEQYF
0.15 CASSQRDGYGYTF
0.15 CASSYANTGWETQYF
TEN-10
Frequency Amino-acid
89.09 CASSFGGPNEKLFF
0.51 CASSPGSNTGELFF
0.34 CASSQDLGPVEYEQYF
0.34 RASSFTGTGASGELFF
0.21 CASSIRGGETQYF
MPE-1
Frequency Amino-acid
3.65 CASSWVQLMNTEAFF
0.23 CASSQDRGSYYGYTF
0.17 CASSQLSGQINEKLFF
0.15 CASSLVQGAGELFF
0.15 CASSVGHSTSYEQYF
TEN-3
Frequency Amino-acid
61.88 CASSPFRDSYNEQFF
1.52 CATLDRYSNQPQHF
0.43 CASSEGSYGYTF
0.19 CASSVSGQTSNEQFF
0.18 CASSEARGGSGELFF
TEN-11
Frequency Amino-acid
13.35 CASSLQEETQYF
12.41 CASSLDDSGFYGYTF
6.66 CASSQGDTEAFF
5.55 CATEREWGNEQFF
3.41 CASSLGYQPQHF
MPE-2
Frequency Amino-acid
0.39 CASTPAGDYNSPLHF
0.38 CASSPTRGYAGELFF
0.27 CASSTAGTGYGYTF
0.23 CASSQGLKVGATNYGYTF
0.20 CASSEARGSYGYTF
TEN-4
Frequency Amino-acid
5.89 CASSFPSENEQFF
4.20 CASLGTSSYEQYF
3.13 CAQGAREQYF
3.05 CSVLQLTDTQYF
2.83 CASSPSLTGSGEQYF
TEN-12
Frequency Amino-acid
7.78 CASSYHGAADGYTF
1.46 CASTLSGGSTGELFF
1.01 CASSLGQAYEQYF
0.84 CASSLGRGGSYEQYF
0.57 CASSPRHQGINYGYTF
MPE-3
Frequency Amino-acid
1.48 CASSLGWADYGYTF
0.91 CASRSEPAPNYGYTF
0.47 CASSLSLGYTF
0.37 CASSPPQGARGIYGYTF
0.37 CSARPGQNTGELFF
TEN-5
Frequency Amino-acid
6.82 CATSRDVAGGGTQYF
2.51 CASSHLAQGGGEQYF
1.67 CASSPTQNGGGGYTF
1.53 CAISGAAANYGYTF
1.39 CASSQDLSDYEKLFF
TEN-13
Frequency Amino-acid
26.12 CASSQDSLGTGSGYTF
1.94 CASSHFPGLAGEEQFF
1.02 CATSDIDNYGYTF
0.97 CASSVSLATEAFF
0.88 CASSPNTGVSGYTF
MPE-4
Frequency Amino-acid
1.84 CATSGPMLIAKNIQYF
1.56 CAWSVLRRRPDAFF
1.54 CASSEWTVSEAFF
1.33 CASSPQGLAIPGDTQYF
0.99 CATHASSSYEQYF
TEN-6
Frequency Amino-acid
34.10 CASSDRGRGTNEKLFF
34.08 CASSFGGPNEKLFF
2.79 CASSPGQGRSYGYTF
2.04 CASSLEPGDSVYGYTF
1.19 CASSQERGRDTIYF
TEN-14
Frequency Amino-acid
0.46 CASSWTENTEAFF
0.32 CAISESGAGLNTEAFF
0.31 CSVGGANTGELFF
0.29 CSVGATNTGELFF
0.27 CASSLRTGHYQPQHF
MPE-5
Frequency Amino-acid
1.92 CASSPLRQGIASSNQPQHF
0.86 CASSIGLAGLTDTQYF
0.84 CASSVDPGPSGRNEQFF
0.82 CASSLGEYYGYTF
0.76 CASSPMGISGNTIYF
TEN-7
Frequency Amino-acid
4.71 CASSEVVAGASSYEQYF
3.55 CASSLNRDRSNTEAFF
3.27 CASSPTSGSSNEQFF
1.06 CASSLGGEGYTF
0.59 CASSQDELEQYF
TEN-15
Frequency Amino-acid
41.71 CASSLAGGLGEQFF
11.99 CASSGGRDQPQHF
11.43 CASSFSGSDTQYF
6.25 CSALGPYGYTF
1.40 CSAGRGRDQPQHF
MPE-6
Frequency Amino-acid
18.01 CASTLRKAGGSGNTIYF
1.59 CASSSVFRTGATEAFF
0.56 CASTRPGSNTEAFF
0.51 CASSLALLRRDVYNEQFF
0.49 CASSEDGGLNQPQHF
TEN-8
Frequency Amino-acid
1.06 CASSNPTGQGHSNQPQHF
0.64 CASRTGPDTQYF
0.39 CASSQEGGGNTGELFF
0.27 CASFTSSYEQYF
0.17 CASSQGAGSTNQPQHF
TEN-16
Frequency Amino-acid
5.23 CASSGRTASYGYTF
3.41 CAIGTGDSNQPQHF
1.72 CSATYLAGVHNEQFF
0.81 CASSPNDGQGDEAFF
0.70 CAWMPLISEKYRGLNYGYTF
MPE-7
Frequency Amino-acid
1.24 CASSAFLTGSIYF
0.62 CASNQGTRTGELFF
0.52 CATSRDRQEAFF
0.43 CARSRGIRSGNTIYF
0.33 CASSLTEAYEQYF
TEN-9
Frequency Amino-acid
44.31 CASSDVGRTSNQPQHF
31.62 CASSYSDPRDMNTEAFF
3.27 CASSKHPGLNTEAFF
3.16 CSVHSFGGASGYTF
2.53 CATSPDPPADEQFF
TCRBV famlies
TCRBV01–01*01
TCRBV02–01*01
TCRBV03
TCRBV03–01*01
TCRBV03–02
TCRBV03–02*01
TCRBV03–02*02
TCRBV04
TCRBV04–01*01
TCRBV04–02*01
TCRBV04–03*01
TCRBV05
TCRBV05–01*01
TCRBV05–02*01
TCRBV05–03
TCRBV05–03*01
TCRBV05–03*02
TCRBV05–04*01
TCRBV05–05*01
TCRBV05–06*01
TCRBV05–07*01
TCRBV05–08*01
TCRBV06
TCRBV06–01*01
TCRBV06–04
TCRBV06–05*01
TCRBV06–06
TCRBV06–07*01
TCRBV06–08*01
TCRBV06–09*01
TCRBV07
TCRBV07–01*01
TCRBV07–02*01
TCRBV07–03
TCRBV07–03*01
TCRBV07–03*02
TCRBV07–03*03
TCRBV07–04*01
TCRBV07–05
TCRBV07–05*01
TCRBV07–05*02
TCRBV07–06*01
TCRBV07–07*01
TCRBV07–08
TCRBV07–08*01
TCRBV07–08*02
TCRBV07–09
TCRBV08–02*01
TCRBV09–01
TCRBV10
TCRBV10–01
TCRBV10–02*01
TCRBV10–03*01
TCRBV11
TCRBV11–01*01
TCRBV11–02*02
TCRBV11–03*01
TCRBV12
TCRBV12–01*01
TCRBV12–02*01
TCRBV12–05*01
TCRBV13–01*01
TCRBV14–01*01
TCRBV15–01*01
TCRBV16–01
TCRBV17–01*01
TCRBV18–01*01
TCRBV19–01
TCRBV20
TCRBV20–01*01
TCRBV20–or09_02*02
TCRBV21–01*01
TCRBV22–01*01
TCRBV23–01*01
TCRBV24
TCRBV25
TCRBV25–01*01
TCRBV26
TCRBV26–01*01
TCRBV27–01*01
TCRBV28–01*01
TCRBV29–01*01
TCRBV30–01
TCRBV30–01*01
TCRBV30–01*02
TCRBVA–or09_02*01
unknown
unresolved

Figure 4

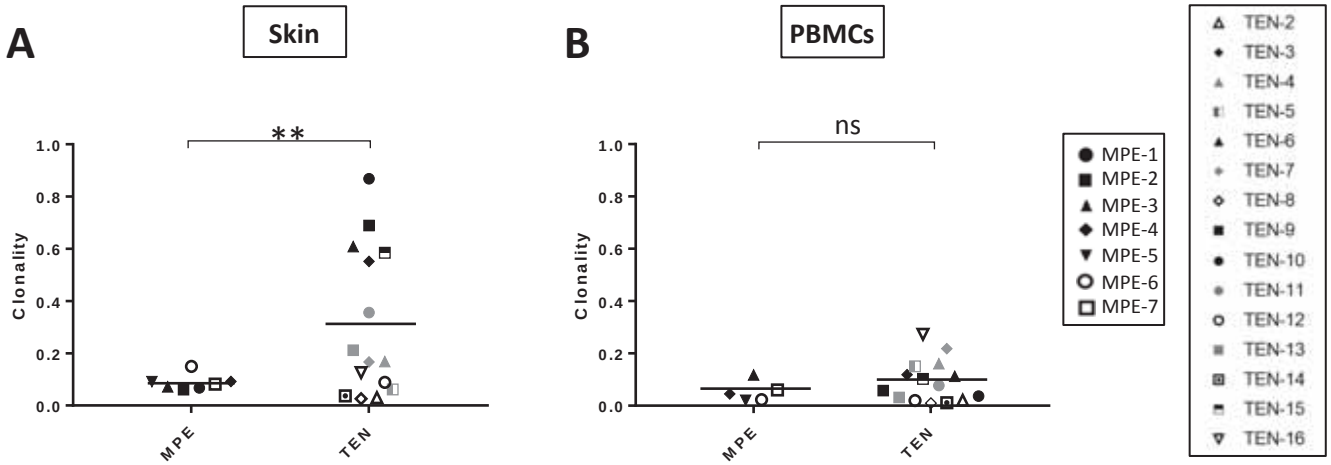
A
Skin
**
Clonality
1.0
0.8
0.6
0.4
0.2
0.0
MPE
TEN
B
PBMCs
ns
Clonality
1.0
0.8
0.6
0.4
0.2
0.0
MPE
TEN
MPE-1
MPE-2
MPE-3
MPE-4
MPE-5
MPE-6
MPE-7
TEN-2
TEN-3
TEN-4
TEN-5
TEN-6
TEN-7
TEN-8
TEN-9
TEN-10
TEN-11
TEN-12
TEN-13
TEN-14
TEN-15
TEN-16

Figure 5

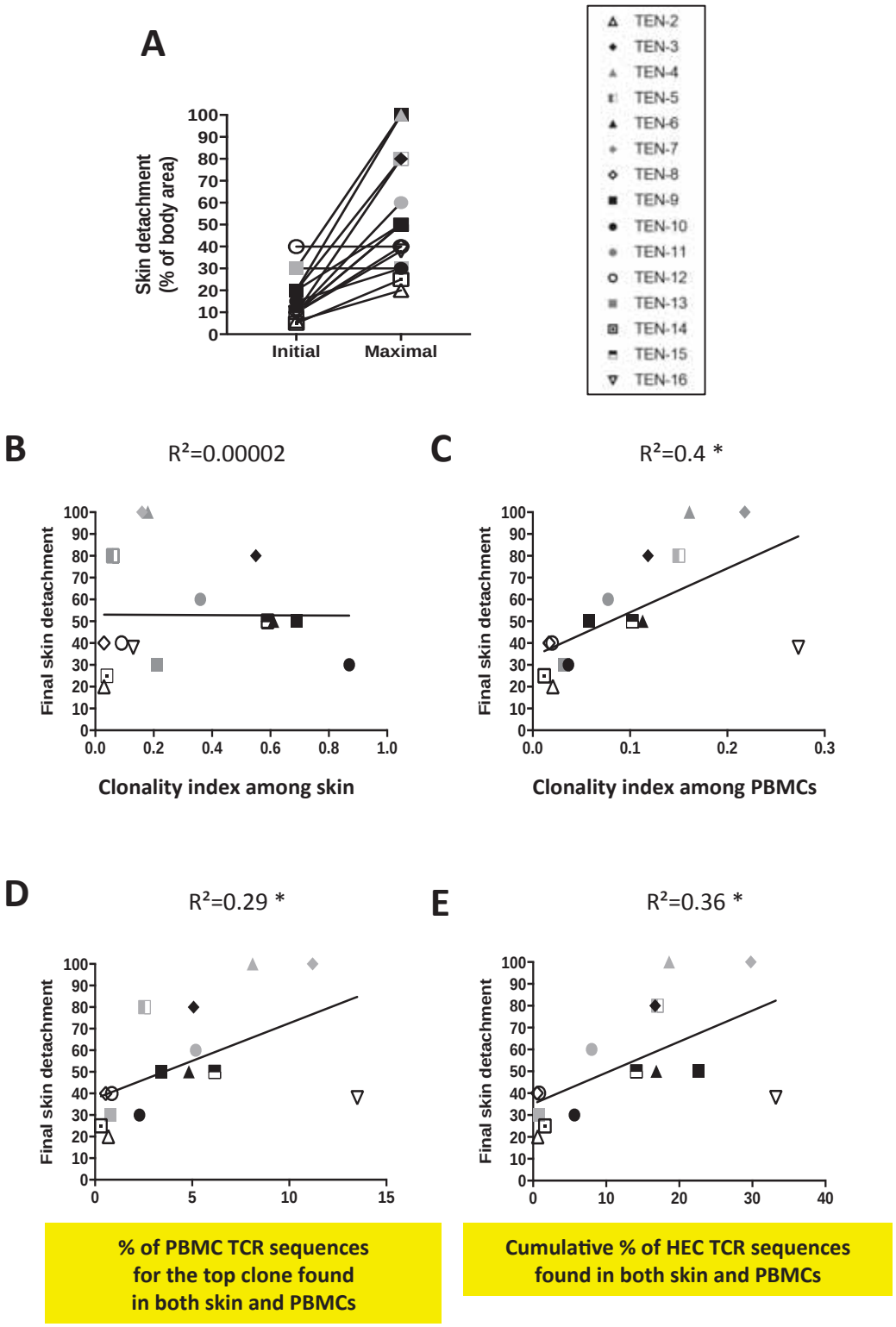
A
Skin detachment (% of body area)
Initial
Maximal
TEN-2
TEN-3
TEN-4
TEN-5
TEN-6
TEN-7
TEN-8
TEN-9
TEN-10
TEN-11
TEN-12
TEN-13
TEN-14
TEN-15
TEN-16
B
R²=0.00002
Final skin detachment
Clonality index among skin
C
R²=0.4 *
Final skin detachment
Clonality index among PBMCs
D
R²=0.29 *
Final skin detachment
% of PBMC TCR sequences for the top clone found in both skin and PBMCs
E
R²=0.36 *
Final skin detachment
Cumulative % of HEC TCR sequences found in both skin and PBMCs

Figure 6

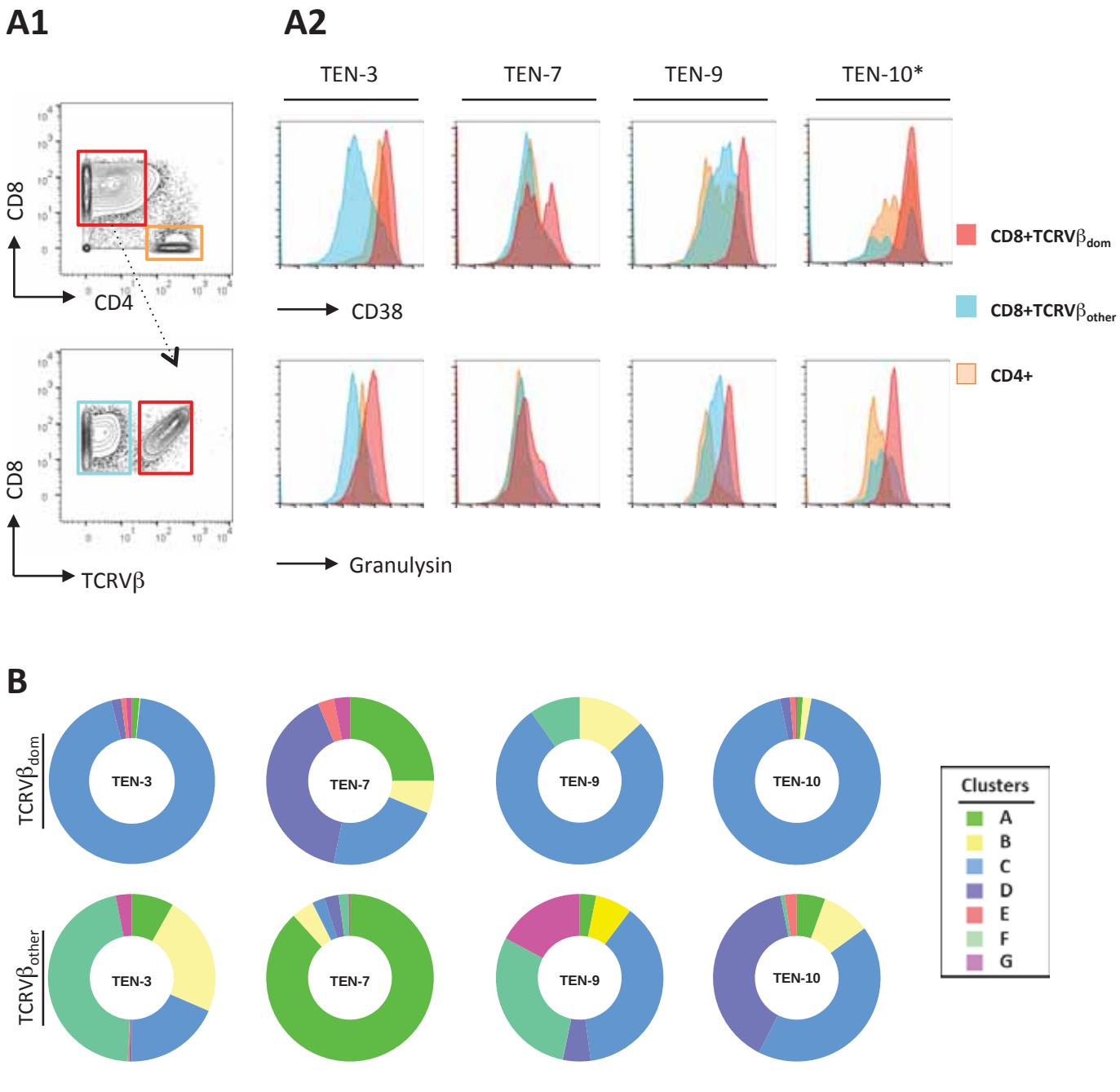
A1
A2
CD8
CD4
CD8
TCRVβ
TEN-3
TEN-7
TEN-9
TEN-10*
CD38
Granulysin
CD8+TCRVβdom
CD8+TCRVβother
CD4+
B
TCRVβdom
TCRVβother
TEN-3
TEN-7
TEN-9
TEN-10
Clusters
A
B
C
D
E
F
G

Figure 7

Biological investigations

	CyTOF	TCRVβ	TCR sequencing	TCR transfectant stimulation assay
TEN-1		D1	-	-
TEN-2	-	D1	D0*	-
TEN-3	D1	D1	D0	D2
TEN-4	D1	D1	D0	-
TEN-5		D1	D0	-
TEN-6	-	D1	D0	-
TEN-7	D1	D0	D1	D2
TEN-8	-	D0	D0	-
TEN-9	D2	D1	D1	D0 & D1
TEN-10	D2	D1	D0	D0 & D2
TEN-11	-	D1	D2	
TEN-12	-	-	D0	-
TEN-13	-	D1	D2	-
TEN-14	-	-	D1*	-
TEN-15	D1	D1	D1	D1
TEN-16	D1	-	D1	-
TEN-17	D0	D0	-	-
TEN-18	D0	-	-	
MPE-1	-	-	D1	-
MPE-2	-	-	D1	-
MPE-3	-	D1	D1	-
MPE-4	-	D1	D1	-
MPE-5	-	D1	D1	-
MPE-6	-	D1	D1	-
MPE-7	-	D1	D1	-
MPE-8	-	D1	-	-
MPE-9	D1	-	-	-
MPE-10	D1	-	-	-
MPE-11	D1	-	-	-
MPE-12	D1	-	-	-
MPE-13	D2	-	-	-
MPE-14	D1	-	-	-

Table S1

Antibodies and panel information				
Isotope Channel	**Antibody/reagent name**	**Clone**	**Source**	**Category**
191/193 Ir	DNA		Miltenyi	Cells isolation
194Pt	Viability		Miltenyi	Viability
89Y	CD45	HI30	Fluidigm	Lineage
142Nd	CD19	LT19	Miltenyi	Lineage
144Nd	TCR Vα14-Jα18	6B11	Miltenyi	Lineage
145Nd	CD11c	M54-27G12	Miltenyi	Lineage
148Nd	CD14	TUK4	Miltenyi	Lineage
150Nd	CD11b	M1/70.15.11.5	Miltenyi	Lineage
153Eu	CD45RA	T6D11	Miltenyi	Lineage
155Gd	CD8β	SIDI8BEE	Miltenyi	Lineage
158Gd	CCR7(CD197)	FR11-11EB	Miltenyi	Lineage
159Tb	TCR Vα7.2	REA179	Miltenyi	Lineage
164Dy	CD4	VIT4	Miltenyi	Lineage
166Er	NKp46	9 E2	Miltenyi	Lineage
168Er	TCR αβ	BW242/412	Miltenyi	Lineage
169Tm	CD8α	BW135/80	Miltenyi	Lineage
175Lu	TCRγδ	11F2	Miltenyi	Lineage
141Pr	CD56	HCD56	Miltenyi	Lineage/Activation
146Nd	CD107a	H4A3	Miltenyi	Activation
152Sm	CD27	M-T271	Miltenyi	Activation
163Di	CD57	HCD57	Miltenyi	Activation
167Er	CD38	REA572	Miltenyi	Activation
170Er	CD137	4B4-1	Miltenyi	Activation
171Yb	Annexin A1	74/3	Miltenyi	Activation
172Yb	CD253	RIK2.1	Miltenyi	Activation
174Yb	CD226	DX11	Miltenyi	Activation
147Sm	PERF	delta G9	Miltenyi	Cytotoxicity
149Sm	GzmB	REA226	Miltenyi	Cytotoxicity
151Eu	GzmA	REA162	Miltenyi	Cytotoxicity
161Dy	CD255	CARL-1	Miltenyi	Cytotoxicity
162Dy	GNLY	AF3138	Miltenyi	Cytotoxicity
154Sm	V-beta 13.2	H132	Beckman Coulter	TCR
156Gd	V-beta 7.2	ZIZOU4	Beckman Coulter	TCR
160Gd	V-beta 21.3	IG125	Beckman Coulter	TCR

Table S2

A

Patient ID	Total templates	Productive templates	Productive fraction	Productive rearrangements	Productive clonality	TCRB accounting for>0.5% total	
						N TCRB sequences	Cum% of TCRB repertoire
TEN-2	15156	12345	0.81	10051	0.03	1	3.65
TEN-3	9911	9083	0.92	2612	0.55	2	63.40
TEN-4	7602	5904	0.78	2261	0.17	16	29.97
TEN-5	951	718	0.76	452	0.06	18	22.98
TEN-6	27148	24951	0.92	2568	0.61	9	77.04
TEN-7	135218	109695	0.81	32357	0.17	7	14.26
TEN-8	91287	73280	0.80	56653	0.03	2	1.70
TEN-9	24344	23321	0.96	1745	0.69	6	85.44
TEN-10	115687	111243	0.96	4319	0.87	2	89.60
TEN-11	7408	5691	0.77	836	0.36	24	70.64
TEN-12	16159	12809	0.79	8121	0.09	5	11.66
TEN-13	2564	2163	0.84	1134	0.21	9	33.24
TEN-14	37,685	30113	0.80	18898	0.04	0	0
TEN-15	51687	30309	0.58	2111	0.59	11	69.94
TEN-16	15801	12384	0.78	4962	0.13	10	13.64
MPE-1	64906	53041	0.81	19223	0.08	2	1.70
MPE-2	211797	170222	0.80	68346	0.07	0	0
MPE-3	45946	36899	0.80	14225	0.09	2	2.39
MPE-4	7087	5775	0.81	2757	0.09	17	14.61
MPE-5	10537	8457	0.80	5139	0.06	8	6.83
MPE-6	5114	4280	0.84	2364	0.15	4	20.68
MPE-7	48944	39474	0.81	20772	0.07	3	2.38

B

Patient ID	Total templates	Productive templates	Productive fraction	Productive rearrangements	Productive clonality	TCRB accounting for>0.5% total	
						N TCRB sequences	Cum% of TCRB repertoire
TEN-2	42212	33656	0.80	26806	0.02	1	0.65
TEN-3	25349	21559	0.85	12802	0.12	11	16.70
TEN-4	22380	16933	0.76	6559	0.16	9	18.68
TEN-5	97423	77785	0.80	38437	0.15	16	17.01
TEN-6	45198	36165	0.80	24135	0.11	11	16.86
TEN-7	68825	50224	0.73	21623	0.22	10	29.79
TEN-8	18785	15003	0.80	13198	0.01	1	0.55
TEN-9	857	676	0.79	471	0.06	14	22.63
TEN-10	5087	4021	0.79	3170	0.04	4	5.65
TEN-11	19359	15443	0.80	9465	0.08	4	8.01
TEN-12	108801	87610	0.81	71003	0.02	1	0.86
TEN-13	97529	80175	0.82	57810	0.03	1	0.81
TEN-14	20670	17286	0.84	11424	0.01	4	22.5
TEN-15	29410	24394	0.83	15989	0,10	6	15.21
TEN-16	61236	47672	0.78	19237	0.27	11	33.27
MPE-3	23185	18627	0.80	10726	0.12	11	15.74
MPE-4	6152	4815	0.78	4176	0.02	3	4.38
MPE-5	11093	8560	0.77	6762	0.06	5	10.68
MPE-6	80269	65498	0.82	50441	0.02	2	1.31
MPE-7	31855	25294	0.79	17336	0.04	2	1.54

Table S3

Patient	V family	TCRBV	TCRBD	TCRBJ	Templates	CDR3 rearrangement	Productive frequency	Respective anti-Vβ mAb	% Vβ+ cells among CD3+CD8+ T cells as determined by FACs analysis
	TCRBV09	TCRBV09-01	TCRBD02-01*01	TCRBJ02-01*01	450	CTGAGCTCTCTGGAGCTGGGGGACTCAGCTTTGTATTTCTGTGCCAGCAGCGTAGATCTGTCGGGGAATGAGCAGTTCTTCGGGCCA	3.64	Vb 1	27.00
	TCRBV06	TCRBV06-06	unresolved	TCRBJ02-01*01	28	CTCAGGCTGGAGTTGGCTGCTCCCTCCCAGACATCTGTGTACTTCTGTGCCAGCAGTTACTCAATCCATGAGCAGTTCTTCGGGCCA	0.23	Vb 13.6	2.55
TEN-2	TCRBV02	TCRBV02-01*01	TCRBD02-01*01	TCRBJ02-07*01	21	TCCACAAAGCTGGAGGACTCAGCCATGTACTTCTGTGCCAGCAGTGAACAACTAGCGGGGTTGTCCTACGAGCAGTACTTCGGGCCG	0.17	Vb 22	5.75
	TCRBV06	TCRBV06-05*01	unresolved	TCRBJ01-02*01	19	AGGCTGCTGTCGGCTGCTCCCTCCCAGACATCTGTGTACTTCTGTGCCAGCAGCCAAAGGGACGGATATGGCTACACCTTCGGTTCG	0.15	Vb 13.1	13.7
	TCRBV06	TCRBV06-05*01	TCRBD01-01*01	TCRBJ02-05*01	19	CTGTCGGCTGCTCCCTCCCAGACATCTGTGTACTTCTGTGCCAGCAGTTACGCCAATACAGGGTGGGAGACCCAGTACTTCGGGCCA	0.15	Vb 13.1	
	TCRBV11	TCRBV11-02*02	unresolved	TCRBJ02-01*01	5621	CAGCCTGCAAAGCTTGAGGACTCGGCCGTGTATCTCTGTGCCAGCAGCCCCTTCCGTGACTCCTACAATGAGCAGTTCTTCGGGCCA	61.88	Vb 21.3	57.00
	TCRBV19	TCRBV19-01	TCRBD01-01*01	TCRBJ01-05*01	138	GTGACATCGGCCCAAAAGAACCCGACAGCTTTCTATCTCTGTGCCACCTTCGACGACAATATAGCAATCAGCCCCAGCATTTTGGTGAT	1.52	Vb 17	1.02
TEN-3	TCRBV19	TCRBV19-01	TCRBD02-01*02	TCRBJ01-02*01	39	CTCACTGTGACATCGGCCCAAAAGAACCCGACAGCTTTCTATCTCTGTGCCAGTAGTGAGGGCAGCTATGGCTACACCTTCGGTTCG	0.43	Vb 17	
	TCRBV09	TCRBV09-01	unresolved	TCRBJ02-01*01	17	AGCTCTCTGGAGCTGGGGGACTCAGCTTTGTATTTCTGTGCCAGCAGTGTCAGCGGACAGACTAGCAATGAGCAGTTCTTCGGGCCA	0.19	Vb 1	3.61
	TCRBV06	TCRBV06-01*01	unresolved	TCRBJ02-02*01	16	GAGTCGGCTGCTCCCTCCCAGACATCTGTGTACTTCTGTGCCAGCAGTGAAGCCAGAGGGGGGTCCGGGGAGCTGTTTTTTGGAGAA	0.18	na	na
	TCRBV05	TCRBV05-06*01	TCRBD02-01	TCRBJ02-01*01	348	AATGTGAACGCCTTGTTGCTGGGGGACTCGGCCCTCTATCTCTGTGCCAGCAGCTTTCCTAGCGAAAATGAGCAGTTCTTCGGGCCA	5.89	Vb 5.2	2.75
	TCRBV28	TCRBV28-01*01	TCRBD02-01	TCRBJ02-07*01	248	ATTCTGGAGTCCGCCAGCACCAACCAGACATCTATGTACCTCTGTGCCAGCCTGGGGACTAGCTCCTACGAGCAGTACTTCGGGCCG	4.20	Vb 3	24.2
TEN-4	TCRBV30	TCRBV30-01*01	TCRBD01-01*01	TCRBJ02-07*01	185	TTCATCCTGAGTTCTAAGAAGCTCCTTCTCAGTGACTCTGGCTTCTATCTCTGTGCCAGGGGGCGCGGGAGCAGTACTTCGGGCCG	3.13	Vb 20	1.56
	TCRBV29	TCRBV29-01*01	unresolved	TCRBJ02-03*01	180	CTGACTGTGAGCAACATGAGCCCTGAAGACAGCAGCATATATCTCTGCAGCGTTCTACAACTCACAGATACGCAGTATTTTGGCCCA	3.05	Vb 4	3.33
	TCRBV14	TCRBV14-01*01	TCRBD01-01*01	TCRBJ02-07*01	167	CAGCCTGCAGAACTGGAGGATTCTGGAGTTTATTTCTGTGCCAGCAGCCCATCTTTGACAGGGAGCGGCGAGCAGTACTTCGGGCCG	2.83	Vb 16	3.62
	TCRBV15	TCRBV15-01*01	TCRBD02-01*01	TCRBJ02-05*01	49	CGCTCACCAGGCCTGGGGGACGCAGCCATGTACCTGTGTGCCACCAGCAGAGATGTAGCGGGGGGCGGGACCCAGTACTTCGGGCCA	6.82	na	na
	TCRBV14	TCRBV14-01*01	na	TCRBJ02-07*01	18	CAGCCTGCAGAACTGGAGGATTCTGGAGTTTATTTCTGTGCCAGCAGCCACTTGGCCCAGGGTGGGGGCGAGCAGTACTTCGGGCCG	2.51	Vb 16	1.88
TEN-5	TCRBV06	TCRBV06-05*01	TCRBD02-01*01	TCRBJ01-02*01	12	CTGTCGGCTGCTCCCTCCCAGACATCTGTGTACTTCTGTGCCAGCAGTCCGACGCAAAACGGGGGGGGTGGCTACACCTTCGGTTCG	1.67	Vb 13.1	0.94
	TCRBV10	TCRBV10-03*01	na	TCRBJ01-02*01	11	CTGGAGTCCGCTACCAGCTCCCAGACATCTGTGTACTTCTGTGCCATCAGTGGAGCTGCAGCCAACTATGGCTACACCTTCGGTTCG	1.53	Vb 12	1.7
	TCRBV04	TCRBV04-03*01	TCRBD02-01	TCRBJ01-04*01	10	CACACCCTGCAGCCAGAAGACTCGGCCCTGTATCTCTGCGCCAGCAGCCAAGATCTCTCGGACTATGAAAAACTGTTTTTTGGCAGT	1.39	Vb 7.2	9.15
	TCRBV21	TCRBV21-01*01	TCRBD01-01*01	TCRBJ01-04*01	8509	TCCACGGAGTCAGGGGACACAGCACTGTATTTCTGTGCCAGCAGCGACAGGGGAAGAGGTACTAATGAAAAACTGTTTTTTGGCAGT	34.10	na	na
	TCRBV28	TCRBV28-01*01	unresolved	TCRBJ01-04*01	8503	CTGGAGTCCGCCAGCACCAACCAGACATCTATGTACCTCTGTGCCAGCAGTTTTGGGGGGCCTAATGAAAAACTGTTTTTTGGCAGT	34.08	Vb 3	48.1
TEN-6	TCRBV18	TCRBV18-01*01	TCRBD01-01*01	TCRBJ01-02*01	695	CAGCAGGTAGTGCGAGGAGATTCGGCAGCTTATTTCTGTGCCAGCTCACCCGGACAGGGAAGAAGCTATGGCTACACCTTCGGTTCG	2.79	Vb 18	3.26
	TCRBV06	TCRBV06-04	TCRBD02-01	TCRBJ01-02*01	508	TCTGCTGTACCCTCTCAGACATCTGTGTACTTCTGTGCCAGCAGCTTGGAACCTGGGGACTCGGTCTATGGCTACACCTTCGGTTCG	2.04	na	na
	TCRBV03	unresolved	TCRBD01-01*01	TCRBJ01-03*01	297	ATCAATTCCCTGGAGCTTGGTGACTCTGCTGTGTATTTCTGTGCCAGCAGCCAAGAAAGGGGAAGGGACACCATATATTTTGGAGAG	1.19	Vb 9	3.56
	TCRBV02	TCRBV02-01*01	TCRBD02-01*01	TCRBJ02-07*01	5168	ACAAAGCTGGAGGACTCAGCCATGTACTTCTGTGCCAGCAGTGAAGTGGTAGCGGGGGCTAGCTCCTACGAGCAGTACTTCGGGCCG	4.71	Vb 22	2.46
	TCRBV05	TCRBV05-05*01	TCRBD01-01*01	TCRBJ01-01*01	3889	GCCTTGTTGCTGGGGGACTCGGCCCTGTATCTCTGTGCCAGCAGCTTGAACAGGGACCGATCGAACACTGAAGCTTTCTTTGGACAA	3.55	Vb 5.3	3.6
TEN-7	TCRBV06	unresolved	TCRBD02-01*02	TCRBJ02-01*01	3588	GAGTCGGCTGCTCCCTCCCAAACATCTGTGTACTTCTGTGCCAGCAGCCCGACTAGCGGGAGTAGTAATGAGCAGTTCTTCGGGCCA	3.27	Vb 13.1; Vb 13.2; Vb 13.6	9.25
	TCRBV06	TCRBV06-05*01	TCRBD02-01*01	TCRBJ01-02*01	1168	CTCAGGCTGCTGTCGGCTGCTCCCTCCCAGACATCTGTGTACTTCTGTGCCAGCAGTCTGGGGGAGAAGGCTACACCTTCGGTTCG	1.06	Vb 13.1	4.39
	TCRBV04	TCRBV04-01*01	TCRBD02-01	TCRBJ02-07*01	652	CTTCACCTACACGCCCTGCAGCCAGAAGACTCAGCCCTGTATCTCTGCGCCAGCAGCCAAGATGAACTCGAGCAGTACTTCGGGCCG	0.59	Vb 7.1	1.25
	TCRBV11	TCRBV11-03*01	TCRBD01-01*01	TCRBJ01-05*01	775	GAGCTTGGGGACTCGGCCGTGTATCTCTGTGCCAGCAGCAACCCGACGGGACAGGGGCATAGCAATCAGCCCCAGCATTTTGGTGAT	1.06	na	na
	TCRBV27	TCRBV27-01*01	TCRBD01-01*01	TCRBJ02-03*01	471	CTGATCCTGGAGTCGCCCAGCCCAACCAGACCTCTCTGTACTTCTGTGCCAGCAGGACAGGGCCAGATACGCAGTATTTTGGCCCA	0.64	Vb 14	1.2
TEN-8	TCRBV04	TCRBV04-03*01	na	TCRBJ02-02*01	289	ACCCTGCAGCCAGAAGACTCGGCCCTGTATCTCTGCGCCAGCAGCCAAGAAGGAGGGGGGGAACACCGGGGAGCTGTTTTTTGGAGAA	0.39	Vb 7.2	5.76
	TCRBV27	TCRBV27-01*01	TCRBD02-01	TCRBJ02-07*01	197	CTGATCCTGGAGTCGCCCAGCCCAACCAGACCTCTCTGTACTTCTGTGCCAGCTTTACTAGCTCCTACGAGCAGTACTTCGGGCCG	0.27	Vb 14	1.2
	TCRBV04	TCRBV04-03*01	TCRBD01-01*01	TCRBJ01-05*01	123	ACCCTGCAGCCAGAAGACTCGGCCCTGTATCTCTGCGCCAGCAGCCAAGGTGCAGGATCGACGAATCAGCCCCAGCATTTTGGTGAT	0.17	Vb 7.2	5.76
	TCRBV02	TCRBV02-01*01	TCRBD02-01*02	TCRBJ01-05*01	10334	TCCACAAAGCTGGAGGACTCAGCCATGTACTTCTGTGCCAGCAGTGATGTGGGGAGAACTAGCAATCAGCCCCAGCATTTTGGTGAT	44.31	Vb 22	35.9
	TCRBV06	TCRBV06	TCRBD01-01*01	TCRBJ01-01*01	7373	GCTGCTCCCTCCCAAACATCTGTGTACTTCTGTGCCAGCAGTTACTCCGATCCGAGGGACATGAACACTGAAGCTTTCTTTGGACAA	31.62	Vb 13.1; Vb 13.2; Vb 13.6	42.26
TEN-9	TCRBV21	TCRBV21-01*01	TCRBD01-01*01	TCRBJ01-01*01	763	CAGTCCACGGAGTCAGGGGACACAGCACTGTATCTCTGTGCCAGCAGCAAACACCCAGGGTTAAACACTGAAGCTTTCTTTGGACAA	3.27	na	na
	TCRBV29	TCRBV29-01*01	TCRBD02-01*01	TCRBJ01-02*01	737	GTGAGCAACATGAGCCCTGAAGACAGCAGCATATATCTCTGCAGCGTTCATTCCTTTGGGGGGCAAGTGGCTACACCTTCGGTTCG	3.16	Vb 4	5.86
	TCRBV24	TCRBV24	na	TCRBJ02-01*01	590	CTAGAGTCTGCCATCCCCAACCAGACAGCTCTTTACTTCTGTGCCACCAGCCCGGACCCCCGGCTGATGAGCAGTTCTTCGGGCCA	2.53	na	na
	TCRBV28	TCRBV28-01*01	TCRBD02-01*01	TCRBJ01-04*01	99110	CTGGAGTCCGCCAGCACCAACCAGACATCTATGTACCTCTGTGCCAGCAGTTTCGGGGGGCCTAATGAAAAACTGTTTTTTGGCAGT	89.09	Vb 3	93.9
	TCRBV28	TCRBV28-01*01	na	TCRBJ02-02*01	566	CTGGAGTCCGCCAGCACCAACCAGACATCTATGTACCTCTGTGCCAGCAGCCCTGGAAGCAACACCGGGGAGCTGTTTTTTGGAGAA	0.51	Vb 3	
TEN-10	TCRBV04	TCRBV04-03*01	TCRBD01-01*01	TCRBJ02-07*01	376	ACCCTGCAGCCAGAAGACTCGGCCCTGTATCTCTGCGCCAGCAGCCAAGATCTGGGGCCAGTAGAGTACGAGCAGTACTTCGGGCCG	0.34	Vb 7.2	0.88
	TCRBV07	TCRBV07-03*03	TCRBD02-01	TCRBJ02-02*01	374	CGCACAGAGCAGGGGGACTCAGCCGCGTATCTCCGTGCCAGCAGCTTCACCGGGACTGGGGCGTCTGGGGAGCTGTTTTTTGGAGAA	0.34	na	na
	TCRBV19	TCRBV19-01	na	TCRBJ02-05*01	238	ACTGTGACATCGGCCCAAAAGAACCCGACAGCTTTCTATCTCTGTGCCAGTAGTATTAGGGGCGGGGAGACCCAGTACTTCGGGCCA	0.21	Vb 17	3.18
	TCRBV12	TCRBV12	TCRBD01-01*01	TCRBJ02-05*01	760	CTGAAGATCCAGCCCTCAGAACCCAGGGACTCAGCTGTGTACTTCTGTGCCAGCAGTTTGCAGGAAGAGACCCAGTACTTCGGGCCA	13.35	na	na
	TCRBV05	TCRBV05-01*01	unknown	TCRBJ01-02*01	706	AGCACCTTGGAGCTGGGGGACTCGGCCCTTTATCTTTGCGCCAGCAGCTTGGACGACAGCGGATTTTATGGCTACACCTTCGGTTCG	12.41	Vb 5.1	11.9
TEN-11	TCRBV04	TCRBV04-01*01	unknown	TCRBJ01-01*01	379	CTTCACCTACACGCCCTGCAGCCAGAAGACTCAGCCCTGTATCTCTGCGCCAGCAGCCAAGGGGACACTGAAGCTTTCTTTGGACAA	6.66	Vb 7.1	6.04
	TCRBV24	TCRBV24	TCRBD02-01*02	TCRBJ02-01*01	316	TCCCTAGAGTCTGCCATCCCCAACCAGACAGCTCTTTACTTCTGTGCCACGGAGCGGGAGTGGGGAAATGAGCAGTTCTTCGGGCCA	5.55	na	na
	TCRBV05	TCRBV05-06*01	unknown	TCRBJ01-05*01	194	CTGAATGTGAACGCCTTGTTGCTGGGGGACTCGGCCCTCTATCTCTGTGCCAGCAGCTTGGGCTATCAGCCCCAGCATTTTGGTGAT	3.41	Vb 5.2	0.086
	TCRBV27	TCRBV27-01*01	na	TCRBJ01-02*01	997	CTGGAGTCGCCCAGCCCCAACCAGACCTCTCTGTACTTCTGTGCCAGCAGTTACCACGGGGCTGCGGATGGCTACACCTTCGGTTCG	7.78	Vb 14	nd
	TCRBV04	TCRBV04-01*01	TCRBD02-01*01	TCRBJ02-02*01	187	CACGCCCTGCAGCCAGAAGACTCAGCCCTGTATCTCTGCGCCAGCACCCTTAGCGGGGGGTCCACCGGGGAGCTGTTTTTTGGAGAA	1.46	Vb 7.1	nd
TEN-12	TCRBV07	TCRBV07-08*01	TCRBD01-01*01	TCRBJ02-07*01	130	AAGATCCAGCGCACACAGCAGGAGGACTCCGCCGTGTATCTCTGTGCCAGCAGCTTAGGCCAGGCCTACGAGCAGTACTTCGGGCCG	1.01	na	nd
	TCRBV05	TCRBV05-04*01	TCRBD02-01*01	TCRBJ02-07*01	107	AACGCCTTGGAGCTGGACGACTCGGCCCTGTATCTCTGTGCCAGCAGCTTGGGTCGGGGGGGCTCCTACGAGCAGTACTTCGGGCCG	0.84	na	nd
	TCRBV04	TCRBV04-01*01	TCRBD01-01*01	TCRBJ01-02*01	73	GCCCTGCAGCCAGAAGACTCAGCCCTGTATCTCTGCGCCAGCAGCCCAGGCACCAGGGGATTAACTATGGCTACACCTTCGGTTCG	0.57	Vb 7.1	nd
	TCRBV04	TCRBV04-01*01	TCRBD01-01*01	TCRBJ01-02*01	565	GCCCTGCAGCCAGAAGACTCAGCCCTGTATCTCTGCGCCAGCAGCCAAGATAGTTTAGGTACAGGGTCTGGCTACACCTTCGGTTCG	26.11	Vb 7.1	18.1
	TCRBV28	TCRBV28-01*01	TCRBD02-01*02	TCRBJ02-01*01	42	TCCGCCAGCACCAACCAGACATCTATGTACCTCTGTGCCAGCAGTCACTTCCCGGGACTAGCGGGAGAGGACGAGTCTTCCGGGCCA	1.94	Vb 3	8.84
TEN-13	TCRBV24	TCRBV24	TCRBD02-01	TCRBJ01-02*01	22	TCCCTAGAGTCTGCCATCCCCAACCAGACAGCTCTTTACTTCTGTGCCACCAGTGATATAGATAACTATGGCTACACCTTCGGTTCG	1.02	na	na
	TCRBV11	TCRBV11-03*01	TCRBD02-01	TCRBJ01-01*01	21	AAGATCCAGCCTGCAGAGCTTGGGGACTCGGCCGTGTATCTCTGTGCCAGCAGCGTAAGTTTAGCAACGGAAGCTTTCTTTGGACAA	0.97	na	na
	TCRBV04	TCRBV04-03*01	TCRBD01-01*01	TCRBJ01-02*01	19	CTACACACCCTGCAGCCAGAAGACTCGGCCCTGTATCTCTGCGCCAGCAGTCCTAACACAGGGGTCTCTGGCTACACCTTCGGTTCG	0.88	Vb 7.2	0.59
	TCRBV07	TCRBV07-03*01	TCRBD01-01*01	TCRBJ01-01*01	139	AAGATCCAGCGCACAGAGCGGGGGGGACTCAGCCGTGTATCTCTGTGCCAGCAGCTGGACAGAGAACACTGAAGCTTTCTTTGGACAA	0.46	na	na
	TCRBV10	TCRBV10-03*01	unknown	TCRBJ01-01*01	95	TCCGCTACCAGCTCCCAGACATCTGTGTACTTCTGTGCCATCAGTGAGTCCGGGGCAGGGCTGAACACTGAAGCTTTCTTTGGACAA	0.32	Vb 12	na
TEN-14	TCRBV29	TCRBV29-01*01	unknown	TCRBJ02-02*01	94	ACTGTGAGCAACATGAGCCCTGAAGACAGCAGCATATATCTCTGCAGCGTTGGTGGGGCGAACACCGGGGAGCTGTTTTTTGGAGAA	0.31	Vb 4	na
	TCRBV29	TCRBV29-01*01	TCRBD01-01*01	TCRBJ02-02*01	86	ACTGTGAGCAACATGAGCCCTGAAGACAGCAGCATATATCTCTGCAGCGTTGGGGCCACGAACACCGGGGAGCTGTTTTTTGGAGAA	0.29	Vb 4	na
	TCRBV27	TCRBV27-01*01	TCRBD01-01*01	TCRBJ01-05*01	80	GAGTCGCCCAGCCCCAACCAGACCTCTCTGTACTTCTGTGCCAGCAGTTTAAGGACGGGACACTATCAGCCCCAGCATTTTGGTGAT	0.27	Vb 14	na
	TCRBV27	TCRBV27-01*01	TCRBD02-01*01	TCRBJ02-01*01	12643	CTGGAGTCGCCCAGCCCCAACCAGACCTCTCTGTACTTCTGTGCCAGCAGTCTACGCGGGGGGCTGGGTGAGCAGTTCTTCGGGCCA	41.71	Vb 14	27.2
	TCRBV18	TCRBV18-01*01	TCRBD01-01*01	TCRBJ01-05*01	3635	AGGATCCAGCAGGTAGTGCGAGGAGATTCGGCAGCTTATTTCTGTGCCAGCTCAGGGGGCAGGGATCAGCCCCAGCATTTTGGTGAT	11.99	Vb 18	0.65
TEN-15	TCRBV06	TCRBV06-05*01	unknown	TCRBJ02-03*01	3463	AGGCTGCTGTCGGCTGCTCCCTCCCAGACATCTGTGTACTTCTGTGCCAGCAGTTTCTCGGGTTCGGATACGCAGTATTTTGGCCCA	11.43	Vb 13.1	16.4
	TCRBV20	TCRBV20-01*01	TCRBD02-01	TCRBJ01-02*01	1893	ACTCTGACAGTGACCAGTGCCCATCCTGAAGACAGCAGCTTCTACATCTGCAGTGCTCTCGGTCCCTATGGCTACACCTTCGGTTCG	6.25	Vb 2	4.72
	TCRBV20	TCRBV20	TCRBD01-01*01	TCRBJ01-05*01	648	ACAGTGACCAGTGCCCATCCTGAAGACAGCAGCTTCTACATCTGCAGTGCAGGCAGGGGAAGGGATCAGCCCCAGCATTTTGGTGAT	1.40	Vb 2	4.72
	TCRBV09	TCRBV09-01	TCRBD01-01*01	TCRBJ01-02*01	648	CTGAGCTCTCTGGAGCTGGGGGACTCAGCTTTGTATTTCTGTGCCAGCAGCGGACAGCAAGTTATGGCTACACCTTCGGTTCG	5.23	Vb 1	na
	TCRBV10	TCRBV10-03*01	TCRBD01-01*01	TCRBJ01-05*01	422	CTGGAGTCCGCTACCAGCTCCCAGACATCTGTGTACTTCTGTGCCATCGGGACAGGGGATAGCAATCAGCCCCAGCATTTTGGTGAT	3.41	Vb 12	na
TEN-16	TCRBV29	TCRBV29-01*01	TCRBD02-01*02	TCRBJ02-01*01	213	AGCAACATGAGCCCTGAAGACAGCAGCATATATCTCTGCAGCGCCACCTATTTAGCGGGAGTTCACAATGAGCAGTTCTTCGGGCCA	1.72	Vb 4	na
	TCRBV12	TCRBV12	TCRBD01-01*01	TCRBJ01-01*01	100	CAGCCCTCAGAACCCAGGGACTCAGCTGTGTACTTCTGTGCCAGCAGTCCGAATGACGGACAGGGGGATGAAGCTTTCTTTGGACAA	0.81	Vb 8	na
	TCRBV30	TCRBV30-01	TCRBD01-01*01	TCRBJ01-02*01	87	AGTGACTCTGGCTTCTATCTCTGTGCCTGGATGCCTCTAATTTCCGAGAAATACAGGGGGCTTAACTATGGCTACACCTTCGGTTCG	0.70	Vb 20	na

Table S4

Patient	V family	TCRBV	TCRBD	TCRBJ	Templates	CDR3 rearrangement	Productive frequency	Respective anti-Vβ mAb	% Vβ+ cells among CD3+CD8+ T cells as determined by FACs analysis
	TCRBV06	TCRBV06-06	na	TCRBJ02-01*01	218	CTCAGGCTGGAGTTGGCTGCTCCCTCCCAGACATCTGTGTACTTCTGTGCCAGCAGTTACTCAATCCATGAGCAGTTCTTCGGGCCA	0.65	Vb 13.6	na
	TCRBV09	TCRBV09-01	TCRBD02-01*01	TCRBJ02-01*01	144	CTGAGCTCTCTGGAGCTGGGGGACTCAGCTTTGTATTTCTGTGCCAGCAGCGTAGATCTGTCGGGGAATGAGCAGTTCTTCGGGCCA	0.43	Vb 1	na
TEN-2	TCRBV06	TCRBV06-05*01	TCRBD01-01*01	TCRBJ02-05*01	117	CTGTCGGCTGCTCCCTCCCAGACATCTGTGTACTTCTGTGCCAGCAGTTACGCCAATACAGGGTGGGAGACCCAGTACTTCGGGCCA	0.35	Vb 13.1	na
	TCRBV05	TCRBV05-01*01	na	TCRBJ02-02*01	99	ATGAATGTGAGCACCTTGGAGCTGGGGGACTCGGCCCTTTATCTTTGCGCCAGCAGCTTGTACACCGGGGAGCTGTTTTTTGGAGAA	0.29	Vb 5.1	na
	TCRBV06	TCRBV06-05*01	TCRBD01-01*01	TCRBJ01-02*01	94	CTGTCGGCTGCTCCCTCCCAGACATCTGTGTACTTCTGTGCCAGCAGTTACTCTGGGCAGGGGATCTATGGCTACACCTTCGGTTCG	0.28	Vb 13.1	na
	TCRBV11	TCRBV11-02*02	na	TCRBJ02-01*01	1094	CAGCCTGCAAAGCTTGAGGACTCGGCCGTGTATCTCTGTGCCAGCAGCCCCTTCCGTGACTCCTACAATGAGCAGTTCTTCGGGCCA	5.07	Vb 21.3	6.54
	TCRBV27	TCRBV27-01*01	TCRBD01-01*01	TCRBJ02-07*01	553	CCCAACCAGACCTCTCTGTACTTCTGTGCCAGCAGATCCTTACAGGGGGCGCGGACGACATTTCTCTACGAGCAGTACTTCGGGCCG	2.57	Vb 14	7.88
TEN-3	TCRBV09	TCRBV09-01	na	TCRBJ02-01*01	420	AGCTCTCTGGAGCTGGGGGACTCAGCTTTGTATTTCTGTGCCAGCAGTGTCAGCGGACAGACTAGCAATGAGCAGTTCTTCGGGCCA	1.95	Vb 1	3.89
	TCRBV28	TCRBV28-01*01	TCRBD02-01	TCRBJ01-01*01	243	ATTCTGGAGTCCGCCAGCACCAACCAGACATCTATGTACCTCTGTGCCAGCCGGGACTCCGGGAGGAACTGAAGCTTTCTTTGGACAA	1.12	Vb 3	4
	TCRBV07	TCRBV07-02*01	TCRBD02-01*02	TCRBJ02-01*01	233	CGCACACAGCAGGAGGACTCGGCCGTGTATCTCTGTGCCAGCAGCTGGGTGGGCGGGAGTAACAACAATGAGCAGTTCTTCGGGCCA	1.08	na	na
	TCRBV19	TCRBV19-01	TCRBD02-01*02	TCRBJ02-05*01	1374	GTGACATCGGCCCAAAAGAACCCGACAGCTTTCTATCTCTGTGCCAGTAGTATAGTTGGAGGAGGGGAGACCCAGTACTTCGGGCCA	8.11	Vb 17	10.5
	TCRBV27	TCRBV27-01*01	TCRBD01-01*01	TCRBJ01-05*01	845	AGCCCCAACCAGACCTCTCTGTACTTCTGTGCCAGCAGTTTAGGAGCCAGGACGGCAGGGCCTGACGGGTACCAGCATTTTGGTGAT	4.99	Vb 14	3.17
TEN-4	TCRBV07	TCRBV07-03*01	TCRBD01-01*01	TCRBJ02-01*01	265	CGCACAGAGCGGGGGGACTCAGCCGTGTATCTCTGTGCCAGCAGCTTGCTGGGACAGGGCGACTACAATGAGCAGTTCTTCGGGCCA	1.56	na	na
	TCRBV07	TCRBV07-02*01	TCRBD01-01*01	TCRBJ02-07*01	176	ACGATCCAGCGCACACAGCAGGAGGACTCGGCCGTGTATCTCTGTGCCAGCAGCTTCTGGCACCCCTACGAGCAGTACTTCGGGCCG	1.04	na	na
	TCRBV06	TCRBV06-05*01	TCRBD02-01*01	TCRBJ02-01*01	123	CTGCTGTCGGCTGCTCCCTCCAGACATCTGTGTACTTCTGTGCCAGCAGTTTAGCGGGGCCCTACAATGAGCAGTTCTTCGGGCCA	0.73	Vb 13.1	0.27
	TCRBV13	TCRBV13-01*01	TCRBD01-01*01	TCRBJ01-02*01	1951	TCCTTGGAGGCTGGGGGACTCAGCCCTGTACTTCTGTGCCAGCAGCTTAAGTACAGGGGGCTGGTTATGATGGCTACACCTTCGGTTCG	2.51	Vb 23	3.6
	TCRBV15	TCRBV15-01*01	TCRBD02-01*01	TCRBJ02-05*01	1776	CGCTCACCAGGCCTGGGGGACGCAGCCATGTACCTGTGTGCCACCAGCAGAGATGTAGCGGGGGGCGGGACCCAGTACTTCGGGCCA	2.28	na	na
TEN-5	TCRBV28	TCRBV28-01*01	TCRBD01-01*01	TCRBJ02-02*01	1701	TCCGCCAGCACCAACCAGACATCTATGTACCTCTGTGCCAGCAGCCCGCCGGGGGACAGGAACACCGGGGAGCTGTTTTTTGGAGAA	2.19	Vb 3	5.43
	TCRBV06	TCRBV06-05*01	TCRBD02-01*01	TCRBJ02-01*01	916	TCGGCTGCTCCCTCCCAGACATCTGTGTACTTCTGTGCCAGCAGTTACTTAGCGGGGGCTTCCTACAATGAGCAGTTCTTCGGGCCA	1.18	Vb 13.1	2.34
	TCRBV27	TCRBV27-01*01	na	TCRBJ02-02*01	779	GAGTCGCCCAGCCCCAACCAGACCTCTCTGTACTTCTGTGCCAGCAGTTTCTCCCCAGAGGGGACCGGGGAGCTGTTTTTTGGAGAA	1.00	Vb 14	2.26
	TCRBV07	TCRBV07-02*01	na	TCRBJ01-02*01	1748	ACGATCCAGCGCACACAGCAGGAGGACTCGGCCGTGTATCTCTGTGCCAGCAGCCTCAGGGAGAACTATGGCTACACCTTCGGTTCG	4.83	na	na
	TCRBV18	TCRBV18-01*01	TCRBD01-01*01	TCRBJ01-02*01	905	CAGCAGGTAGTGCGAGGAGATTCGGCAGCTTATTTCTGTGCCAGCTCACCCGGACAGGGAAGAAGCTATGGCTACACCTTCGGTTCG	2.50	Vb 18	3.07
TEN-6	TCRBV19	TCRBV19-01	TCRBD01-01*01	TCRBJ02-01*01	769	ACTGTGACATCGGCCCAAAAGAACCCGACAGCTTTCTATCTCTGTGCCAGTAGGATGCCAGGGTCGAATGAGCAGTTCTTCGGGCCA	2.13	Vb 17	6.78
	TCRBV30	TCRBV30-01*01	TCRBD01-01*01	TCRBJ01-02*01	754	AAGAAGCTCCTTCTCAGTGACTCTGGCTTCTATCTCTGTGCCTGGAGCGGGGGGGACAGGGGCCTCCTATGGCTACACCTTCGGTTCG	2.08	Vb 20	1.63
	TCRBV27	TCRBV27-01*01	na	TCRBJ02-02*01	398	GAGTCGCCCAGCCCCAACCAGACCTCTCTGTACTTCTGTGCCAGCAGAAGGCCGGGACCGAACACCGGGGAGCTGTTTTTTGGAGAA	1.10	Vb 14	0.74
	TCRBV06	TCRBV06	TCRBD02-01*02	TCRBJ02-01*01	5623	GAGTCGGCTGCTCCCTCCCAAACATCTGTGTACTTCTGTGCCAGCAGCCCGACTAGCGGGAGTAGTAATGAGCAGTTCTTCGGGCCA	11.20	Vb 13.1; Vb 13.2; Vb 13.6	na
	TCRBV02	TCRBV02-01*01	TCRBD02-01*01	TCRBJ02-07*01	4141	ACAAAGCTGGAGGACTCAGCCATGTACTTCTGTGCCAGCAGTGAAGTGGTAGCGGGGGCTAGCTCCTACGAGCAGTACTTCGGGCCG	8.25	Vb 22	4.83
TEN-7	TCRBV20	TCRBV20	na	TCRBJ02-05*01	1525	ACAGTGACCAGTGCCCATCCTGAAGACAGCAGCTTCTACATCTGCAGTGCTAAGCAGCTTAACCAAGAGACCCAGTACTTCGGGCCA	3.04	na	na
	TCRBV06	TCRBV06-01*01	TCRBD01-01*01	TCRBJ02-02*01	997	GCTCCCTCCCAGACATCTGTGTACTTCTGTGCCAGCAGTGAACTTTTATGGGACAGAATATCCGGCAAGGAGCTGTTTTTTGGAGAA	1.99	na	na
	TCRBV05	TCRBV05-05*01	TCRBD01-01*01	TCRBJ01-01*01	646	GCCTTGTTGCTGGGGGACTCGGCCCTGTATCTCTGTGCCAGCAGCTTGAACAGGGACCGATCGAACACTGAAGCTTTCTTTGGACAA	1.29	Vb 5.3	2.74
	TCRBV11	TCRBV11-03*01	TCRBD01-01*01	TCRBJ01-05*01	82	GAGCTTGGGGACTCGGCCGTGTATCTCTGTGCCAGCAGCAACCCGACGGGACAGGGGCATAGCAATCAGCCCCAGCATTTTGGTGAT	0.55	na	na
	TCRBV27	TCRBV27-01*01	TCRBD01-01*01	TCRBJ02-03*01	47	CTGATCCTGGAGTCGCCCAGCCCCAACCAGACCTCTCTGTACTTCTGTGCCAGCAGGACAGGGCCAGATACGCAGTATTTTGGCCCA	0.31	Vb 14	0.97
TEN-8	TCRBV04	TCRBV04-03*01	na	TCRBJ02-02*01	27	ACCCTGCAGCCAGAAGACTCGGCCCTGTATCTCTGCGCCAGCAGCCAAGAAGGAGGGGGGAACACCGGGGAGCTGTTTTTTGGAGAA	0.18	Vb 7.2	1.29
	TCRBV27	TCRBV27-01*01	TCRBD02-01	TCRBJ02-07*01	25	CTGATCCTGGAGTCGCCCAGCCCCAACCAGACCTCTCTGTACTTCTGTGCCAGCTTTACTAGCTCCTACGAGCAGTACTTCGGGCCG	0.17	Vb 14	0.97
	TCRBV04	TCRBV04-03*01	TCRBD01-01*01	TCRBJ01-05*01	20	ACCCTGCAGCCAGAAGACTCGGCCCTGTATCTCTGCGCCAGCAGCCAAGGTGCAGGATCGACGAATCAGCCCCAGCATTTTGGTGAT	0.13	Vb 7.2	1.29
	TCRBV29	TCRBV29-01*01	TCRBD02-01*01	TCRBJ01-02*01	23	GTGAGCAACATGAGCCCTGAAGACAGCAGCATATATCTCTGCAGCGTTCATTCCTTTGGGGGGGCAAGTGGCTACACCTTCGGTTCG	3.40	Vb 4	0.14
	TCRBV21	TCRBV21-01*01	TCRBD01-01*01	TCRBJ01-01*01	22	CAGTCCACGGAGTCAGGGGACACAGCACTGTATCTCTGTGCCAGCAGCAAACACCCAGGGTTAAACACTGAAGCTTTCTTTGGACAA	3.25	na	na
TEN-9	TCRBV06	TCRBV06	TCRBD01-01*01	TCRBJ01-01*01	18	GCTGCTCCCTCCCAAACATCTGTGTACTTCTGTGCCAGCAGTTACTCCGATCCGAGGGACATGAACACTGAAGCTTTCTTTGGACAA	2.66	na	na
	TCRBV24	TCRBV24	na	TCRBJ02-01*01	17	CTAGAGTCTGCCATCCCCAACCAGACAGCTCTTTACTTCTGTGCCACCAGCCCGGACCCCCCGGCTGATGAGCAGTTCTTCGGGCCA	2.51	na	na
	TCRBV02	TCRBV02-01*01	TCRBD02-01*02	TCRBJ01-05*01	15	TCCACAAAGCTGGAGGACTCAGCCATGTACTTCTGTGCCAGCAGTGATGTGGGGAGAACTAGCAATCAGCCCCAGCATTTTGGTGAT	2.22	Vb 22	2.49
	TCRBV28	TCRBV28-01*01	TCRBD02-01*01	TCRBJ01-04*01	87	CTGGAGTCCGCCAGCACCAACCAGACATCTATGTACCTCTGTGCCAGCAGTTTCGGGGGGCCTAATGAAAAACTGTTTTTGGCAGT	2.16	Vb 3	0.17
	TCRBV06	TCRBV06	TCRBD01-01*01	TCRBJ02-02*01	81	GAGTCGGCTGCTCCCTCCCAAACATCTGTGTACTTCTGTGCCAGCAGTTATGGACAGGTCGCCACCGGGGAGCTGTTTTTGGAGAA	2.01	na	na
TEN-10	TCRBV27	TCRBV27-01*01	TCRBD02-01*02	TCRBJ01-01*01	32	CTGGAGTCGCCCAGCCCCAACCAGACCTCTCTGTACTTCTGTGCCAGCAACCTAGGAGGGGTGAACACTGAAGCTTTCTTTGGACAA	0.80	Vb 14	0.11
	TCRBV04	TCRBV04-03*01	TCRBD01-01*01	TCRBJ02-07*01	27	ACCCTGCAGCCAGAAGACTCGGCCCTGTATCTCTGCGCCAGCAGCCAAGATCTGGGGCCAGTAGAGTACGAGCAGTACTTCGGGCCG	0.67	Vb 7.2	0.34
	TCRBV24	TCRBV24	TCRBD01-01*01	TCRBJ02-07*01	20	GAGTCTGCCATCCCCAACCAGACAGCTCTTTACTTCTGTGCCACCAAGGATTTAAGGGGCCCTGCTTCAGAGCAGTACTTCGGGCCG	0.50	na	na
	TCRBV28	TCRBV28-01*01	TCRBD02-01	TCRBJ02-01*01	800	TCCGCCAGCACCAACCAGACATCTATGTACCTCTGTGCCAGCAGTTTAACGACTAGCGGATCCTACAATGAGCAGTTCTTCGGGCCA	5.18	Vb 3	14.9
	TCRBV07	TCRBV07-06*01	na	TCRBJ02-03*01	258	ATCCAGCGCACAGAGCAGCGGGACTCGGCCATGTATCGCTGTGCCAGCAGCTTATGGGTGAGCACAGATACGCAGTATTTTGGCCCA	1.67	na	na
TEN-11	TCRBV27	TCRBV27-01*01	TCRBD02-01	TCRBJ02-07*01	100	GAGTCGCCCAGCCCCAACCAGACCTCTCTGTACTTCTGTGCCAGCAGTTTGGTCCCGGGACTCAACTACGAGCAGTACTTCGGGCCG	0.65	Vb 14	0.021
	TCRBV10	TCRBV10-02*01	na	TCRBJ02-05*01	79	CTCACTCTGGAGTCAGCTACCCGCTCCCAGACATCTGTGTATTTCTGCGCCAGCAGTGGTGTTTACGAGACCCAGTACTTCGGGCCA	0.51	Vb 12	0.51
	TCRBV19	TCRBV19-01	TCRBD02-01	TCRBJ01-01*01	74	TCGGCCCAAAAGAACCCGACAGCTTTCTATCTCTGTGCCAGTAGTCCCATTCCCTGGACTTTGAACACTGAAGCTTTCTTTGGACAA	0.48	Vb 17	3.55
	TCRBV27	TCRBV27-01*01	na	TCRBJ01-02*01	755	CTGGAGTCGCCCAGCCCCAACCAGACCTCTCTGTACTTCTGTGCCAGCAGTTACCACGGGGCTGCGGATGGCTACACCTTCGGTTCG	0.86	Vb 14	nd
	TCRBV03	TCRBV03	TCRBD01-01*01	TCRBJ01-01*01	186	ATCAATTCCCTGGAGCTTGGTGACTCTGCTGTGTATTTCTGTGCCAGCAGCCCGCATGACAAGAACACTGAAGCTTTCTTTGGACAA	0.21	na	nd
TEN-12	TCRBV14	TCRBV14-01*01	TCRBD02-01*01	TCRBJ02-01*01	166	CAGCCTGCAGAACTGGAGGATTCTGGAGTTTATTTCTGTGCCAGCAGCCAACTAGCGGGGGCCTACAATGAGCAGTTCTTCGGGCCA	0.19	Vb 16	nd
	TCRBV05	TCRBV05-04*01	TCRBD02-01*01	TCRBJ02-07*01	154	AACGCCTTGGAGCTGGACGACTCGGCCCTGTATCTCTGTGCCAGCAGCTTGGGTCGGGGGGGCTCCTACGAGCAGTACTTCGGGCCG	0.18	na	nd
	TCRBV07	TCRBV07-08*01	TCRBD01-01*01	TCRBJ02-07*01	151	AAGATCCAGCGCACACAGCAGGAGGACTCCGCCGTGTATCTCTGTGCCAGCAGCTTAGGCCAGGCCTACGAGCAGTACTTCGGGCCG	0.17	na	nd
	TCRBV28	TCRBV28-01*01	TCRBD02-01	TCRBJ02-01*01	646	CTGGAGTCCGCCAGCACCAACCAGACATCTATGTACCTCTGTGCCAGCAGTTTGACTACAACACGGAATGAGCAGTTCTTCGGGCCA	0.81	Vb 3	8.17
	TCRBV11	TCRBV11-03*01	TCRBD02-01	TCRBJ01-01*01	349	AAGATCCAGCCTGCAGAGCTTGGGGACTCGGCCGTGTATCTCTGTGCCAGCAGCGTAAGTTTAGCAACGGAAGCTTTCTTTGGACAA	0.44	na	na
TEN-13	TCRBV06	TCRBV06-01*01	TCRBD02-01*01	TCRBJ01-05*01	201	GAGTCGGCTGCTCCCTCCCAGACATCTGTGTACTTCTGTGCCAGCAGTTGGGGGTCGGGGGGCAATCAGCCCCAGCATTTTGGTGAT	0.25	na	na
	TCRBV05	TCRBV05-01*01	na	TCRBJ02-02*01	172	GTGAGCACCTTGGAGCTGGGGGACTCGGCCCTTTATCTTTGCGCCAGCAGCTTTGATGGGGGAGACGGGGAGCTGTTTTTTGGAGAA	0.21	Vb 5.1	5.03
	TCRBV06	TCRBV06-05*01	TCRBD02-01*02	TCRBJ02-01*01	146	TCGGCTGCTCCCTCCCAGACATCTGTGTACTTCTGTGCCAGCAGTTACACGGGCGGGAGGGCCTACAATGAGCAGTTCTTCGGGCCA	0.18	Vb 13.1	4.02
	TCRBV06	TCRBV06-05*01	TCRBD02-01*01	TCRBJ02-05*01	97	TCGGCTGCTCCCTCCCAGACATCTGTGTACTTCTGTGCCAGCAGTTTCGTGGGCGGGGGGGGCCGAGAGACCCAGTACTTCGGGCCA	0.30	Vb 13.1	na
	TCRBV07	TCRBV07-03*01	TCRBD01-01*01	TCRBJ01-01*01	87	AAGATCCAGCGCACAGAGCGGGGGGACTCAGCCGTGTATCTCTGTGCCAGCAGCTGGACAGAGAACACTGAAGCTTTCTTTGGACAA	0.27	na	na
TEN-14	TCRBV07	TCRBV07-08*01	unknown	TCRBJ01-05*01	79	ACTCTGAAGATCCAGCGCACACAGCAGGAGGACTCCGCCGTGTATCTCTGTGCCAGCCCCTTGTGGCAGCCCCAGCATTTTGGTGAT	0.24	na	na
	TCRBV05	TCRBV05-06*01	unknown	TCRBJ02-01*01	50	CTGAATGTGAACGCCTTGTTGCTGGGGGACTCGGCCCTCTATCTCTGTGCCAGCAGCTGGGGGATCAATGAGCAGTTCTTCGGGCCA	0.15	Vb 5.2	na
	TCRBV29	TCRBV29-01*01	TCRBD01-01*01	TCRBJ02-02*01	47	ACTGTGAGCAACATGAGCCCTGAAGACAGCAGCATATATCTCTGCAGCGTTGGGGCCACGAACACCGGGGAGCTGTTTTTTGGAGAA	0.14	Vb 4	na
	TCRBV06	TCRBV06-05*01	unknown	TCRBJ02-03*01	1504	AGGCTGCTGTCGGCTGCTCCCTCCAGACATCTGTGTACTTCTGTGCCAGCAGTTTCTCGGGTTCGGATACGCAGTATTTTGGCCCA	6.17	Vb 13.1	48
	TCRBV21	TCRBV21-01*01	unknown	TCRBJ01-01*01	877	TTGGAGATCCAGTCCACGGAGTCAGGGGACACAGCACTGTATTTCTGTGCCAGCTCCTGGGGGAACACTGAAGCTTTCTTTGGACAA	3.60	na	na
TEN-15	TCRBV12	TCRBV12	unknown	TCRBJ01-05*01	721	ATCCAGCCCTCAGAACCCAGGGACTCAGCTGTGTACTTCTGTGCCAGCAGTGTGAATTATAGCAATCAGCCCAGCATTTTGGTGAT	2.96	Vb 8	13.8
	TCRBV07	TCRBV07-09	TCRBD02-01*01	TCRBJ02-07*01	250	CAGCGCACAGAGCAGGGGGACTCGGCCATGTATCTCTGTGCCAGCACCCCGGGGGATAGGGCAACCTACGAGCAGTACTTCGGGCCG	1.02	na	na
	TCRBV12	TCRBV12	unknown	TCRBJ01-04*01	234	ATCCAGCCCTCAGAACCCAGGGACTCAGCTGTGTACTTCTGTGCCAGCAGTCCGAATTATTCCAATGAAAAACTGTTTTTTGGCAGT	0.96	Vb 8	13.8
	TCRBV19	TCRBV19-01	TCRBD01-01*01	TCRBJ02-02*01	6434	GTGACATCGGCCCAAAAGAACCCGACAGCTTTCTATCTCTGTGCCAGTAGTAAGGTACAGACCCCGGGGGAGCTGTTTTTTGGAGAA	13.50	Vb 17	na
	TCRBV12	TCRBV12	TCRBD01-01*01	TCRBJ01-01*01	6380	CAGCCCTCAGAACCCAGGGACTCAGCTGTGTACTTCTGTGCCAGCAGTCCGAATGACGGACAGGGGGATGAAGCTTTCTTTGGACAA	13.38	Vb 8	na
TEN-16	TCRBV10	TCRBV10-01	TCRBD02-01*02	TCRBJ02-03*01	1119	CTGGAGTCTGCTGCCTCCTCCCAGACATCTGTATATTTCTGCGCCAGCAGTGATAGCGGGAGCCCAATACCGGAGTATTTGGCCCA	2.35	Vb 12	na
	TCRBV02	TCRBV02-01*01	TCRBD01-01*01	TCRBJ02-07*01	682	ATCCGGTCCACAAAGCTGGAGGACTCAGCCATGTACTTCTGTGCCAGCAGTCGGACAGGGGGGATTTACGAGCAGTACTTCGGGCCG	1.43	Vb 22	na
	TCRBV07	TCRBV07-06*01	TCRBD02-01*01	TCRBJ01-04*01	485	CGCACAGAGCAGCGGGACTCGGCCATGTATCGCTGTGCCAGCAGCTTAGCGCCGGGGTCAACTAATGAAAAACTGTTTTTTGGCAGT	1.02	na	na

Table S5

Patient	V family	TCRBV	TCRBD	TCRBJ	Templates	CDR3 rearrangement	Productive frequency	Respective anti-Vβ mAb	% Vβ+ cells among CD3+CD8+ T cells as determined by FACs analysis
	TCRBV05	TCRBV05-06*01	unresolved	TCRBJ01-01*01	499	AACGCCTTGTTGCTGGGGGACTCGGCCCTCTATCTCTGTGCCAGCAGTTGGGTCCAGCTAATGAACACTGAAGCTTTCTTTGGACAA	3.65	Vb 1	na
	TCRBV04	TCRBV04-01*01	unresolved	TCRBJ01-02*01	404	CACGCCCTGCAGCCAGAAGACTCAGCCCTGTATCTCTGCGCCAGCAGCCAAGATCGGGGCAGTTACTATGGCTACACCTTCGGTTCG	0.23	Vb 13.6	na
MPE-1	TCRBV03	unresolved	TCRBD01-01*01	TCRBJ01-04*01	253	TCCCTGGAGCTTGGTGACTCTGCTGTGTATTTCTGTGCCAGCAGCCAATTATCTGGTCAGATTAATGAAAAACTGTTTTTTGGCAGT	0.17	Vb 22	na
	TCRBV07	TCRBV07-06*01	TCRBD01-01*01	TCRBJ02-02*01	246	ATCCAGCGCACAGAGCAGCGGGACTCGGCCATGTATCGCTGTGCCAGCAGCTTAGTACAGGGGGCCGGGGAGCTGTTTTTTGGAGAA	0.15	Vb 13.1	na
	TCRBV09	TCRBV09-01	TCRBD01-01*01	TCRBJ02-07*01	232	AGCTCTCTGGAGCTGGGGGACTCAGCTTTGTATTTCTGTGCCAGCAGCGTAGGGCACAGCACCTCCTACGAGCAGTACTTCGGGCCG	0.15	Vb 13.1	na
	TCRBV27	TCRBV27-01*01	TCRBD02-01	TCRBJ01-06*01	660	GAGTCGCCCAGCCCCAACCAGACCTCTCTGTACTTCTGTGCCAGCACCCCGGCGGGCGACTATAATTCACCCCTCCACTTTGGGAAC	0.39	Vb 14	na
	TCRBV04	TCRBV04-03*01	TCRBD01-01*01	TCRBJ02-02*01	654	CACACCCTGCAGCCAGAAGACTCGGCCCTGTATCTCTGCGCCAGCAGCCCGACCAGGGGATATGCCGGGGAGCTGTTTTTTGGAGAA	0.38	Vb 7.2	na
MPE-2	TCRBV11	TCRBV11-02*02	TCRBD01-01*01	TCRBJ01-02*01	452	ATCCAGCCTGCAAAGCTTGAGGACTCGGCCGTGTATCTCTGTGCCAGCAGCACAGCCGGGACAGGGTATGGCTACACCTTCGGTTCG	0.27	Vb 21.3	na
	TCRBV03	unresolved	TCRBD01-01*01	TCRBJ01-02*01	399	GAGCTTGGTGACTCTGCTGTGTATTTCTGTGCCAGCAGCCAAGGTTTAAAAGTAGGGGCAACTAACTATGGCTACACCTTCGGTTCG	0.23	unknown	na
	TCRBV02	TCRBV02-01*01	TCRBD02-01*01	TCRBJ01-02*01	334	ATCCGGTCCACAAAGCTGGAGGACTCAGCCATGTACTTCTGTGCCAGCAGTGAAGCGCGGGGAAGCTATGGCTACACCTTCGGTTCG	0.20	Vb 22	na
	TCRBV05	TCRBV05-04*01	TCRBD01-01*01	TCRBJ01-02*01	547	GTGAACGCCTTGGAGCTGGACGACTCGGCCCTGTATCTCTGTGCCAGCAGCTTGGGGTGGGCTGACTATGGCTACACCTTCGGTTCG	1.48	unknown	na
	TCRBV04	TCRBV04-01*01	unknown	TCRBJ01-02*01	334	CACGCCCTGCAGCCAGAAGACTCAGCCCTGTATCTCTGCGCCAGCAGGTCAGAGCCGGCCCCTAACTATGGCTACACCTTCGGTTCG	0.90	Vb 7.1	6.36
MPE-3	TCRBV07	TCRBV07-02*01	TCRBD02-01	TCRBJ01-02*01	175	ACTCTGACGATCCAGCGCACACAGCAGGAGGACTCGGCCGTGTATCTCTGTGCCAGCAGCTTAAGCCTTGGCTACACCTTCGGTTCG	0.47	unknown	na
	TCRBV07	TCRBV07-09	TCRBD01-01*01	TCRBJ01-02*01	137	ACAGAGCAGGGGGACTCGGCCATGTATCTCTGTGCCAGCAGCCCACCACAGGGGGCGCGGGGGATCTATGGCTACACCTTCGGTTCG	0.37	unknown	na
	TCRBV20	TCRBV20	unknown	TCRBJ02-02*01	136	GTGACCAGTGCCCATCCTGAAGACAGCAGCTTCTACATCTGCAGTGCTAGACCGGGCCAGAACACCGGGGAGCTGTTTTTTGGAGAA	0.37	unknown	na
	TCRBV24	TCRBV24	unknown	TCRBJ02-04*01	106	TCTGCCATCCCCAACCAGACAGCTCTTTACTTCTGTGCCACCAGTGGCCCAATGTTAATAGCCAAAAACATTCAGTACTTCGGCGCC	1.84	unknown	na
	TCRBV30	TCRBV30-01*01	unknown	TCRBJ01-01*01	90	TCTAAGAAGCTCCTTCTCAGTGACTCTGGCTTCTATCTCTGTGCCTGGAGTGTACTGAGACGCAGACCTGATGCTTTCTTTGGACAA	1.56	Vb 20	6.07
MPE-4	TCRBV09	TCRBV09-01	unknown	TCRBJ01-01*01	89	AACCTGAGCTCTCTGGAGCTGGGGGACTCAGCTTTGTATTTCTGTGCCAGCAGCGAGTGGACCGTAAGCGAAGCTTTCTTTGGACAA	1.54	Vb 1	12.5
	TCRBV05	TCRBV05-04*01	TCRBD02-01	TCRBJ02-03*01	77	TTGGAGCTGGACGACTCGGCCCTGTATCTCTGTGCCAGCAGCCCCCAGGGCCTAGCGATACCAGGGGATACGCAGTATTTTGGCCCA	1.33	unknown	na
	TCRBV19	TCRBV19-01	TCRBD02-01	TCRBJ02-07*01	57	ACTGTGACATCGGCCCAAAAGAACCCGACAGCTTTCTATCTCTGTGCCACCCATGCGTCAAGTTCCTACGAGCAGTACTTCGGGCCG	0.99	Vb 17	12.2
	TCRBV02	TCRBV02-01*01	TCRBD01-01*01	TCRBJ01-05*01	162	CTGGAGGACTCAGCCATGTACTTCTGTGCCAGCAGTCCCCTTAGACAGGGCATCGCCTCTAGCAATCAGCCCCAGCATTTTGGTGAT	1.92	Vb 22	5.68
	TCRBV19	TCRBV19-01	TCRBD02-01*02	TCRBJ02-03*01	73	TCGGCCCAAAAGAACCCGACAGCTTTCTATCTCTGTGCCAGTAGTATAGGCCTAGCGGGACTCACAGATACGCAGTATTTTGGCCCA	0.86	Vb 17	5.07
MPE-5	TCRBV09	TCRBV09-01	TCRBD02-01	TCRBJ02-01*01	71	CTGGAGCTGGGGGACTCAGCTTTGTATTTCTGTGCCAGCAGCGTAGATCCAGGGCCTAGCGGGCGTAATGAGCAGTTCTTCGGGCCA	0.84	Vb 1	2.1
	TCRBV07	TCRBV07-06*01	TCRBD02-01	TCRBJ01-02*01	69	ACGATCCAGCGCACAGAGCAGCGGGACTCGGCCATGTATCGCTGTGCCAGCAGCTTAGGCGAGTACTATGGCTACACCTTCGGTTCG	0.82	unknown	na
	TCRBV02	TCRBV02-01*01	unknown	TCRBJ01-03*01	64	CGGTCCACAAAGCTGGAGGACTCAGCCATGTACTTCTGTGCCAGCAGTCCCATGGGGATCTCTGGAAACACCATATATTTTGGAGAG	0.76	Vb 22	5.68
	TCRBV07	TCRBV07-03*01	TCRBD02-01*02	TCRBJ01-03*01	771	ACAGAGCGGGGGGACTCAGCCGTGTATCTCTGTGCCAGCACCCTCCGAAAGGCGGGAGGGTCTGGAAACACCATATATTTTGGAGAG	18.01	unknown	na
	TCRBV28	TCRBV28-01*01	TCRBD01-01*01	TCRBJ01-01*01	68	TCCGCCAGCACCAACCAGACATCTATGTACCTCTGTGCCAGCAGTTCGGTGTTCAGGACAGGGGCCACTGAAGCTTTCTTTGGACAA	1.59	Vb 3	na
MPE-6	TCRBV25	TCRBV25-01*01	TCRBD02-01*01	TCRBJ01-01*01	24	CTGGAGTCTGCCAGGCCCTCACATACCTCTCAGTACCTCTGTGCCAGCACGAGACCGGGGTCGAACACTGAAGCTTTCTTTGGACAA	0.56	Vb 11	na
	TCRBV07	TCRBV07-09	TCRBD02-01*02	TCRBJ02-01*01	22	GAGCAGGGGGGACTCGGCCATGTATCTCTGTGCCAGCAGCTTAGCTCTTTTGCGGCGGGATGTCTACAATGAGCAGTTCTTCGGGCCA	0.51	unknown	na
	TCRBV09	TCRBV09-01	TCRBD02-01	TCRBJ01-05*01	21	AGCTCTCTGGAGCTGGGGGACTCAGCTTTGTATTTCTGTGCCAGCAGCGAGGACGGGGGACTGAATCAGCCCCAGCATTTTGGTGAT	0.49	Vb 1	na
	TCRBV06	TCRBV06-01*01	TCRBD02-01*01	TCRBJ01-03*01	489	AGGCTGGAGTCGGCTGCTCCCTCCCAGACATCTGTGTACTTCTGTGCCAGCAGTGCATTTCTTACGGGGTCCATATATTTTGGAGAG	1.24	unknown	na
	TCRBV03	TCRBV03	TCRBD02-01	TCRBJ02-02*01	243	ATCAATTCCCTGGAGCTTGGTGACTCTGCTGTGTATTTCTGTGCCAGCAACCAAGGGACTCGCACCGGGGAGCTGTTTTTTGGAGAA	0.62	unknown	na
MPE-7	TCRBV15	TCRBV15-01*01	TCRBD01-01*01	TCRBJ01-01*01	207	CTTGACATCCGCTCACCAGGCCTGGGGGACGCAGCCATGTACCTGTGTGCCACCAGCAGAGATCGACAGGAAGCTTTCTTTGGACAA	0.52	unknown	na
	TCRBV05	TCRBV05-03	TCRBD01-01*01	TCRBJ01-03*01	171	AGTGCCTTGGAGCTGGGGGACTCGGCCCTGTATCTCTGTGCCAGAAGCAGGGGAATTAGGTCTGGAAACACCATATATTTTGGAGAG	0.43	unknown	na
	TCRBV11	TCRBV11-03*01	TCRBD02-01*02	TCRBJ02-07*01	132	AAGATCCAGCCTGCAGAGCTTGGGGACTCGGCCGTGTATCTCTGTGCCAGCAGCTTAACGGAGGCCTACGAGCAGTACTTCGGGCCG	0.33	unknown	na

Table S6

Patient	V family	TCRBV	TCRBD	TCRBJ	Templates	CDR3 rearrangement	Productive frequency	Respective anti-Vβ mAb	% Vβ+ cells among CD3+CD8+ T cells as determined by FACs analysis
	TCRBV05	TCRBV05-04*01	TCRBD01-01*01	TCRBJ01-02*01	621	GTGAACGCCTTGGAGCTGGACGACTCGGCCCTGTATCTCTGTGCCAGCAGCTTGGGGTGGGCTGACTATGGCTACACCTTCGGTTCG	3.33	unknown	na
	TCRBV05	TCRBV05-06*01	TCRBD01-01*01	TCRBJ01-04*01	391	GTGAACGCCTTGTTGCTGGGGGACTCGGCCCTCTATCTCTGTGCCAGCAGCGACAGATACAGGGCCGAAAAACTGTTTTTTGGCAGT	2.10	Vb 5.2	0.81
MPE-3	TCRBV04	TCRBV04-03*01	TCRBD02-01*02	TCRBJ02-01*01	386	CTGCAGCCAGAAGACTCGGCCCTGTATCTCTGCGCCAGCAGCCCATCTGGGGGAGGGCGACTCTCCAATGAGCAGTTCTTCGGGCCA	2.07	Vb 7.2	0
	TCRBV15	TCRBV15-01*01	TCRBD02-01*02	TCRBJ02-05*01	377	ATCCGCTCACCAGGCCTGGGGGACGCAGCCATGTACCTGTGTGCCACCAGCCGAACGGGGAGGTGGGAGACCCAGTACTTCGGGCCA	2.02	unknown	na
	TCRBV11	TCRBV11-02*02	TCRBD01-01*01	TCRBJ02-07*01	354	ATCCAGCCTGCAAAGCTTGAGGACTCGGCCGTGTATCTCTGTGCCAGCAGCTCCCGGGACAGGGGCTACGAGCAGTACTTCGGGCCG	1.90	Vb 21.3	3.94
	TCRBV07	TCRBV07-09	TCRBD01-01*01	TCRBJ01-02*01	101	ATCCAGCGCACAGAGCAGGGGGACTCGGCCATGTATCTCTGTGCCAGCAGCTTAGCGGGGACAGGATATGGCTACACCTTCGGTTCG	2.10	unknown	na
	TCRBV06	TCRBV06	TCRBD01-01*01	TCRBJ01-02*01	59	TCGGCTGCTCCCTCCCAGACATCTGTGTACTTCTGTGCCAGCAGTCCCGGGACAGGCTCTCTTGGCTATGGCTACACCTTCGGTTCG	1.23	unknown	na
MPE-4	TCRBV07	TCRBV07-09	unknown	TCRBJ01-03*01	51	ACAGAGCAGGGGGACTCGGCCATGTATCTCTGTGCCAGCAGCTCACTTACAGTACTCCTCGGGGGAAACACCATATATTTTGGAGAG	1.06	unknown	na
	TCRBV05	TCRBV05-04*01	TCRBD02-01	TCRBJ02-01*01	19	CTGAATGTGAACGCCTTGGAGCTGGACGACTCGGCCCTGTATCTCTGTGCCAGCAGCTTGGGGACTTTGGAGCAGTTCTTCGGGCCA	0.39	unknown	na
	TCRBV07	TCRBV07-02*01	TCRBD02-01*01	TCRBJ01-02*01	13	ATCCAGCGCACACAGCAGGAGGACTCGGCCGTGTATCTCTGTGCCAGCAGCCCCACGGGGGGCGGGGAATGGCTACACCTTCGGTTCG	0.27	unknown	na
	TCRBV04	TCRBV04-01*01	unknown	TCRBJ02-01*01	283	CTTCACCTACACGCCCTGCAGCCAGAAGACTCAGCCCTGTATCTCTGCGCCAGCAGCCTACTGGACGGAGAGCAGTTCTTCGGGCCA	3.31	Vb 7.1	2.81
	TCRBV10	TCRBV10-03*01	TCRBD01-01*01	TCRBJ02-07*01	281	TCCGCTACCAGCTCCCAGACATCTGTGTACTTCTGTGCCATCAGTGAGGGGGGCGCCGGGACAGGCTCCGAGCAGTACTTCGGGCCG	3.28	Vb 12	7.74
MPE-5	TCRBV20	TCRBV20	TCRBD02-01*02	TCRBJ02-01*01	155	ACCAGTGCCCATCCTGAAGACAGCAGCTTCTACATCTGCAGTGCTAGAGATCTCGAGGTTGGGTGGAATGAGCAGTTCTTCGGGCCA	1.81	unknown	na
	TCRBV07	TCRBV07-09	unknown	TCRBJ01-01*01	127	ATCCAGCGCACAGAGCAGGGGGACTCGGCCATGTATCTCTGTGCCAGCGTACCCTTGTCGGGCAACACTGAAGCTTTCTTTGGACAA	1.48	unknown	na
	TCRBV07	TCRBV07-02*01	TCRBD01-01*01	TCRBJ02-07*01	68	CAGCAGGAGGACTCGGCCGTGTATCTCTGTGCCACCAGGCCCGGGCCGACGAGGGGGCCGAGCTCCTACGAGCAGTACTTCGGGCCG	0.79	unknown	na
	TCRBV03	TCRBV03	TCRBD02-01	TCRBJ02-01*01	447	ATCAATTCCCTGGAGCTTGGTGACTCTGCTGTGTATTTCTGTGCCAGCAGGGGGAGCGGCTCCTACAATGAGCAGTTCTTCGGGCCA	0.68	unknown	na
	TCRBV28	TCRBV28-01*01	TCRBD01-01*01	TCRBJ01-01*01	410	TCCGCCAGCACCAACCAGACATCTATGTACCTCTGTGCCAGCAGTTCGGTGTTCAGGACAGGGGCCACTGAAGCTTTCTTTGGACAA	0.63	Vb 3	na
MPE-6	TCRBV07	TCRBV07-09	TCRBD01-01*01	TCRBJ01-04*01	75	CGCACAGAGCAGGGGGACTCGGCCATGTATCTCTGTGCCAGCAGCCCCGCGTCCGGGACAGAGGGTGAAAAACTGTTTTTTGGCAGT	0.11	unknown	na
	TCRBV28	TCRBV28-01*01	TCRBD02-01*02	TCRBJ02-07*01	74	CTGGAGTCCGCCAGCACCAACCAGACATCTATGTACCTCTGTGCCAGCAGTTTAGGAGGGGTGGCCTACGAGCAGTACTTCGGGCCG	0.11	Vb 3	na
	TCRBV05	TCRBV05-01*01	TCRBD01-01*01	TCRBJ01-02*01	64	AATGTGAGCACCTTGGAGCTGGGGGACTCGGCCCTTTATCTTTGCGCCAGCAGCCGGACAGGCTATTATGGCTACACCTTCGGTTCG	0.10	Vb 5.1	na
	TCRBV30	TCRBV30-01*01	unknown	TCRBJ01-01*01	249	CTGAGTTCTAAGAAGCTCCTTCTCAGTGACTCTGGCTTCTATCTCTGTGCCTGGAGTTTGGAGAACACTGAAGCTTTCTTTGGACAA	0.98	Vb 20	6.42
	TCRBV03	TCRBV03	unknown	TCRBJ01-06*01	140	ATCAATTCCCTGGAGCTTGGTGACTCTGCTGTGTATTTCTGTGCCAGCAGCTCCGGCAATGGGAATTCACCCCTCCACTTTGGGAAC	0.55	unknown	na
MPE-7	TCRBV09	TCRBV09-01	TCRBD01-01*01	TCRBJ02-02*01	125	CTGGGGGACTCAGCTTTGTATTTCTGTGCCAGCAGCCGCCGAAGACGTGCAGGGAATCCGAACACCGGGGAGCTGTTTTTTGGAGAA	0.49	Vb 1	2.72
	TCRBV12	TCRBV12	TCRBD01-01*01	TCRBJ02-07*01	121	ATCCAGCCCTCAGAACCCAGGGACTCAGCTGTGTACTTCTGTGCCAGCAGTTTTGGTGGGACAAATTACGAGCAGTACTTCGGGCCG	0.48	unknown	na
	TCRBV15	TCRBV15-01*01	TCRBD01-01*01	TCRBJ01-01*01	99	CTTGACATCCGCTCACCAGGCCTGGGGGACGCAGCCATGTACCTGTGTGCCACCAGCAGAGATCGACAGGAAGCTTTCTTTGGACAA	0.39	unknown	na

Table S7

sample_name	Sorted Vβ	v_family	v_resolved	d_resolved	j_resolved	templates	amino_acid	rearrangement	productive_frequency
		TCRAV25	TCRAV25-01*01	unresolved	TCRAJ43-01*01	13167	CANNDMRF	CAGCTCCCTGCACATCACAGCCACCCAGACTACAGATGTAGGAACCTACTTCTGTGCCAACAATGACATGCGCTTTGGAGCA	87.6
		TCRAV25	TCRAV25-01*01	unresolved	TCRAJ43-01*01	1309	CANNDMRF	CAGTTCCCTGCACATCACAGCCACCCAGACTACAGATGTAGGAACCTACTTCTGTGCCAACAATGACATGCGCTTTGGAGCA	8.5
TEN-3	Vβ 21,3	TCRAV19	TCRAV19-01*01	unresolved	TCRAJ17-01*01	55	CALSEAHPRGKAAGNKLTF	GGACTCAGCAGTATACTTCTGTGCTCTGAGTGAGGCGCATCCCCGTGGTAAAGCTGCAGGCAACAAGCTAACTTTTGGAGGA	0.4
		TCRAV39	TCRAV39-01*01	unresolved	TCRAJ27-01*01	32	CAVVRPNAGKSTF	CACAGCTGCCGTGCATGACCTCTCTGCCACCTACTTCTGTGCCGTGGTCAGACCCAATGCAGGCAAATCAACCTTTGGGGAT	0.1
		TCRAV20	TCRAV20-01	TCRDD02-01	TCRAJ42-01*01	10	CAVQVLYGGSQGNLIF	TAAACCTGAAGACTCAGCCACTTATCTCTGTGCTGTGCAGGTCTTATATGGAGGAAGCCAAGGAAATCTCATCTTTGGAAAA	0.07
		TCRAV13	TCRAV13-01	TCRDD01-01	TCRAJ39-01*01	284	CADNAGNMLTF	GCACATCACAGAGACCCAACCTGAAGACTCGGCTGTCTACTTCTGTGCCGATAATGCAGGCAACATGCTCACCTTTGGAGGG	86.95
		TCRAV14	TCRAV14-01	TCRDD02-01	TCRAJ53-01*01	24	CAMREGQSGGSNYKLTF	ACTGGGGGACTCAGCAATGTATTTCTGTGCAATGAGAGAGGGCCAGAGTGGAGGTAGCAACTATAAACTGACATTTGGAAAA	7.52
TEN-7	Vβ 13,2	TCRAV29	TCRAV29-01	TCRDD03-01	TCRAJ52-01*01	4	CAANSGYGKLTF	CATTGTGCCCTCCCAGCCTGGAGACTCTGCAGTGTACTTCTGTGCAGCAAATAGCGGCTATGGAAAGCTGACATTTGGACAA	1.62
		TCRAV39	TCRAV39-01*01	TCRDD02-01	TCRAJ45-01*01	2	CAVPPGGGADGLTF	AGCTGCCGTGCATGACCTCTCTGCCACCTACTTCTGTGCCGTCCCCCCAGGAGGAGGTGCTGACGGACTCACCTTTGGCAAA	0.93
		TCRAV12	TCRAV12-01	unknown	TCRAJ50-01*01	2	CVVLYDKVIF	CCTGCTCATCAGAGACTCCAAGCTCAGTGATTCAGCCACCTACCTCTGTGTGGTTCTCTACGACAAGGTGATATTTGGGCCA	0.66
		TCRAV19	TCRAV19-01*01	unknown	TCRAJ30-01*01	1022	CALSVYMNRDDKIIF	CTCACAAGTCGTGGACTCAGCAGTATACTTCTGTGCTCTGAGTGTGTATATGAACAGAGATGACAAGATCATCTTTGGAAAA	51.93
		TCRAV19	TCRAV19-01*01	TCRDD01-01	TCRAJ29-01*01	951	CALSEAWGNTPLVF	AGCCTCACAAGTCGTGGACTCAGCAGTATACTTCTGTGCTCTGAGTGAGGCGTGGGGAAACACACCTCTTGTCTTTGGAAAG	47.88
TEN-9	Vβ 22	TCRAV16	TCRAV12-02	unknown	TCRAJ54-01*01	2	CALRGPAAGNKLTF	ATTTGCTCAAGAGGAAGACTCAGCCATGTATTACTGTGCTCTAAGGGGCCCCGCTGCAGGCAACAAGCTAACTTTTGGAGGA	0.08
		TCRAV12	TCRAV17-01*01	TCRDD01-01	TCRAJ06-01*01	1	CAVTSQGAQKLVF	CAGAGACTCCCAGCCCAGTGATTCAGCCACCTACCTCTGTGCCGTGACTAGCCAGGGAGCCCAGAAGCTGGTATTTGGCCAA	0.05
		TCRAV17	TCRAV16-01*01	TCRDD01-01	TCRAJ17-01*01	1	CATDAGAGGSYIPTF	TTCCCGGGCAGCAGACACTGCTTCTTACTTCTGTGCTACGGACGCGGGGGCAGGAGGAAGCTACATACCTACATTTGGAAGA	0.03
		TCRAV19	TCRAV19-01*01	unknown	TCRAJ30-01*01	128	CALSVYMNRDDKIIF	CTCACAAGTCGTGGACTCAGCAGTATACTTCTGTGCTCTGAGTGTGTATATGAACAGAGATGACAAGATCATCTTTGGAAAA	49.41
		TCRAV19	TCRAV19-01*01	TCRDD01-01	TCRAJ29-01*01	112	CALSEAWGNTPLVF	AGCCTCACAAGTCGTGGACTCAGCAGTATACTTCTGTGCTCTGAGTGAGGCGTGGGGAAACACACCTCTTGTCTTTGGAAAG	42.88
TEN-9	Vβ 13,2	TCRAV26	TCRAV26-02	TCRDD02-01	TCRAJ34-01*01	4	CILLNTDKLIF	GATCCTGCACCGTGCTACCTTGAGAGATGCTGCTGTGTACTACTGCATCCTCCTCAACACCGACAAGCTCATCTTTGGGACT	1.7
		TCRAV17	TCRAV17-01*01	TCRDD01-01	TCRAJ06-01*01	3	CATDAGAGGSYIPTF	TTCCCGGGCAGCAGACACTGCTTCTTACTTCTGTGCTACGGACGCGGGGGCAGGAGGAAGCTACATACCTACATTTGGAAGA	1.25
		TCRAV19	TCRAV19-01*01	TCRDD02-01	TCRAJ54-01*01	2	CALRPVTPQGAQKLVF	ACAAGTCGTGGACTCAGCAGTATACTTCTGTGCTCTGCGCCCCGTTACCCCTCAGGGAGCCCAGAAGCTGGTATTTGGCCAA	0.57
		TCRAV27	TCRAV27-01*01	TCRDD01-01	TCRAJ26-01*01	170295	CAGDDNYGQNFVF	CACTGCAGCCCAGCCTGGTGATACAGGCCTCTACCTCTGTGCAGGGGACGATAACTATGGTCAGAATTTTGTCTTTGGTCCC	89.84
		TCRAV21	TCRAV21-01	unknown	TCRAJ20-01*01	817	CAVRPNDYKLSF	CATTGCAGCTTCTCAGCCTGGTGACTCAGCCACCTACCTCTGTGCTGTGAGGCCAAACGACTACAAGCTCAGCTTTGGAGCC	4.,11
TEN-10	Vβ 3	TCRDV02	TCRDV02-01	TCRDD01-01	TCRDJ01-01*01	752	CACDPVSWETGDQTDKLIF	AGATGAAGGGTCTTACTACTGTGCCTGTGACCCTGTTTCCTGGGAGACTGGGGATCAAACCGATAAACTCATCTTTGGAAAA	39.76
		TCRAV21	TCRAV21-01	unknown	TCRAJ47-01*01	544	CAVKELEYGNKLVF	AGCTTCTCAGCCTGGTGACTCAGCCACCTACCTCTGTGCTGTGAAGGAATTGGAATATGGAAACAAACTGGTCTTTGGCGCA	29.68
		TCRAV21	TCRAV21-01	unknown	TCRAJ49-01*01	436	CAVRPTFTGNQFYF	AGCTTCTCAGCCTGGTGACTCAGCCACCTACCTCTGTGCTGTGAGGCCAACTTTCACCGGTAACCAGTTCTATTTTGGGACA	22.82
		TCRAV39	TCRAV39-01*01	TCRDD01-01	TCRAJ40-01*01	2732	CAVDIVGYKYIF	CATCACAGCTGCCGTGCATGACCTCTCTGCCACCTACTTCTGTGCCGTGGACATTGTTGGCTACAAATACATCTTTGGAACA	96.08
		TCRAV24	TCRAV24-01*01	unknown	TCRAJ22-01*01	32	CASLSGSARQLTF	CAAAGGATCCCAGCCTGAAGACTCAGCCACATACCTCTGTGCCTCTCTTTCTGGTTCTGCAAGGCAACTGACCTTTGGATCT	1.23
TEN-15	Vβ 14	TCRAV12	TCRAV12-01	TCRDD01-01	TCRAJ41-01*01	11	CVVRDSGYALNF	CATCAGAGACTCCAAGCTCAGTGATTCAGCCACCTACCTCTGTGTGGTGAGGGATTCCGGGTATGCACTCAACTTCGGCAAA	0.42
		TCRAV26	TCRAV26-01	unknown	TCRAJ37-01	9	CIGGFRVCTQL	GATCCTGCCCCACGCTACGCTGAGAGACACTGCTGTGTACTATTGCATCGGCGGATTCCGGGTATGCACTCAACTTCGGCAA	0.38
		TCRAV19	TCRAV19-01*01	unknown	TCRAJ18-01*01	6	CAPDRGSTLGRLYF	AGCCTCACAAGTCGTGGACTCAGCAGTATACTTCTGTGCTCCCGACAGAGGCTCAACCCTGGGGAGGCTATACTTTGGAAGA	0.19
		TCRAV12	TCRAV12-01	TCRDD01-01	TCRAJ41-01*01	177	CVVRDSGYALNF	CATCAGAGACTCCAAGCTCAGTGATTCAGCCACCTACCTCTGTGTGGTGAGGGATTCCGGGTATGCACTCAACTTCGGCAAA	9.,41
		TCRAV29	TCRAV29-01	unknown	TCRAJ49-01*01	3	CAARYTGNQFYF	CATTGTGCCCTCCCAGCCTGGAGACTCTGCAGTGTACTTCTGTGCAGCAAGGTACACCGGTAACCAGTTCTATTTTGGGACA	1.51
TEN-15	Vβ 13,1	TCRAV08	TCRAV08-06	unknown	TCRAJ23-01	2	CAVSRAGSIL	CTTGAGGAAACCCTCAGTCCATATAAGCGACACGGCTGAGTACTTCTGTGCTGTGAGTCGGGCGGGTTCTATTTTGGGACAG	0.35
		TCRAV12	TCRAV12-01	TCRDD01-01	TCRAJ41-01*01	2	CVVRDSVYALNF	CATCAGAGACTCCAAGCTCAGTGATTCAGCCACCTACCTCTGTGTGGTGAGGGATTCCGTGTATGCACTCAACTTCTGCAAA	0.02
		TCRAV08	TCRAV08-06	unknown	TCRAJ49-01*01	2	CAVSRAGSIF	CTTGAGGAAACCCTCAGTCCATATAAGCGACACGGCTGAGTACTTCTGTGCTGTGAGTCGGGCGGGTTCTATTTTTGGGACA	0.02

Table S8

	Target clone	Dominant clonotypes obtained through Vβ sorting					TCR transfectant ID
		Chains	V family	TCRBV	TCRBJ	Rearrangement	
TEN-3	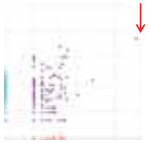	β	TCRBV11	TCRBV11-02*02	TCRBJ02-01*01	CAGCCTGCAAAGCTTGAGGACTCGGCCGTGTATCTCTGTGCCAGCAGCCCCTTCCGTGACTCCTACAATGAGCAGTTCTTCGGGCCA	C1
		α	TCRAV25	TCRAV25-01*01	TCRAJ43-01*01	CAGCTCCCTGCACATCACAGCCACCCAGACTACAGATGTAGGAACCTACTTCTGTGCCAACAATGACATGCGCTTTGGAGCA	
TEN-7	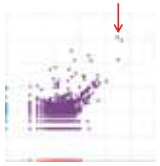	β	TCRBV06	TCRBV06	TCRBJ02-01*01	GAGTCGGCTGCTCCCTCCCAAACATCTGTGTACTTCTGTGCCAGCAGCCCGACTAGCGGGAGTAGTAATGAGCAGTTCTTCGGGCCA	C2
		α	TCRAV13	TCRAV13-01	TCRAJ39-01*01	GCACATCACAGAGACCCAACCTGAAGACTCGGCTGTCTACTTCTGTGCCGATAATGCAGGCAACATGCTCACCTTTGGAGGG	
TEN-9		β	TCRBV02	TCRBV02-01*01	TCRBJ01-05*01	TCCACAAAGCTGGAGGACTCAGCCATGTACTTCTGTGCCAGCAGTGATGTGGGGAGAACTAGCAATCAGCCCCAGCATTTTGGTGAT	C3
		α	TCRAV19	TCRAV19-01*01	TCRAJ30-01*01	CTCACAAGTCGTGGACTCAGCAGTATACTTCTGTGCTCTGAGTGTGTATATGAACAGAGATGACAAGATCATCTTTGGAAAA	
		β	TCRBV02	TCRBV02-01*01	TCRBJ01-05*01	TCCACAAAGCTGGAGGACTCAGCCATGTACTTCTGTGCCAGCAGTGATGTGGGGAGAACTAGCAATCAGCCCCAGCATTTTGGTGAT	C4
		α	TCRAV19	TCRAV19-01*01	TCRAJ29-01*01	AGCCTCACAAGTCGTGGACTCAGCAGTATACTTCTGTGCTCTGAGTGAGGCGTGGGGAAACACACCTCTTGTCTTTGGAAAG	
		β	TCRBV06	TCRBV06	TCRBJ01-01*01	GCTGCTCCCTCCCAAACATCTGTGTACTTCTGTGCCAGCAGTTACTCCGATCCGAGGGACATGAACACTGAAGCTTTCTTTGGACAA	C5
		α	TCRAV19	TCRAV19-01*01	TCRAJ29-01*01	AGCCTCACAAGTCGTGGACTCAGCAGTATACTTCTGTGCTCTGAGTGAGGCGTGGGGAAACACACCTCTTGTCTTTGGAAAG	
		β	TCRBV06	TCRBV06	TCRBJ01-01*01	GCTGCTCCCTCCCAAACATCTGTGTACTTCTGTGCCAGCAGTTACTCCGATCCGAGGGACATGAACACTGAAGCTTTCTTTGGACAA	C6
		α	TCRAV19	TCRAV19-01*01	TCRAJ30-01*01	CTCACAAGTCGTGGACTCAGCAGTATACTTCTGTGCTCTGAGTGTGTATATGAACAGAGATGACAAGATCATCTTTGGAAAA	
TEN-10		β	TCRBV06	TCRBV06	TCRBJ02-02*01	GAGTCGGCTGCTCCCTCCCAAACATCTGTGTACTTCTGTGCCAGCAGTTATGGACAGGTCGCCACCGGGGAGCTGTTTTTTGGAGAA	C7
		α	TCRAV38	TCRAV38-02*01	TCRAJ43-01*01	CAAGATCTCAGACTCACAGCTGGGGGATGCCGCGATGTATTTCTGTGCCTTGTACAATAACAATGACATGCGCTTTGGAGCA	
		β	TCRBV28	TCRBV28-01*01	TCRBJ01-04*01	CTGGAGTCCGCCAGCACCAACCAGACATCTATGTACCTCTGTGCCAGCAGTTTCGGGGGGCCTAATGAAAAACTGTTTTTTGGCAGT	C8
		α	TCRA27	TCRAV27-01*01	TCRAJ26-01*01	AGCCTCACAAGTCGTGGACTCAGCAGTATACTTCTGTGCTCTGAGTGAGGCGTGGGGAAACACACCTCTTGTCTTTGGAAAG	
TEN-15	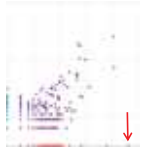	β	TCRBV27	TCRBV27-01*01	TCRBJ02-01*01	CTGGAGTCGCCCAGCCCCAACCAGACCTCTCTGTACTTCTGTGCCAGCAGTCTAGCGGGGGGGCTGGGTGAGCAGTTCTTCGGGCCA	C9
		α	TCRAV39	TCRAV39-01*01	TCRAJ40-01*01	CATCACAGCTGCCGTGCATGACCTCTCTGCCACCTACTTCTGTGCCGTGGACATTGTTGGCTACAAATACATCTTTGGAACA	

Table S9

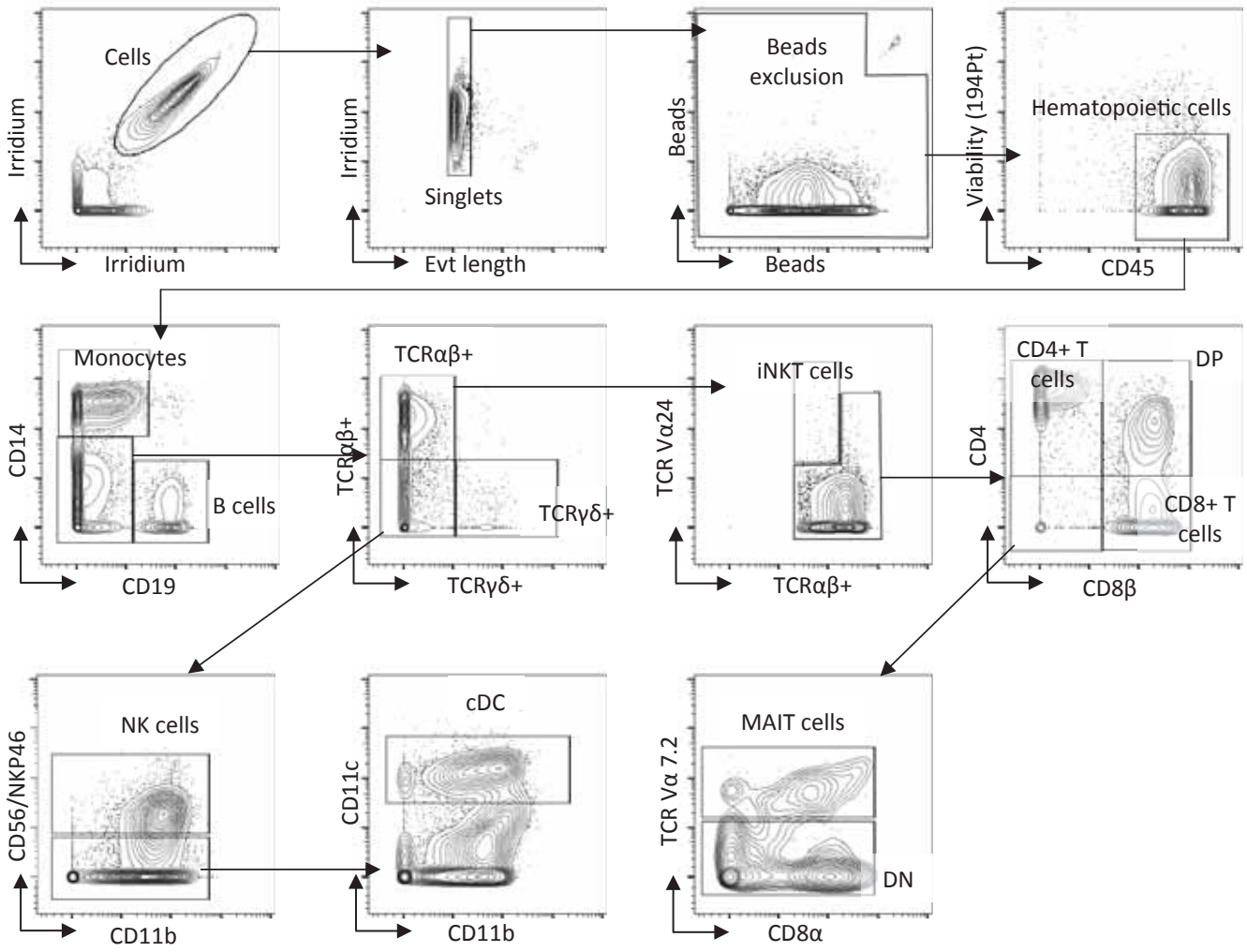
Cells
Irridium
Irridium
Singlets
Evt length
Beads
exclusion
Beads
Beads
Viability (194Pt)
Hematopoietic cells
CD45
Monocytes
CD14
B cells
CD19
TCRαβ+
TCRαβ+
TCRγδ+
TCRγδ+
iNKT cells
TCR Vα24
TCRαβ+
CD4+ T
cells
DP
CD4
CD8+ T
cells
CD8β
NK cells
CD56/NKP46
CD11b
cDC
CD11c
CD11b
MAIT cells
TCR Vα 7.2
DN
CD8α

Figure S1

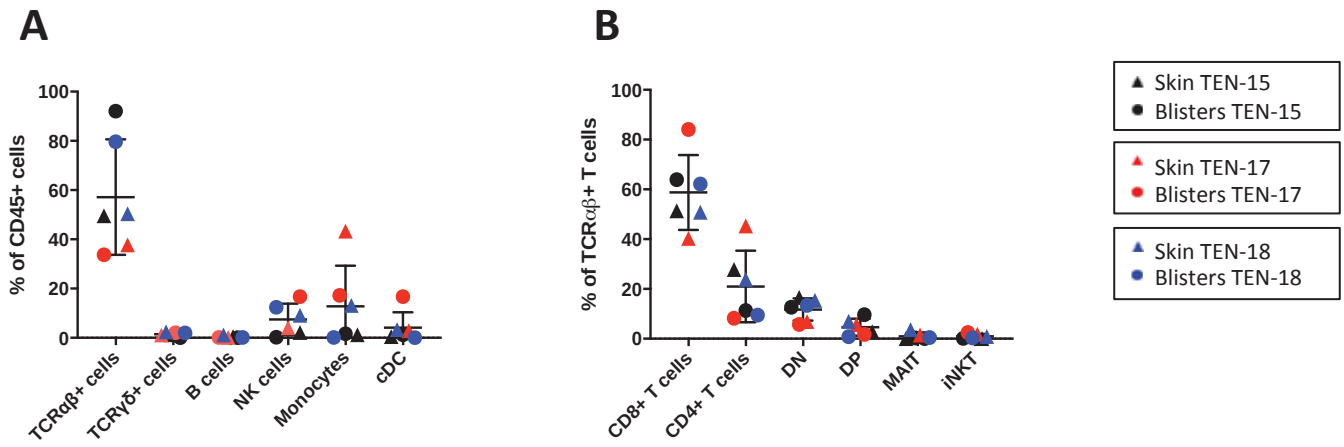
A
B
% of CD45+ cells
100
80
60
40
20
0
TCRαβ+ cells
TCRγδ+ cells
B cells
NK cells
Monocytes
cDC
% of TCRαβ+ T cells
CD8+ T cells
CD4+ T cells
DN
DP
MAIT
iNKT
Skin TEN-15
Blisters TEN-15
Skin TEN-17
Blisters TEN-17
Skin TEN-18
Blisters TEN-18

Figure S2

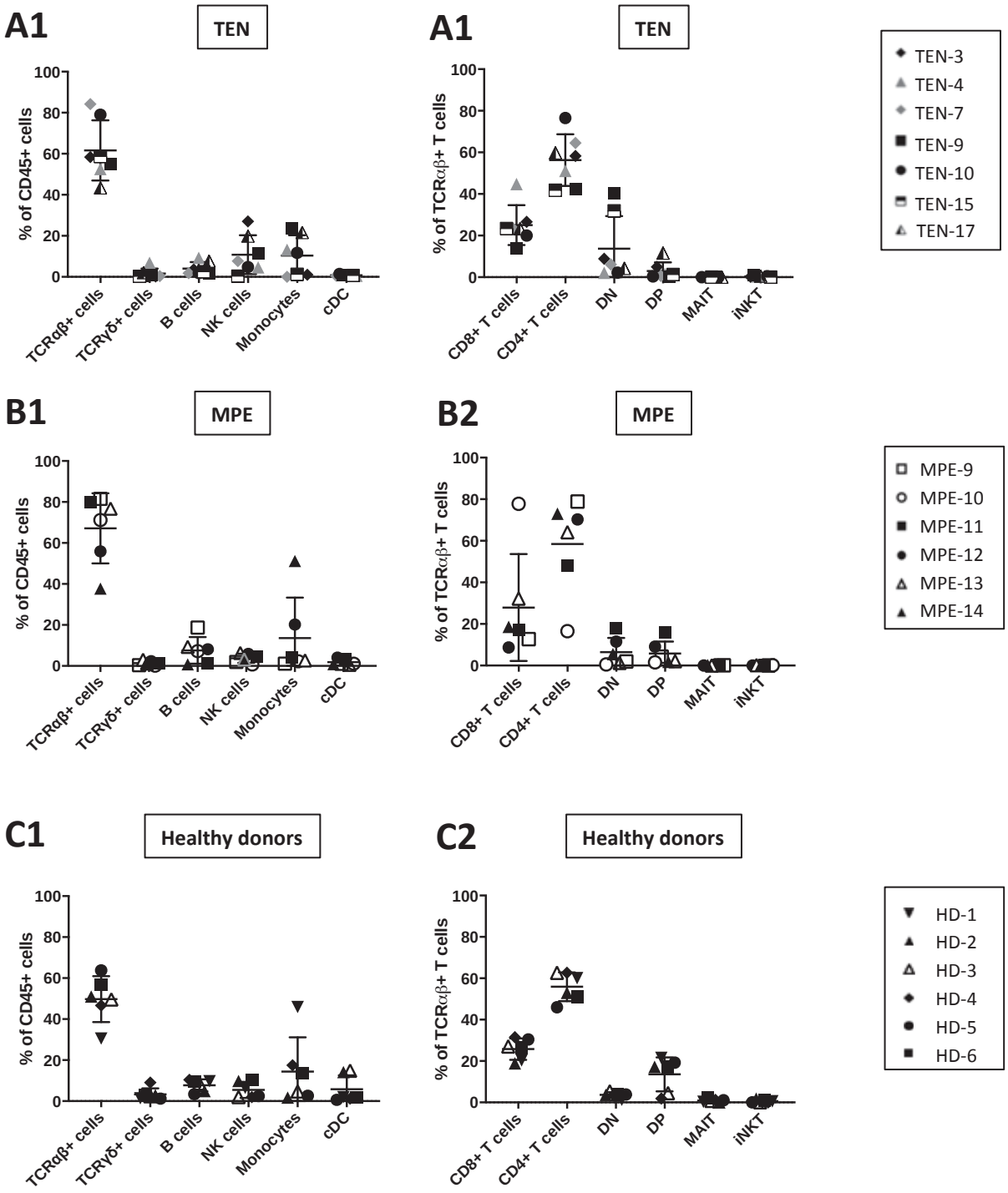
A1
TEN
% of CD45+ cells
TCRαβ+ cells
TCRγδ+ cells
B cells
NK cells
Monocytes
cDC
A1
TEN
% of TCRαβ+ T cells
CD8+ T cells
CD4+ T cells
DN
DP
MAIT
iNKT
TEN-3
TEN-4
TEN-7
TEN-9
TEN-10
TEN-15
TEN-17
B1
MPE
B2
MPE
MPE-9
MPE-10
MPE-11
MPE-12
MPE-13
MPE-14
C1
Healthy donors
C2
Healthy donors
HD-1
HD-2
HD-3
HD-4
HD-5
HD-6

Figure S3

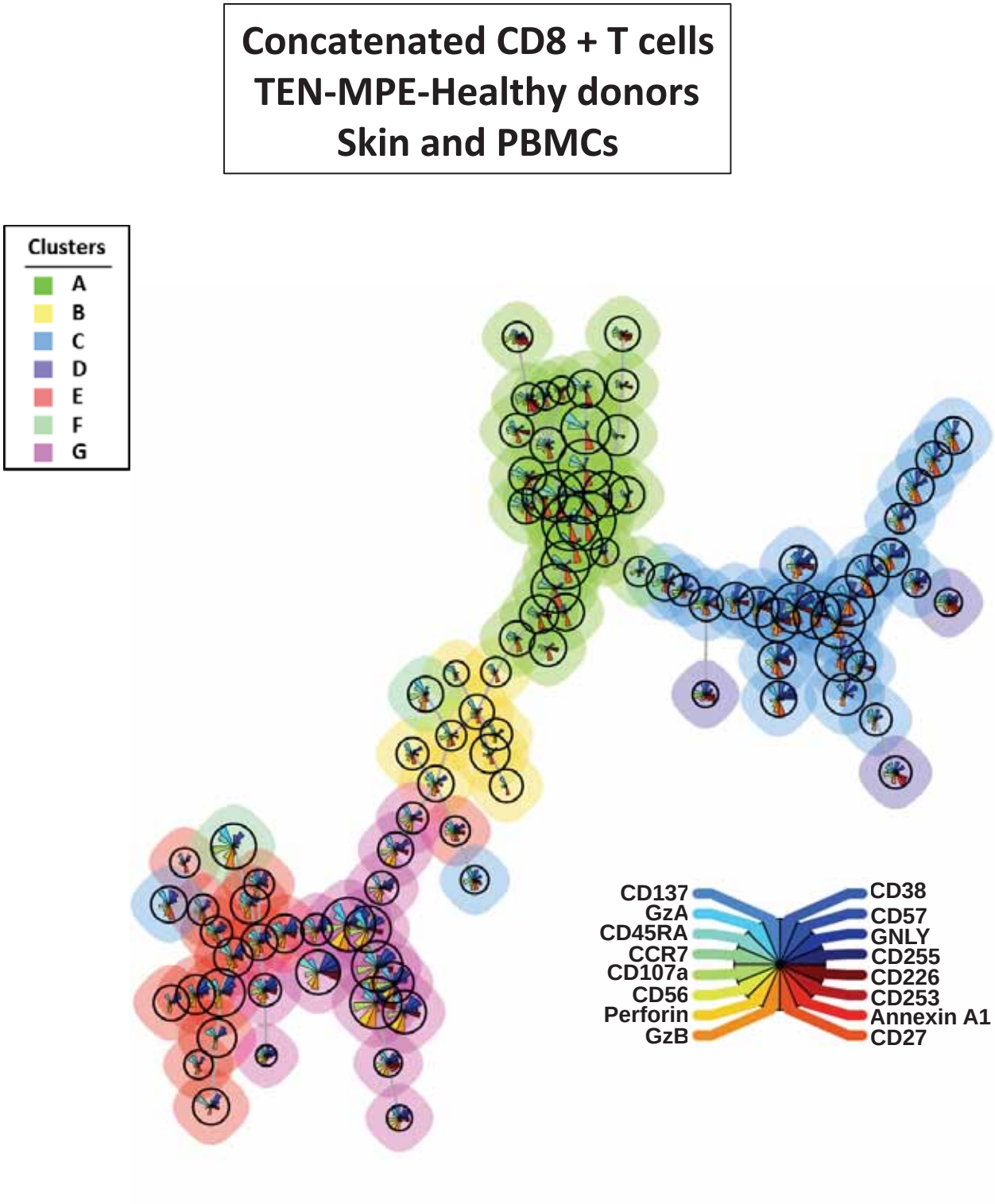
Concatenated CD8 + T cells
TEN-MPE-Healthy donors
Skin and PBMCs
Clusters
A
B
C
D
E
F
G
CD137
GzA
CD45RA
CCR7
CD107a
CD56
Perforin
GzB
CD38
CD57
GNLY
CD255
CD226
CD253
Annexin A1
CD27

Figure S4

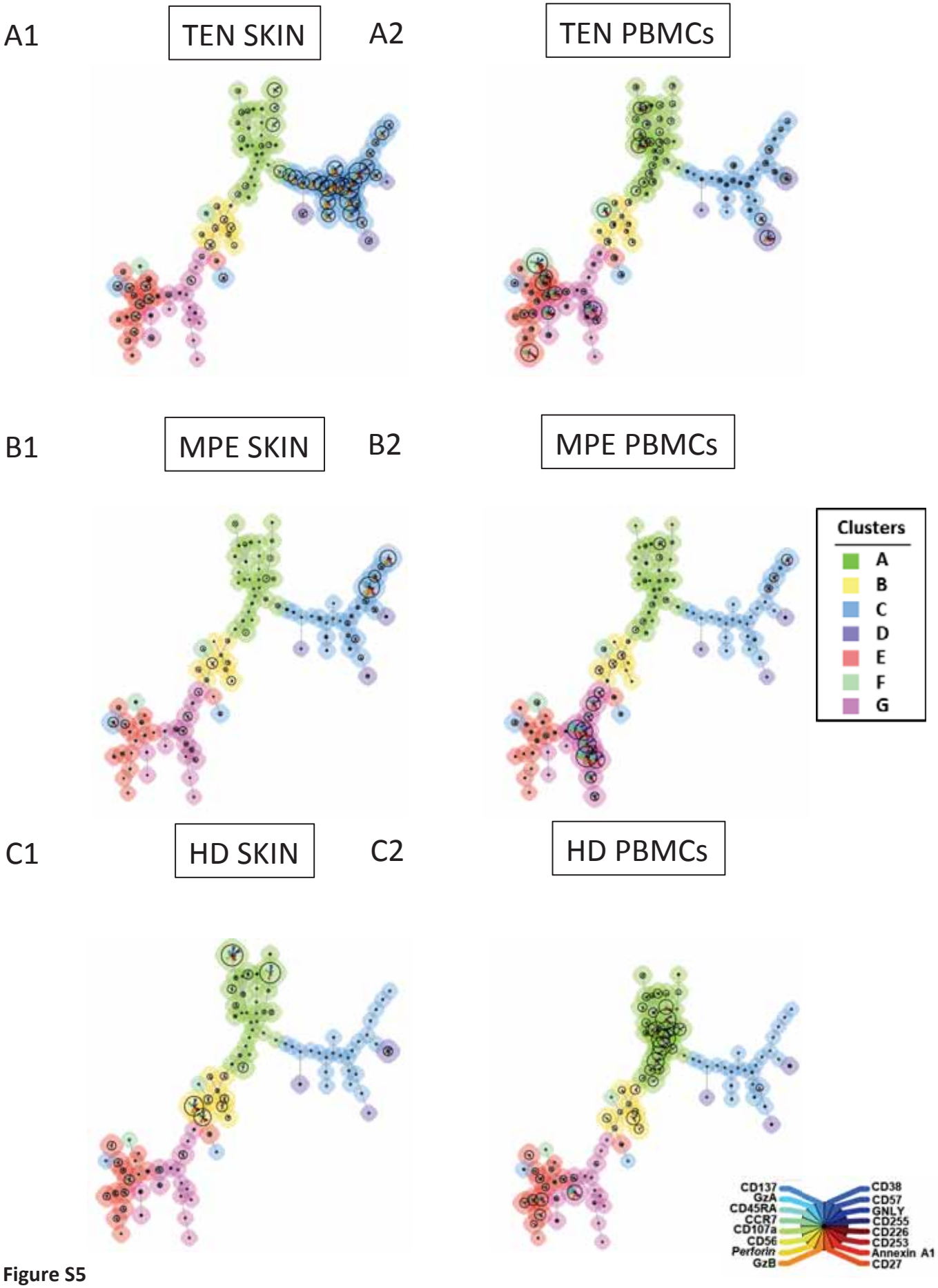
A1
TEN SKIN
A2
TEN PBMCs
B1
MPE SKIN
B2
MPE PBMCs
Clusters
A
B
C
D
E
F
G
C1
HD SKIN
C2
HD PBMCs
CD137
GzA
CD45RA
CCR7
CD107a
CD56
Perforin
GzB
CD38
CD57
GNLY
CD255
CD226
CD253
Annexin A1
CD27

Figure S5

TEN SKIN

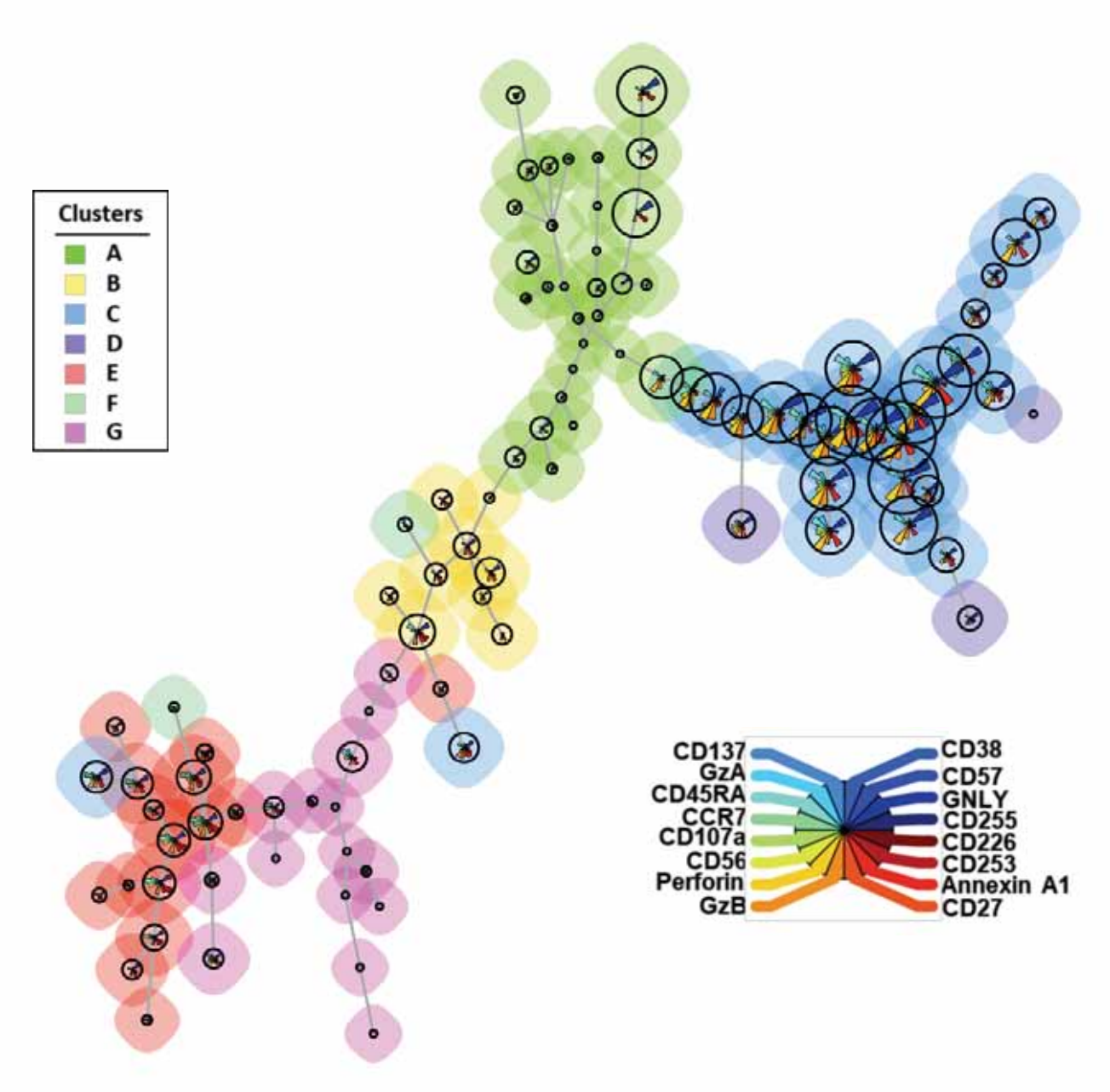

Figure S6

TEN PBMCs

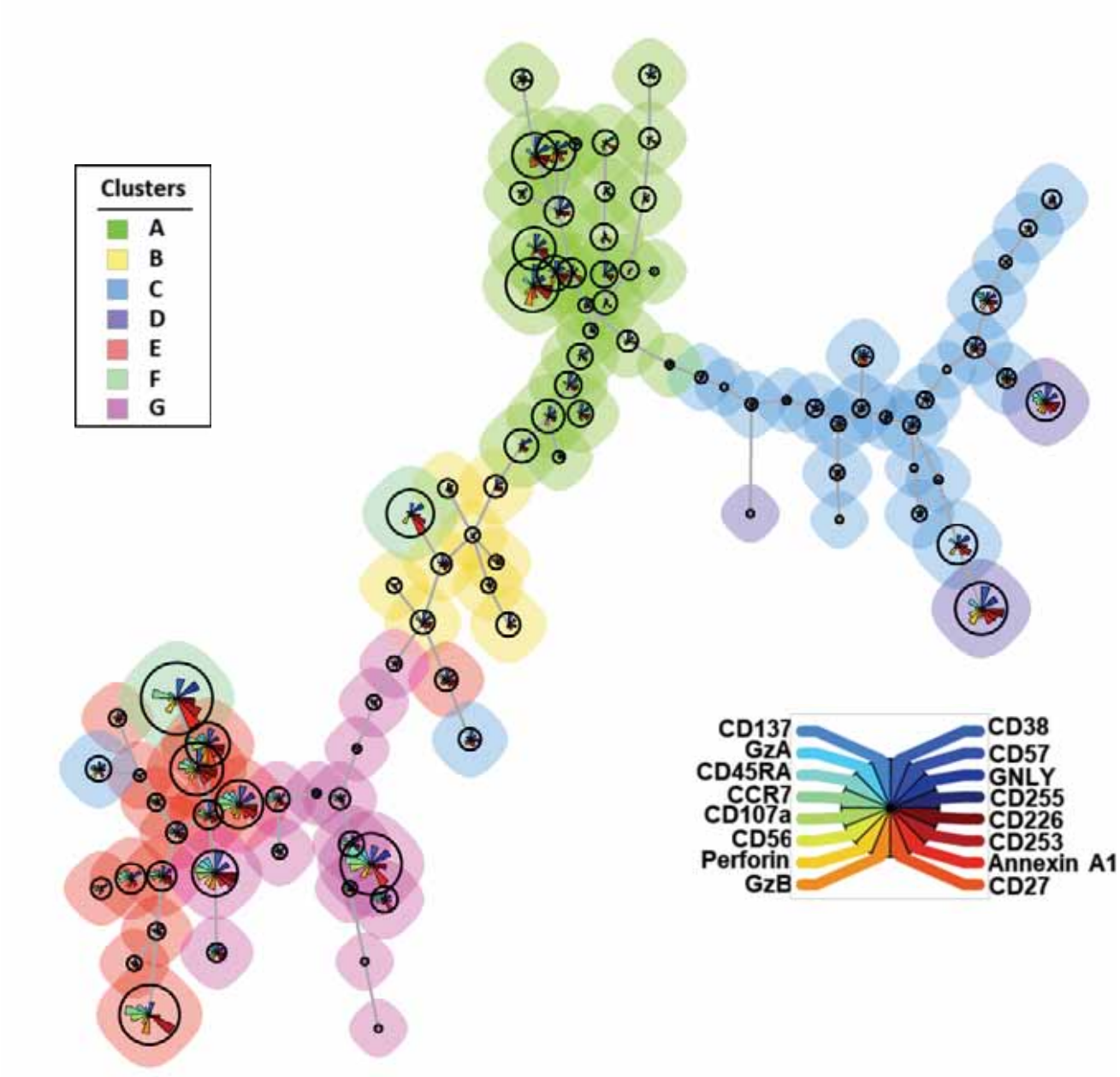

Figure S7

MPE SKIN

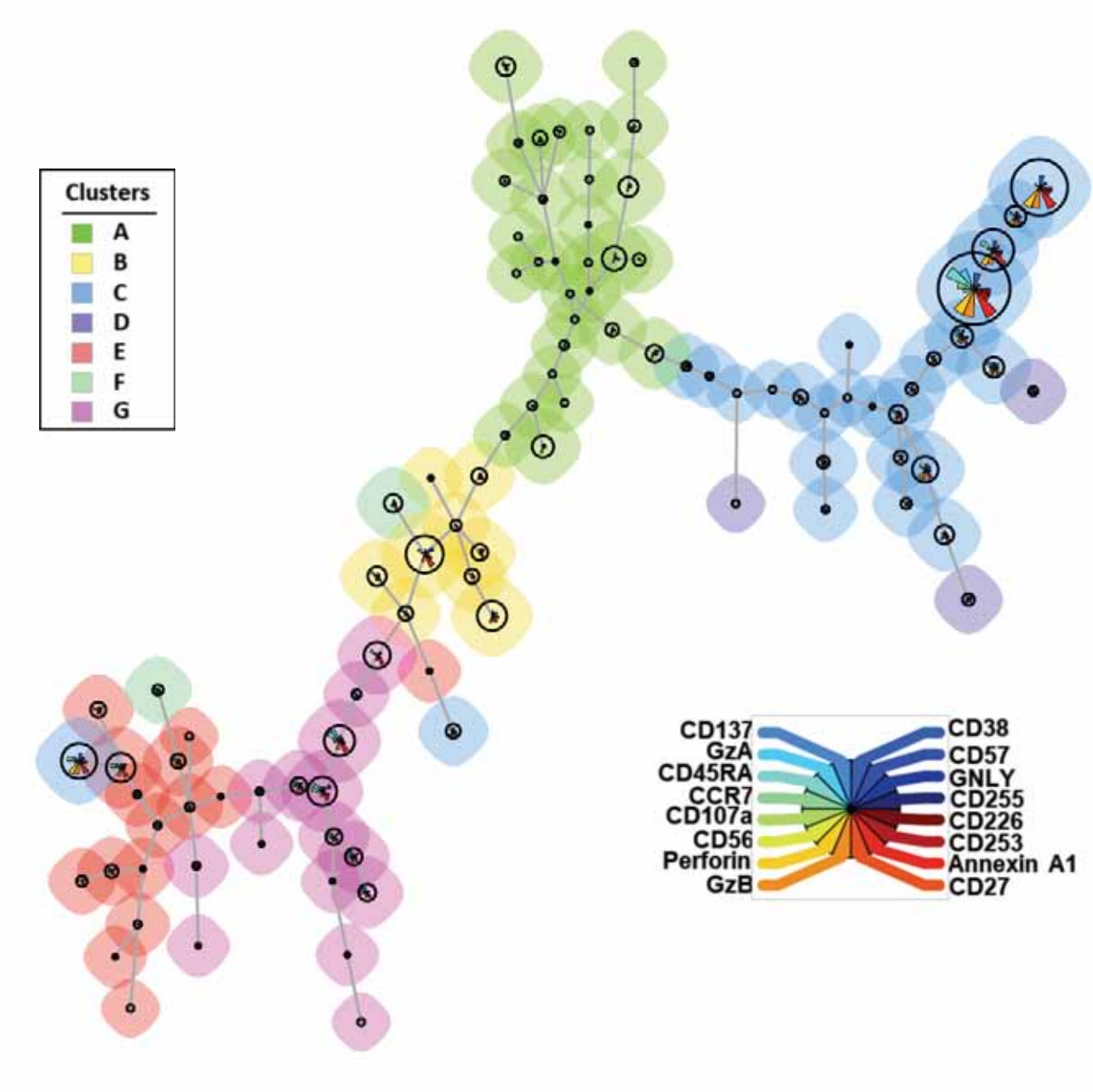

Figure S8

MPE PBMCs

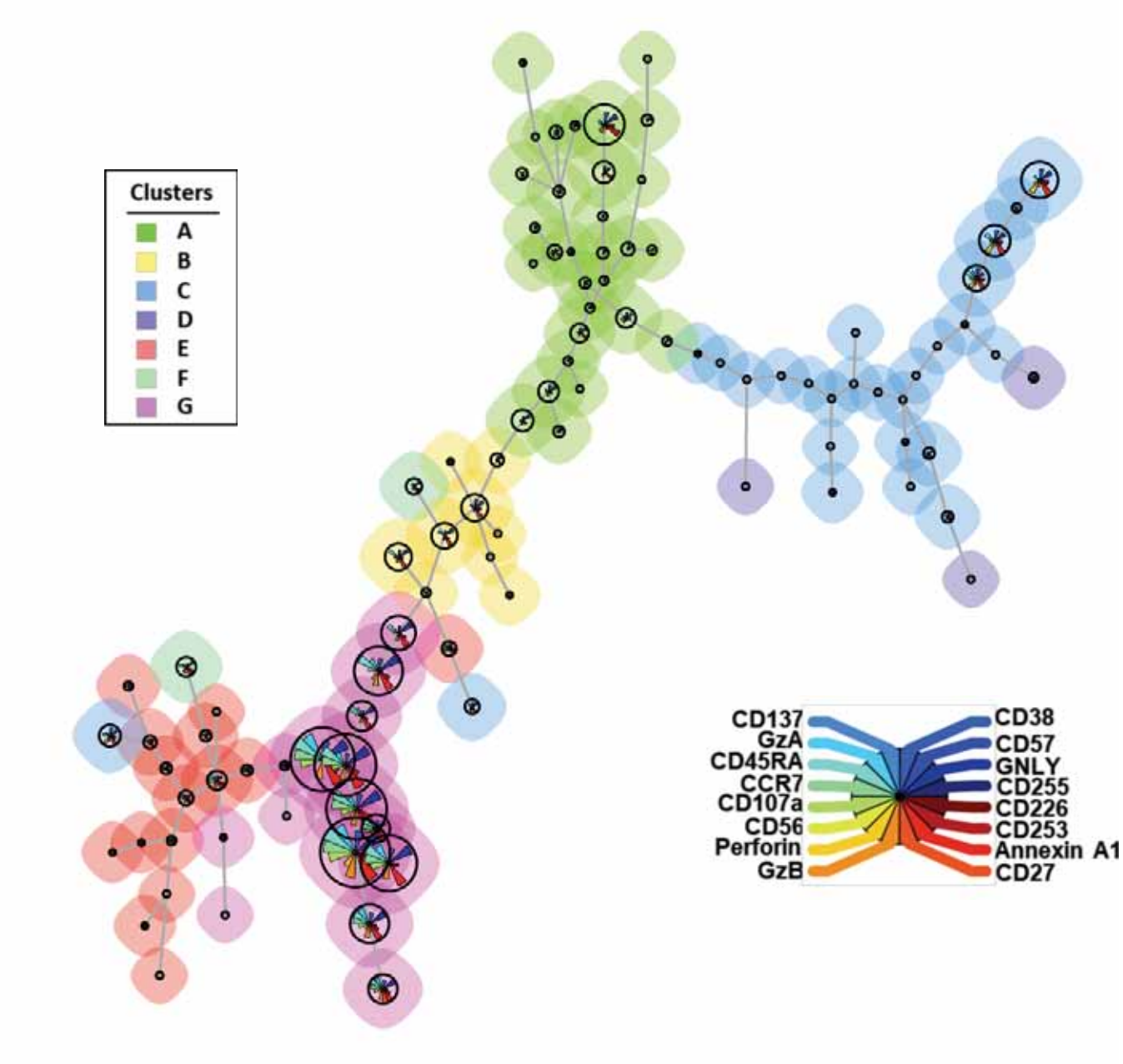

Figure S9

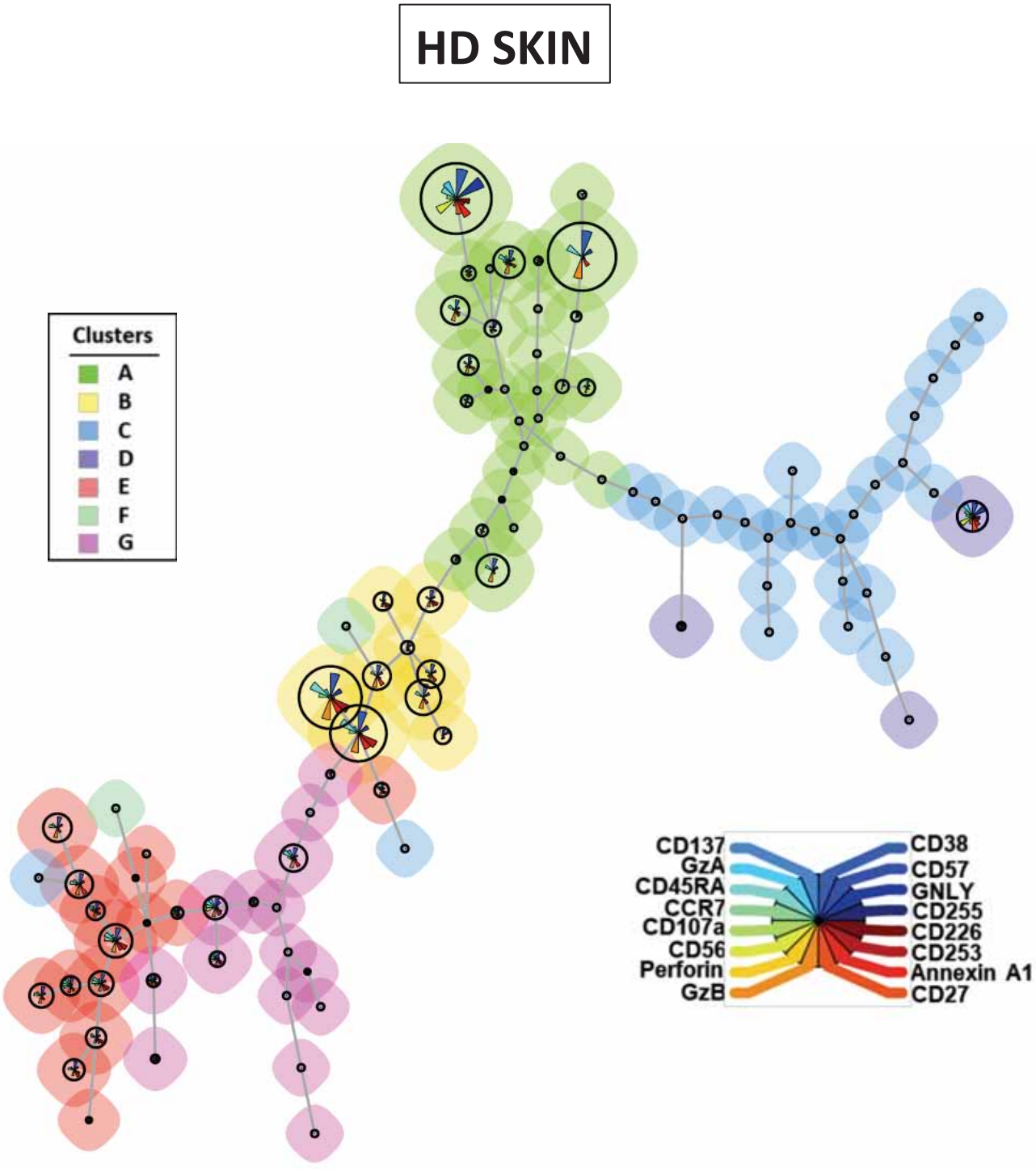
HD SKIN
Clusters
A
B
C
D
E
F
G
CD137
GzA
CD45RA
CCR7
CD107a
CD56
Perforin
GzB
CD38
CD57
GNLY
CD255
CD226
CD253
Annexin A1
CD27

Figure S10

HD PBMCs

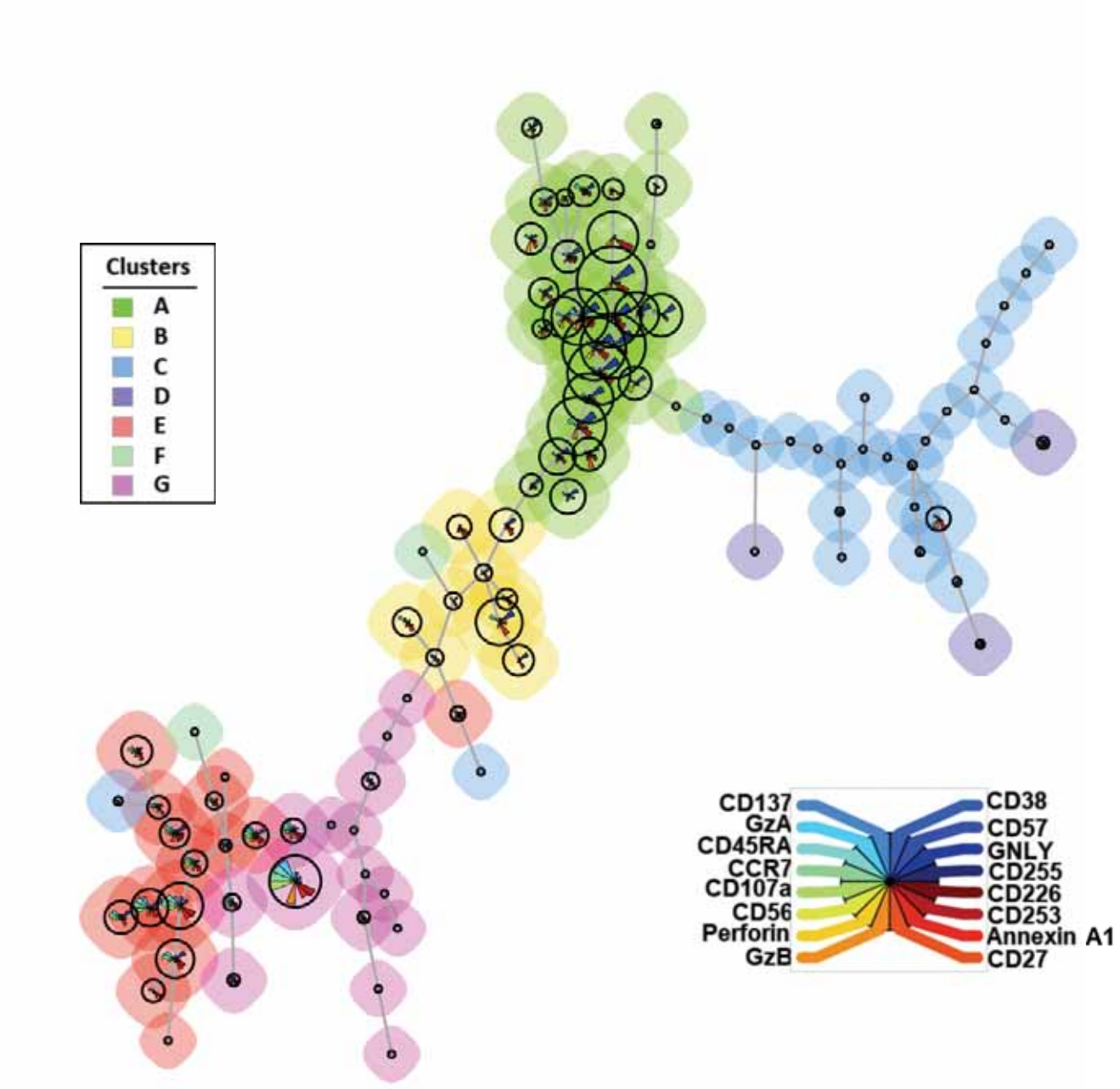

Figure S11

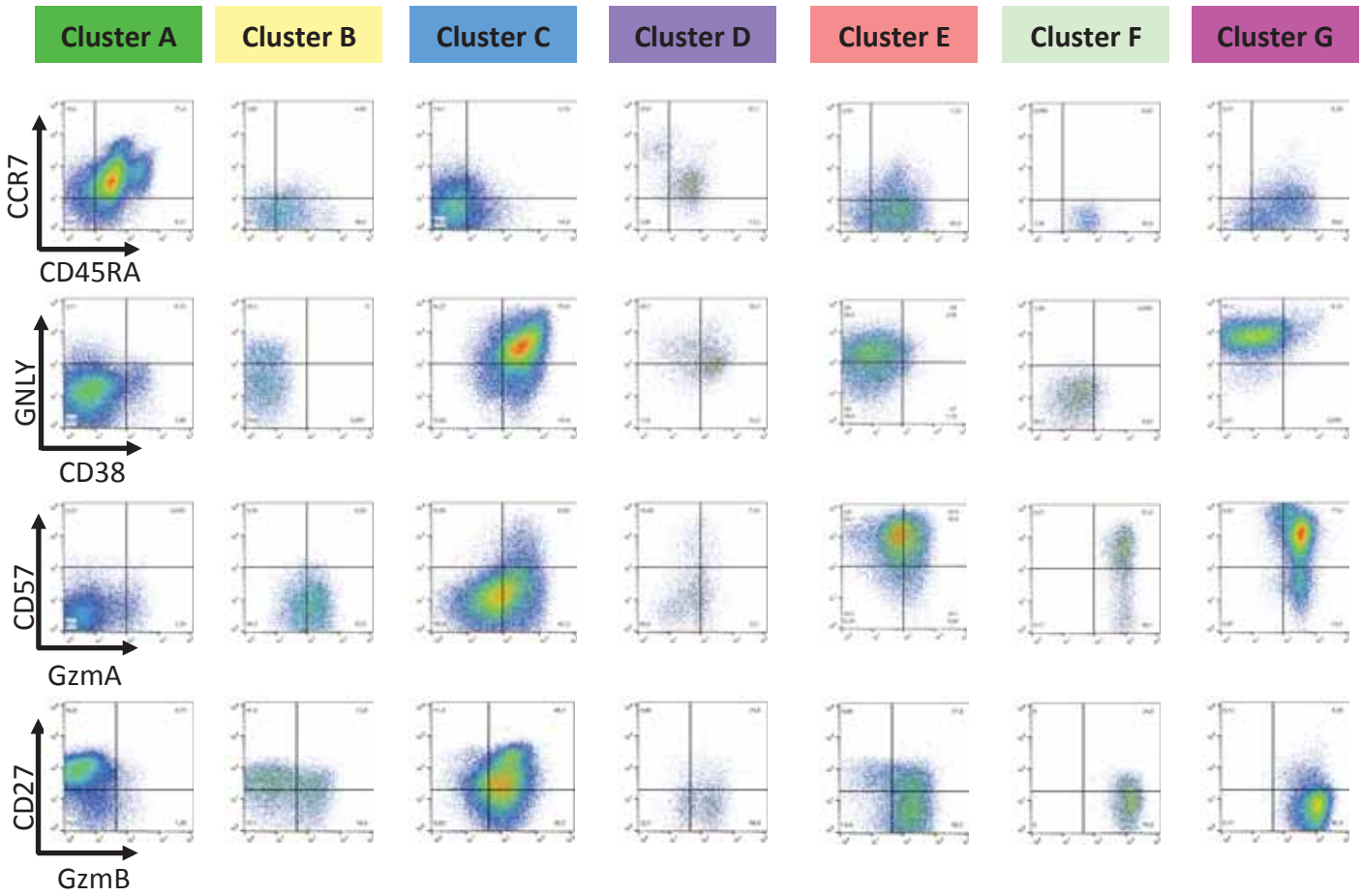
Cluster A
Cluster B
Cluster C
Cluster D
Cluster E
Cluster F
Cluster G
CCR7
CD45RA
GNLY
CD38
CD57
GzmA
CD27
GzmB

Figure S12

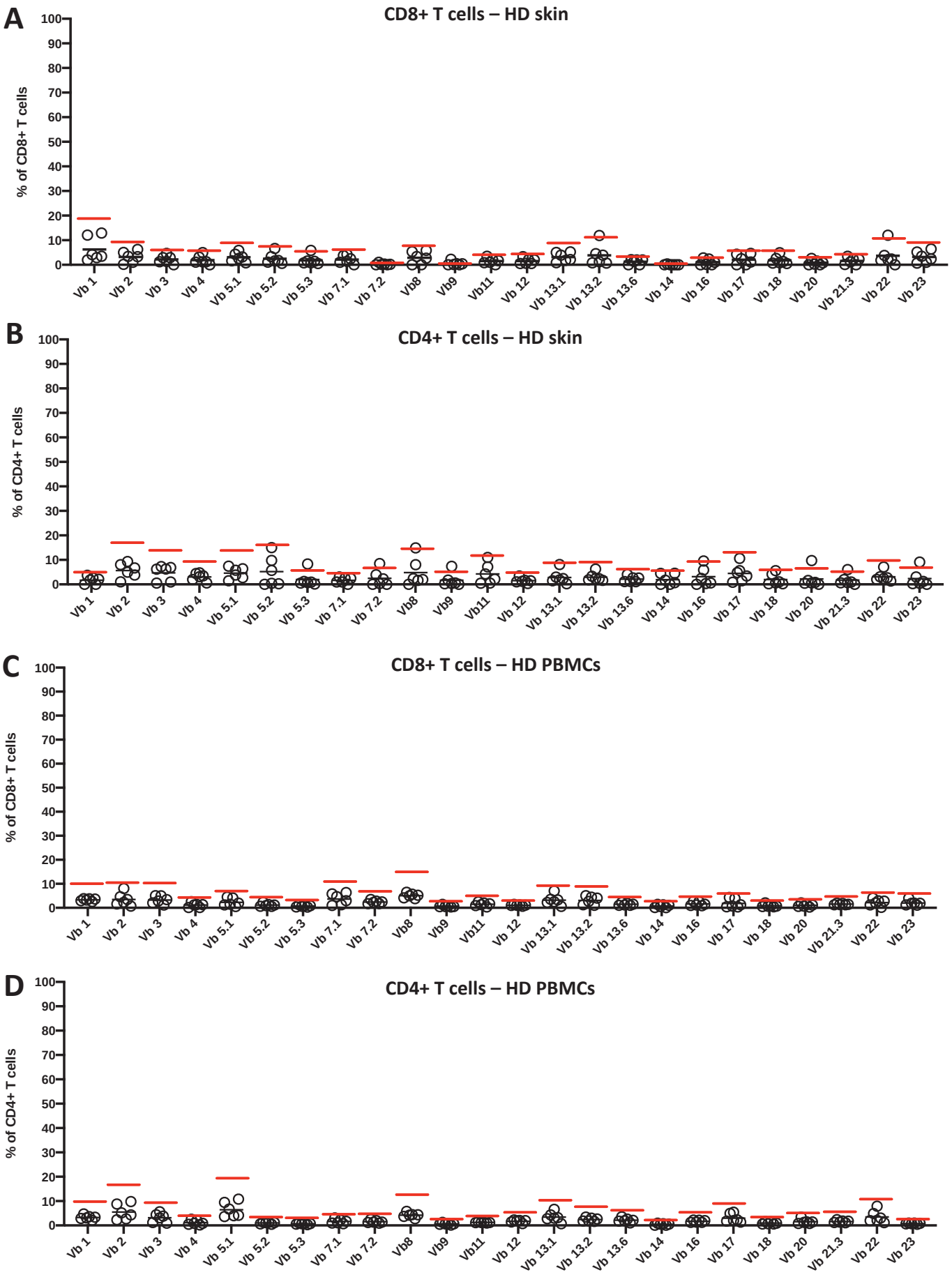
A
CD8+ T cells – HD skin
% of CD8+ T cells
B
CD4+ T cells – HD skin
% of CD4+ T cells
C
CD8+ T cells – HD PBMCs
% of CD8+ T cells
D
CD4+ T cells – HD PBMCs
% of CD4+ T cells
Vb 1
Vb 2
Vb 3
Vb 4
Vb 5.1
Vb 5.2
Vb 5.3
Vb 7.1
Vb 7.2
Vb8
Vb9
Vb11
Vb 12
Vb 13.1
Vb 13.2
Vb 13.6
Vb 14
Vb 16
Vb 17
Vb 18
Vb 20
Vb 21.3
Vb 22
Vb 23

Figure S13

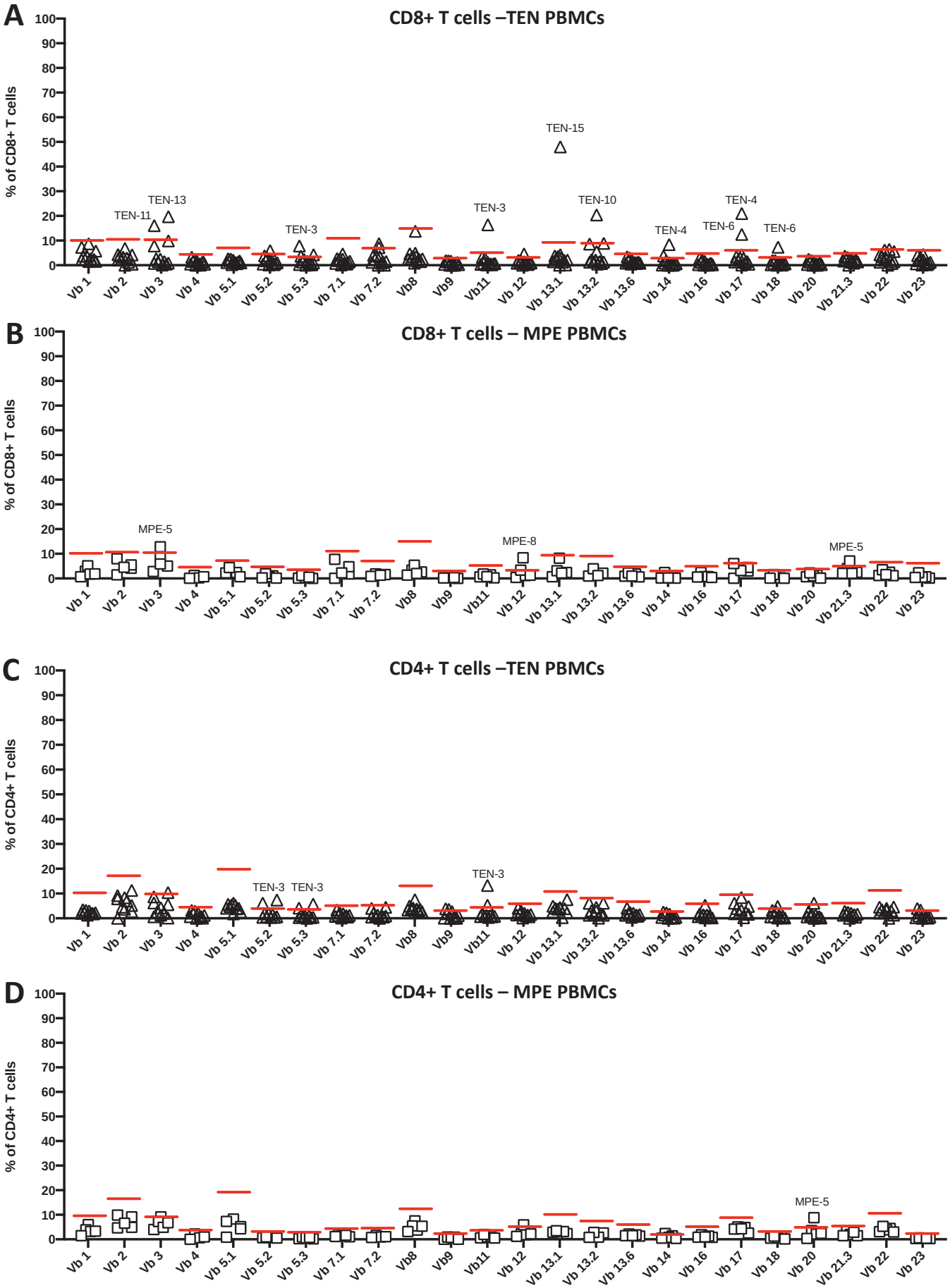
A
CD8+ T cells –TEN PBMCs
% of CD8+ T cells
TEN-11
TEN-13
TEN-3
TEN-3
TEN-15
TEN-10
TEN-4
TEN-6
TEN-4
TEN-6
B
CD8+ T cells – MPE PBMCs
% of CD8+ T cells
MPE-5
MPE-8
MPE-5
C
CD4+ T cells –TEN PBMCs
% of CD4+ T cells
TEN-3
TEN-3
TEN-3
D
CD4+ T cells – MPE PBMCs
% of CD4+ T cells
MPE-5
Vb 1
Vb 2
Vb 3
Vb 4
Vb 5.1
Vb 5.2
Vb 5.3
Vb 7.1
Vb 7.2
Vb8
Vb9
Vb11
Vb 12
Vb 13.1
Vb 13.2
Vb 13.6
Vb 14
Vb 16
Vb 17
Vb 18
Vb 20
Vb 21.3
Vb 22
Vb 23

Figure S14

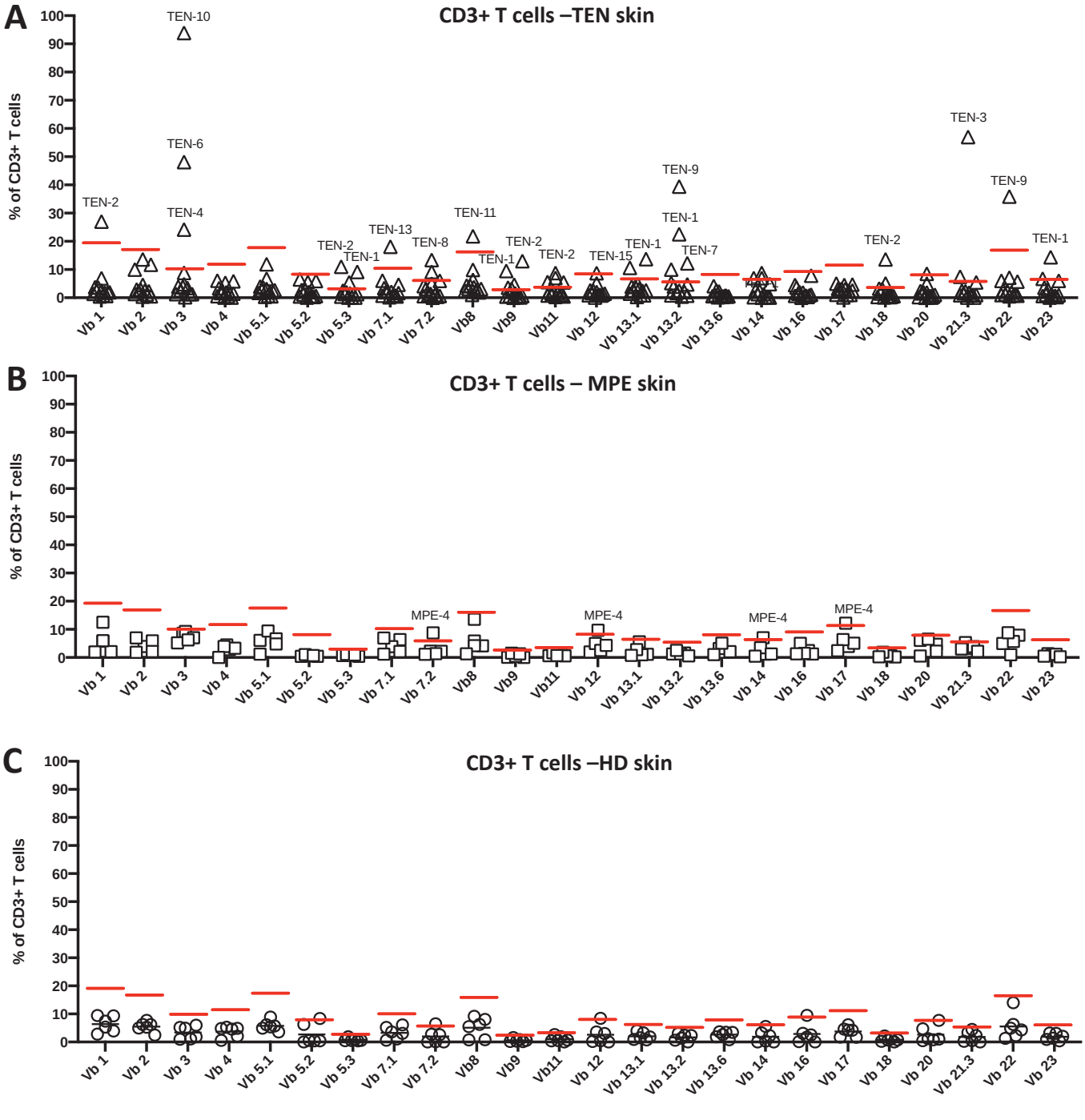
A
CD3+ T cells –TEN skin
% of CD3+ T cells
TEN-10
TEN-6
TEN-4
TEN-2
TEN-2
TEN-1
TEN-13
TEN-8
TEN-11
TEN-1
TEN-2
TEN-2
TEN-15
TEN-1
TEN-9
TEN-1
TEN-7
TEN-2
TEN-3
TEN-9
TEN-1
B
CD3+ T cells – MPE skin
% of CD3+ T cells
MPE-4
MPE-4
MPE-4
MPE-4
C
CD3+ T cells –HD skin
% of CD3+ T cells
Vb 1
Vb 2
Vb 3
Vb 4
Vb 5.1
Vb 5.2
Vb 5.3
Vb 7.1
Vb 7.2
Vb8
Vb9
Vb11
Vb 12
Vb 13.1
Vb 13.2
Vb 13.6
Vb 14
Vb 16
Vb 17
Vb 18
Vb 20
Vb 21.3
Vb 22
Vb 23

Figure S15

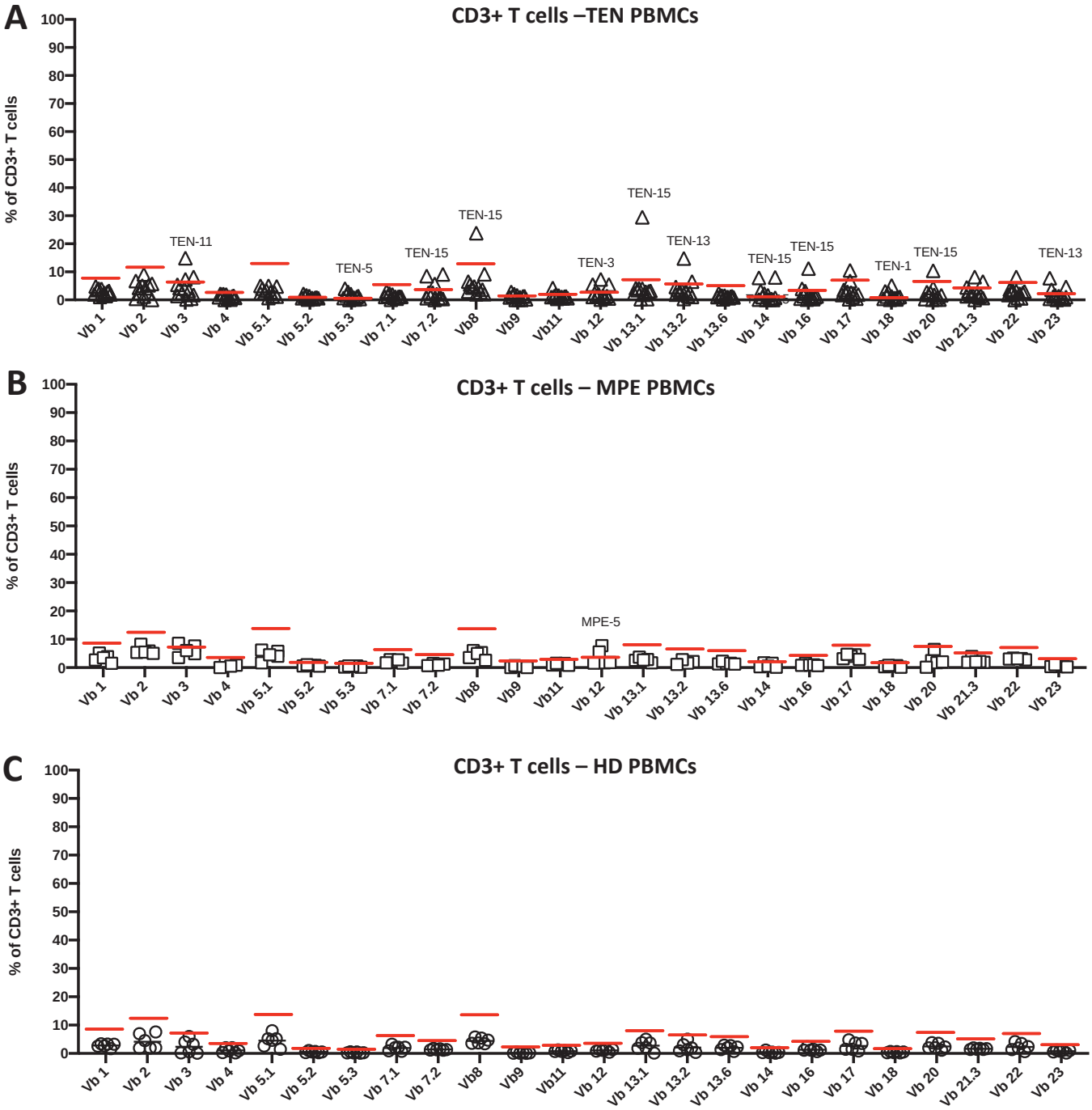
A
CD3+ T cells –TEN PBMCs
% of CD3+ T cells
TEN-11
TEN-5
TEN-15
TEN-15
TEN-3
TEN-15
TEN-13
TEN-15
TEN-15
TEN-1
TEN-15
TEN-13
B
CD3+ T cells – MPE PBMCs
% of CD3+ T cells
MPE-5
C
CD3+ T cells – HD PBMCs
% of CD3+ T cells
Vb 1
Vb 2
Vb 3
Vb 4
Vb 5.1
Vb 5.2
Vb 5.3
Vb 7.1
Vb 7.2
Vb8
Vb9
Vb11
Vb 12
Vb 13.1
Vb 13.2
Vb 13.6
Vb 14
Vb 16
Vb 17
Vb 18
Vb 20
Vb 21.3
Vb 22
Vb 23

Figure S16

TEN-2 SKIN
TEN-2 PBMCs
TEN-3 SKIN
TEN-3 PBMCs
TEN-4 SKIN
TEN-4 PBMCs
TEN-5 SKIN
TEN-5 PBMCs
TEN-6 SKIN
TEN-6 PBMCs
TEN-7 SKIN
TEN-7 PBMCs
TEN-8 SKIN
TEN-8 PBMCs
TEN-9 SKIN
TEN-9 PBMCs
TEN-10 SKIN
TEN-10 PBMCs
TEN-11 SKIN
TEN-11 PBMCs
TEN-12 SKIN
TEN-12 PBMCs
TEN-13 SKIN
TEN-13 PBMCs
TEN-14 SKIN
TEN-14 PBMCs
TEN-15 SKIN
TEN-15 PBMCs
TEN-16 SKIN
TEN-16 PBMCs
MPE-3 SKIN
MPE-3 PBMCs
MPE-4 SKIN
MPE-4 PBMCs
MPE-5 SKIN
MPE-5 PBMCs
MPE-6 SKIN
MPE-6 PBMCs
MPE-7 SKIN
MPE-7 PBMCs

Figure S17

TEN-2 SKIN
TEN-2 PBMCs
TEN-3 SKIN
TEN-3 PBMCs
TEN-4 SKIN
TEN-4 PBMCs
TEN-5 SKIN
TEN-5 PBMCs
TEN-6 SKIN
TEN-6 PBMCs
TEN-7 SKIN
TEN-7 PBMCs
TEN-8 SKIN
TEN-8 PBMCs
TEN-9 SKIN
TEN-9 PBMCs
TEN-10 SKIN
TEN-10 PBMCs
TEN-11 SKIN
TEN-11 PBMCs
TEN-12 SKIN
TEN-12 PBMCs
TEN-13 SKIN
TEN-13 PBMCs
TEN-14 SKIN
TEN-14 PBMCs
TEN-15 SKIN
TEN-15 PBMCs
TEN-16 SKIN
TEN-16 PBMCs
MPE-3 SKIN
MPE-3 PBMCs
MPE-4 SKIN
MPE-4 PBMCs
MPE-5 SKIN
MPE-5 PBMCs
MPE-6 SKIN
MPE-6 PBMCs
MPE-7 SKIN
MPE-7 PBMCs

Figure S18

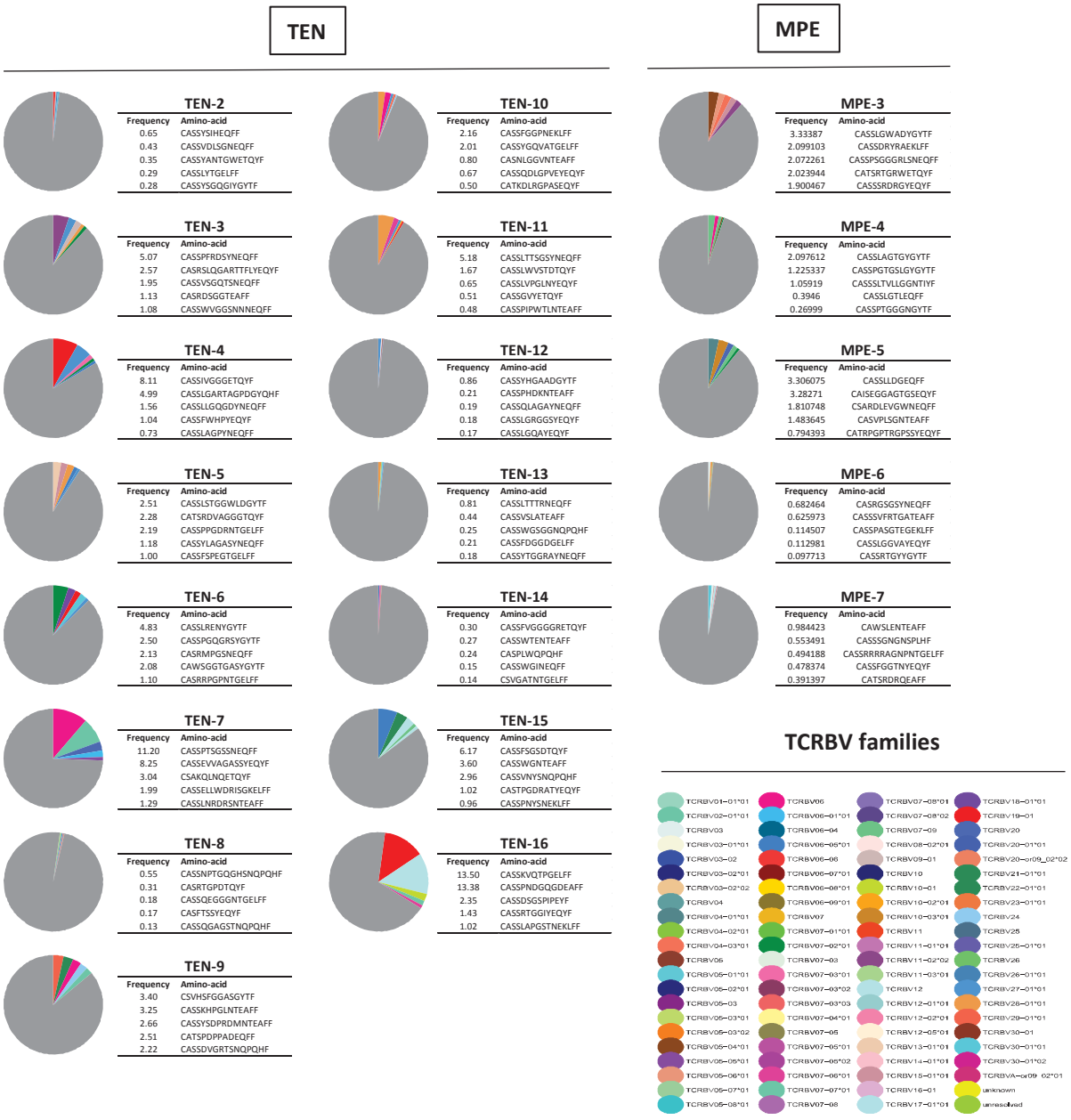
TEN
MPE
TEN-2
Frequency Amino-acid
0.65 CASSYSIHEQFF
0.43 CASSVDLSGNEQFF
0.35 CASSYANTGWETQYF
0.29 CASSLYTGELFF
0.28 CASSYSGQGIYGYTF
TEN-10
Frequency Amino-acid
2.16 CASSFGGPNEKLFF
2.01 CASSYGQVATGELFF
0.80 CASNLGGVNTEAFF
0.67 CASSQDLGPVEYEQYF
0.50 CATKDLRGPASEQYF
MPE-3
Frequency Amino-acid
3.33387 CASSLGWADYGYTF
2.099103 CASSDRYRAEKLFF
2.072261 CASSPSGGGRLSNEQFF
2.023944 CATSRTGRWETQYF
1.900467 CASSSRDRGYEQYF
TEN-3
Frequency Amino-acid
5.07 CASSPFRDSYNEQFF
2.57 CASRSLQGARTTFLYEQYF
1.95 CASSVSGQTSNEQFF
1.13 CASRDSGGTEAFF
1.08 CASSWVGGSNNNEQFF
TEN-11
Frequency Amino-acid
5.18 CASSLTTSGSYNEQFF
1.67 CASSLWVSTDTQYF
0.65 CASSLVPGLNYEQYF
0.51 CASSGVYETQYF
0.48 CASSPIPWTLNTEAFF
MPE-4
Frequency Amino-acid
2.097612 CASSLAGTGYGYTF
1.225337 CASSPGTGSLGYGYTF
1.05919 CASSSLTVLLGGNTIYF
0.3946 CASSLGTLEQFF
0.26999 CASSPTGGGNGYTF
TEN-4
Frequency Amino-acid
8.11 CASSIVGGGETQYF
4.99 CASSLGARTAGPDGYQHF
1.56 CASSLLGQGDYNEQFF
1.04 CASSFWHPYEQYF
0.73 CASSLAGPYNEQFF
TEN-12
Frequency Amino-acid
0.86 CASSYHGAADGYTF
0.21 CASSPHDKNTEAFF
0.19 CASSQLAGAYNEQFF
0.18 CASSLGRGGSYEQYF
0.17 CASSLGQAYEQYF
MPE-5
Frequency Amino-acid
3.306075 CASSLLDGEQFF
3.28271 CAISEGGAGTGSEQYF
1.810748 CSARDLEVGWNEQFF
1.483645 CASVPLSGNTEAFF
0.794393 CATRPGPTRGPSSYEQYF
TEN-5
Frequency Amino-acid
2.51 CASSLSTGGWLDGYTF
2.28 CATSRDVAGGGTQYF
2.19 CASSPPGDRNTGELFF
1.18 CASSYLAGASYNEQFF
1.00 CASSFSPEGTGELFF
TEN-13
Frequency Amino-acid
0.81 CASSLTTTRNEQFF
0.44 CASSVSLATEAFF
0.25 CASSWGSGGNQPQHF
0.21 CASSFDGGDGELFF
0.18 CASSYTGGRAYNEQFF
MPE-6
Frequency Amino-acid
0.682464 CASRGSGSYNEQFF
0.625973 CASSSVFRTGATEAFF
0.114507 CASSPASGTEGEKLFF
0.112981 CASSLGGVAYEQYF
0.097713 CASSRTGYYGYTF
TEN-6
Frequency Amino-acid
4.83 CASSLRENYGYTF
2.50 CASSPGQGRSYGYTF
2.13 CASRMPGSNEQFF
2.08 CAWSGGTGASYGYTF
1.10 CASRRPGPNTGELFF
TEN-14
Frequency Amino-acid
0.30 CASSFVGGGGRETQYF
0.27 CASSWTENTEAFF
0.24 CASPLWQPQHF
0.15 CASSWGINEQFF
0.14 CSVGATNTGELFF
MPE-7
Frequency Amino-acid
0.984423 CAWSLENTEAFF
0.553491 CASSSGNGNSPLHF
0.494188 CASSRRRRAGNPNTGELFF
0.478374 CASSFGGTNYEQYF
0.391397 CATSRDRQEAFF
TEN-7
Frequency Amino-acid
11.20 CASSPTSGSSNEQFF
8.25 CASSEVVAGASSYEQYF
3.04 CSAKQLNQETQYF
1.99 CASSELLWDRISGKELFF
1.29 CASSLNRDRSNTEAFF
TEN-15
Frequency Amino-acid
6.17 CASSFSGSDTQYF
3.60 CASSWGNTEAFF
2.96 CASSVNYSNQPQHF
1.02 CASTPGDRATYEQYF
0.96 CASSPNYSNEKLFF
TCRBV families
TEN-8
Frequency Amino-acid
0.55 CASSNPTGQGHSNQPQHF
0.31 CASRTGPDTQYF
0.18 CASSQEGGGNTGELFF
0.17 CASFTSSYEQYF
0.13 CASSQGAGSTNQPQHF
TEN-16
Frequency Amino-acid
13.50 CASSKVQTPGELFF
13.38 CASSPNDGQGDEAFF
2.35 CASSDSGSPIPEYF
1.43 CASSRTGGIYEQYF
1.02 CASSLAPGSTNEKLFF
TEN-9
Frequency Amino-acid
3.40 CSVHSFGGASGYTF
3.25 CASSKHPGLNTEAFF
2.66 CASSYSDPRDMNTEAFF
2.51 CATSPDPPADEQFF
2.22 CASSDVGRTSNQPQHF

Figure S19

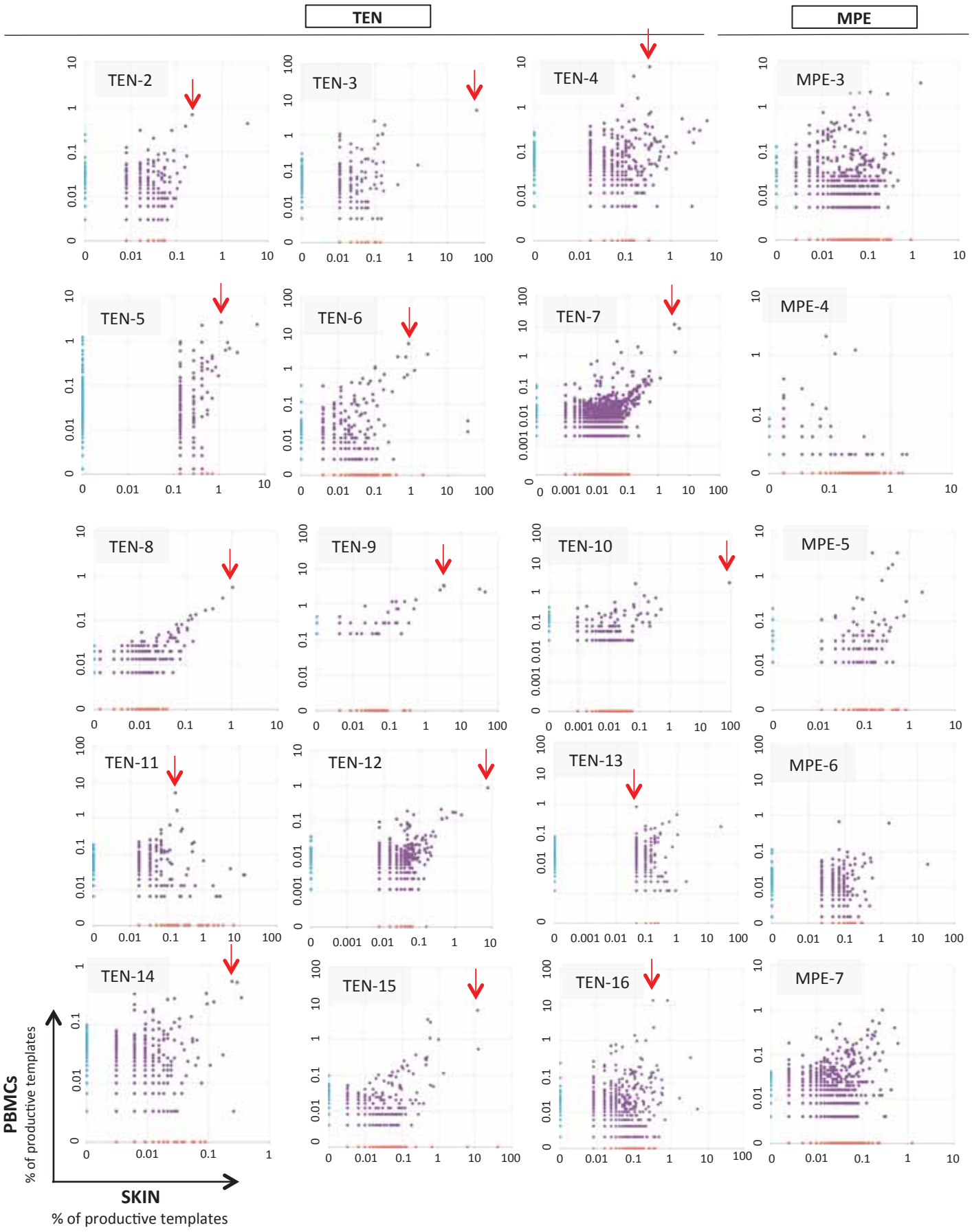
TEN
MPE
TEN-2
TEN-3
TEN-4
MPE-3
TEN-5
TEN-6
TEN-7
MPE-4
TEN-8
TEN-9
TEN-10
MPE-5
TEN-11
TEN-12
TEN-13
MPE-6
TEN-14
TEN-15
TEN-16
MPE-7
PBMCs
% of productive templates
SKIN
% of productive templates

Figure S20